Biochemical and Genetic Mechanisms Underlying Basal Salicylic Acid Synthesis
In *Arabidopsis thaliana*

By

Michael Allan Steinwand

A dissertation submitted in partial satisfaction of the

requirements for the degree of

Doctor of Philosophy

In

Plant Biology

in the

Graduate Division

of the

University of California, Berkeley

Committee in charge:

Professor Mary C. Wildermuth, Chair
Professor Steven Lindow
Professor David Savage

Fall 2017

Abstract

Biochemical and Genetic Mechanisms Underlying Basal Salicylic Acid Synthesis
In *Arabidopsis thaliana*

By

Michael Allan Steinwand

Doctor of Philosophy in Plant Biology

University of California, Berkeley

Professor Mary C. Wildermuth, Chair

The research of plant –microbe interactions is a field with broad applications and strong economic importance to society, as plants are the primary producers that we rely upon for food, textiles, air quality and ornamental value. Global climate change is predicted have a dramatic impact on plant-microbe and pest interactions, and better understanding of how plants respond to pathogen threats is important. The plant hormone salicylic acid (SA) is a crucial signaling molecule in the response to infection by (hemi)biotrophic microbes, as well as other abiotic stress responses. However, our understanding of the mechanisms governing its synthesis is lacking. Pathogen challenge induces rapid and robust SA synthesis, increasing the amount of the hormone 10-fold within 48 hours. However, SA synthesis also occurs at a low rate in uninfected plants, accumulating as a storage form that can be readily converted to active SA. Herein, I detail two studies using the model dicot *Arabidopsis thaliana* examining the processes governing SA accumulation through metabolic manipulation of SA precursors and transporters, and show that the pre-infection levels of endogenous SA can play a role in priming plant immunity.

In chapter 2, I present evidence that chorismate mutases can influence basal SA synthesis by their competition with isochorismate synthase enzymes for the substrate chorismate. Transient overexpression of these enzymes reduced SA accumulation *in planta*, suggesting these enzymes redirected chorismate flux away from SA synthesis. Plants with reduced expression of chorismate mutase 1 (CM1) exhibited elevated basal SA levels, which conferred enhanced disease resistance to a virulent bacterial *Pseudomonas syringae* foliar pathogen. This phenotype comes without an obvious fitness cost to the plant; they don't exhibit increased basal expression of defense genes, or a reduction in plant growth. Rather, it appears that this elevated basal SA quickens early responses to pathogens, a key moment in the infection process.

In contrast, chapter 3 details the discovery that the transcriptional repressor DEL1, previously characterized for its role as a cell cycle regulator, also mediates basal SA synthesis. Loss of DEL1 repression leads to increased expression of SA biosynthesis and transporter genes, which alters SA signaling responses and primes the plant for greater disease resistance to both bacterial and fungal pathogens. *CM1* and *DEL1* mutant plants represent a continuum of defense priming by endogenous SA, and illustrate new approaches for modulating increased disease resistance in plants by influencing metabolic flux of chorismate products. The discovery that DEL1 also mediates expression of an SA hub suggests that it plays a broader role in coordinating developmental and stress response cues.

TABLE OF CONTENTS

CHAPTER 4

APPENDIX

ACKNOWLEDGMENTS

CHAPTER 1: Salicylate Biosynthesis and Innate Immunity in *Arabidopsis thaliana*

Plants have evolved a variety of hormones to coordinate local and distal responses to environmental and biotic stimuli. The phytohormone salicylic acid (SA, 2-hydroxybenzoic acid) is an important plant phenolic shown to be a critical endogenous signal induced by pathogen attack, activating a broad network of transcriptional defense responses that limit the extent of infection, including production of anti-microbial compounds and in some cases, programmed cell death of host tissues (Vlot et al., 2009). SA also mediates responses to a number of abiotic stressors, and influences plant development, as reviewed in (Rivas-San Vicente and Plasencia, 2011). In this dissertation, I examine the coordination of primary metabolism and SA biosynthesis, and the impact of altered basal SA on pathogen outcomes.

Role of SA in coordinating plant immunity

Plants cells possess an innate immunity that functions through tiers of pathogen perception proteins and a connective network of cellular communication (Figure 1.1). At the cell surface are transmembrane pattern recognition receptors (PRRs) that recognize highly conserved components of microbes, such as flagellin from bacteria or chitin from fungi, and can stimulate pattern-triggered immunity (PTI). PTI is typified by induction of defense response genes, production of reactive oxygen species (ROS) and other antimicrobial compounds, and callose deposition at the cell wall (Bigeard et al., 2015). These responses can limit pathogen growth. Pathogens have evolved secreted effector proteins that manipulate host processes to enhance virulence or attenuate PTI in the host cell. Perception of these effectors or their action by intracellular surveillance proteins elicits effector-triggered immunity (ETI), a more robust response that often culminates in localized host cell death to limit pathogen growth (Jones and Dangl, 2006). Accompanying ETI is the establishment of systemic acquired resistance (SAR) that primes distal regions of the plant against secondary infection (Fu and Dong, 2013).

SA has been shown to be an important player mediating these immune responses, and its synthesis is induced in response to both virulent and avirulent (hemi)biotrophic pathogens. Among the early responses upon pathogen perception are mitogen activated protein kinase signaling, formation of reactive oxygen species (ROS) and an influx of Ca^{2+}, causing DNA binding protein SARD1, calmodulin binding protein CBP60g and WRKY28 transcription factor to stimulate expression of the SA biosynthesis gene *ISOCHORISMATE SYNTHASE 1(ICS1)* (Seyfferth and Tsuda, 2014; Zheng et al., 2015). SARD1 and CBP60g have recently been shown to also bind to *EDS5* as well as other components that positively and negatively influence PTI and ETI, suggesting they play a broad role in regulating immune responses (Sun et al., 2015). EDS1 and PAD4 function upstream of SA synthesis and contribute to a positive feedback loop on SA accumulation (Vlot et al., 2009; Seyfferth and Tsuda, 2014).

SA functions in a concentration-dependent manner through interaction with the master

Abbreviations:
Genes: *SARD1- systemic acquired resistance deficient 1; CBP60g- calmodulin binding protein 60g; ICS1- isochorismate synthase 1; EDS5- enhanced disease susceptibility 5; EDS1- enhanced disease susceptibility 1; PAD4- phytoalexin deficient 4; NPR1- non-expresser of PR genes 1; NPR3- non-expresser of PR genes 3; NPR4- non-expresser of PR genes 4; UGT74F1- UDP-glycosyltransferase 74F1; UGT74F2- UDP-glycosyltransferase 74F2; DEL1- DP-E2F-like 1; ASA1- anthranilate synthase alpha subunit 1; MAPK3- mitogen activated protein kinase 3; MAPK6- mitogen activated protein kinase 6*
Terms: PRR- pattern recognition receptor; PTI- pattern triggered immunity; ETI- effector triggered immunity; SAR- systemic acquired resistance; ROS- reactive oxygen species
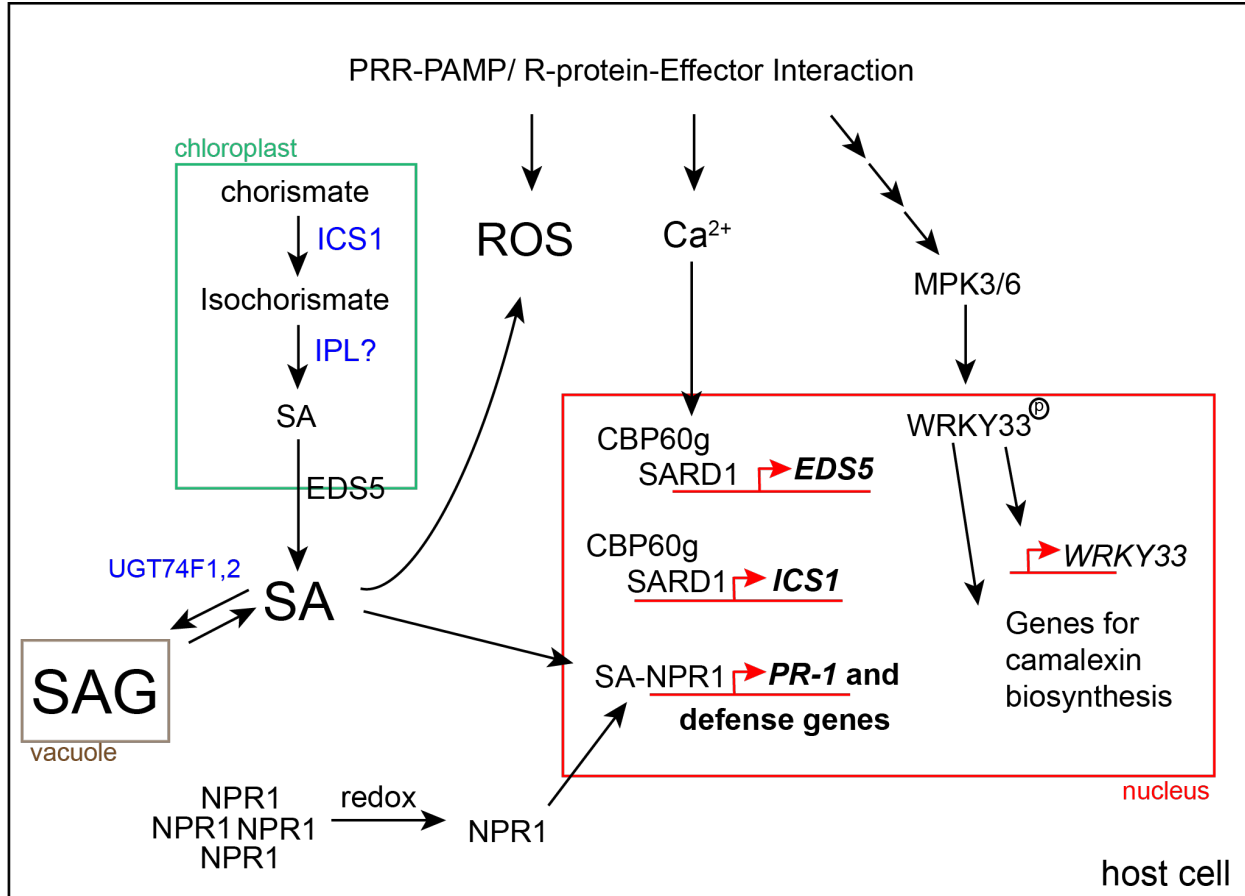
Figure 1.1: Overview of SA synthesis and signaling responses in *Arabidopsis* discussed in this dissertation

Upon perception of the pathogen by the host cell through surveillance proteins, reactive oxygen species (ROS), influx of Ca^{2+} and activation of MAP kinase cascade, including MPK3/6, activate SA synthesis. ROS formation is influenced by SA. Transcriptional activators CBP60g and SARD1 bind to *ICS1* and *EDS5* promoters to upregulate expression. PAD4 and EDS1 function upstream of SA synthesis, but their role is complex and context-dependent, and omitted for clarity. Induced SA synthesis occurs in the chloroplast via ICS1 and a putative IPL protein, then is exported into the cytosol via SA transporter EDS5. Cytosolic SA can be glucosylated to the dominant storage form SAG and transported to vacuole. Cytosolic SA and SAG is considered total active SA. Enzymes that mediate conversion of SA or its precursors are shown in blue. Changes in cellular redox conditions releases NPR1 from its oligomer form and monomeric NPR1 relocates to the nucleus, where, bound to SA, it upregulates expression of *PR-1* and other defense genes. NPR1 also negatively regulates *ICS1* expression as a negative feedback loop on SA synthesis. Activated MPK3 phosphorylates WRKY33, which induces its own expression and activates genes for synthesis of the antimicrobial compound camalexin.

defense transcriptional regulator NPR1 and its paralogs NPR3 and NPR4, which function as adaptors for CUL3 E3 ligases and bind SA with different affinities. At basal SA concentrations, NPR1 exists largely in the cytosol as an oligomer, while NPR4 binds NPR1 and facilitates its ubiquitination for proteosomal degradation, keeping NPR1-mediated gene expression at a basal level. Upon pathogen challenge and SA synthesis, SA-mediated cellular redox changes facilitate NPR1 nuclear import. NPR1 binds to SA, inducing conformational changes thought to enhance activity (Mou et al., 2003; Wu et al., 2012). High SA concentration at the site of infection promotes NPR3-NPR1 interaction, leading to NPR1 degradation and programmed cell death. In neighboring cells, intermediate SA concentration alters activated nuclear NPR1 to promote defense (Spoel et al., 2009; Fu et al., 2012). NPR1 also acts as a negative regulator of *ICS1* expression upon nuclear localization, serving as a feedback mechanism to restrain SA synthesis (Zhang et al., 2010). SA also influences additional NPR1-independent responses, which is discussed briefly in (An and Mou, 2011). Thus both rapidity of synthesis and concentration are key for SA-mediated responses and restriction of pathogen growth.

In the cytosol, SA concentration can be reduced by glucosylation into inactive storage forms SA 2-*O*-β-glucoside (SAG) or salicylate glucose ester (SGE) by salicylic acid glucosyltransferases UGT74F1 and UGT74F2 (Dean and Delaney, 2008; George Thompson et al., 2017) for storage in the vacuole. This glucose can be readily hydrolyzed to form active SA. Additional SA modifications include conjugation to amino acids (*ie* aspartate, to form salicyloyl-L-aspartic acid), hydroxylation (*ie* to 2,3-dihydroxybenzoate) to form precursors for catabolism, or methylation (*ie* the volatile methylsalicylate) to form a mobile signal, among others, which are detailed in (Dempsey et al., 2011).

Routes of SA biosynthesis in plants: Biochemical evidence of PAL and ICS pathways

Unlike many other plant hormones, the full biosynthetic pathway for SA has yet to be defined. To date, two possible routes to SA have been proposed and partially characterized in several plant species, both of which originate from the metabolite chorismate, the end product of the plastid-localized shikimate pathway (Dempsey et al., 2011): the isochorismate synthase pathway (ICS) and the phenylalanine ammonia lyase pathway (PAL) (Figure 1.2).

As SA is a benzoate, initial experiments theorized that SA's synthesis derived from phenylalanine and other benzoates precursors. Radiolabeled tracer studies feeding [^{14}C]phenylalanine, [^{14}C]*trans*-cinnamic acid or [^{14}C]benzoic acid were used in American wintergreen, viral-infected tobacco, cucumber and healthy rice seedlings (El-Basyouni et al., 1964; Yalpani et al., 1993; Meuwly et al., 1995; Silverman et al., 1995) to demonstrate the incorporation of these substrates into endogenously derived [^{14}C]SA. These studies determined that phenylalanine was first converted to *trans*-cinnamic acid, a reaction mediated by PAL enzymes (EC 4.3.1.5.). Application of the PAL chemical inhibitor 2-aminoindan-2-phosphonic acid (AIP) inhibited incorporation of [^{14}C]phenylalanine to [^{14}C]SA (Meuwly et al., 1995), yet [^{14}C]SA was still produced when supplied [^{14}C]benzoic acid under AIP treatment. A viral-induced benzoic acid-2-hydroxylase (BA2H) was isolated and partially purified from infected tobacco (León et al., 1993; León et al., 1995), hydroxylating the *ortho-* position of benzoic acid to form SA. However, no gene encoding this enzyme has been reported in plants to date.

There are four *PAL* genes in *Arabidopsis*, some of which are transcriptionally responsive to biotic and abiotic stresses (Mauch-Mani and Slusarenko, 1996; Cochrane et al., 2004; Olsen et al., 2008). PAL activity was reduced 66% in genetic knockouts of *pal1,2* double mutants and
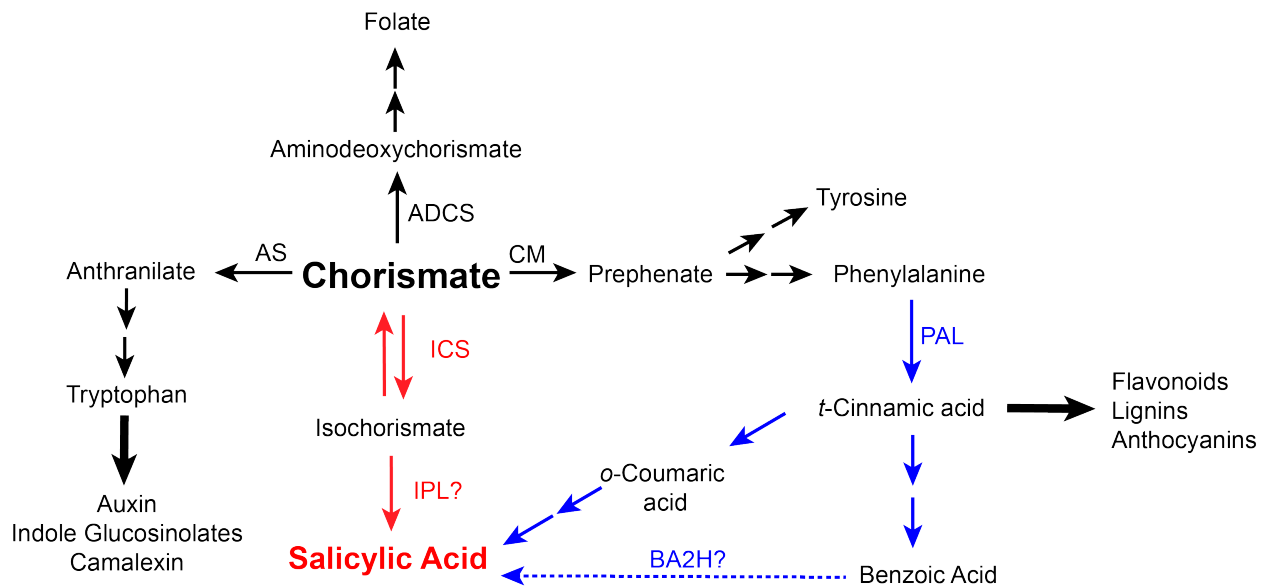
Figure 1.2: ICS and PAL pathways to SA biosynthesis in plants
Schematic of proposed routes to SA in plants shows that chorismate is a common precursor to both pathways. In *Arabidopsis*, ICS pathway is dominant route of synthesis. Red: ICS pathway, catalyzed by ICS enzyme and a putative IPL protein; Blue: PAL pathway, benzoate synthesis derives from phenylalanine to SA. BA2H activity was identified in tobacco but no corresponding gene has been identified. Aromatic amino acids tryptophan, phenylalanine and tyrosine are precursors to defense induced compounds derived from chorismate, including camalexin and phenylpropanoids such as lignin and anthocyanins.

further reduced in triple and quadruple mutants, though 10% residual PAL activity remained (Huang et al., 2010). *PAL* double, triple and quadruple mutants show many pleiotropic effects, including altered phenylpropanoid metabolism and extremely reduced size. However, pre-infection total SA and total SA induced upon infection with avirulent *Pseudomonas syringae* pv DC3000 were not significantly reduced except in quadruple mutants, in which pre-infection and induced total SA were 25% and 50% of wild type, respectively. This suggests that in *Arabidopsis*, another pathway independent of PAL is responsible for SA synthesis. The observed reduction in SA in the *PAL* quadruple mutants could be due to partial use of the PAL pathway to SA or an indirect effect on the ICS pathway.

The labeling approach supplying phenylalanine, *trans*-cinnamic acid or benzoic acid demonstrates that these compounds can be converted to SA *in planta*, but they are not necessarily substrates of the dominant pathway. Mustafa et al. 2009 performed a similar substrate feeding experiment in *Catharanthus roseus* cells upon fungal elicitation, but supplied [1-^{13}C] glucose, which is incorporated into primary metabolism. The positional incorporation of the radiolabel into the molecules of the shikimate pathway was used to distinguish SA derived from either the PAL and ICS routes, which proceed via different mechanisms from chorismate and result in differently labeled SA. This demonstrated that chorismate is converted to the intermediate isochorismate, then converted to SA (Mustafa et al., 2009) in *Catharanthus roseus*, adding additional proof to the growing evidence that an alternative pathway for SA synthesis exists in plants, as elucidated by *Arabidopsis*.

Arabidopsis Isochorismate Synthases mediate SA biosynthesis

Several screens of EMS- and fast neutron-mutagenized *Arabidopsis* for enhanced disease susceptibility and salicylic-acid deficiency identified mutants *sid2* and *eds16,* which exhibited severe reduction in pathogen-induced SA and were more susceptible to infection with the obligate biotrophic fungus *Golovinomyces orontii* (Nawrath and Metraux, 1999; Dewdney et al., 2000). Subsequent analysis determined these mutants to be allelic for a single gene *ICS1* (EC 5.4.4.2), which encodes an ICS that converts chorismate into isochorismate (Wildermuth et al., 2001). Expression of *ICS1* was pathogen-inducible and correlated with SA accumulation; mutants produced just 10% of wild type SA. The homolog *ICS2* was characterized by (Garcion et al., 2008), and shares similar gene exon structure and 88% sequence similarity at the protein level. The two genes exhibit unique expression patterns; ICS1 is responsive to abiotic and biotic stressors, but ICS2 is not induced by these stressors and localized predominantly to vascular tissues in GUS reporter assays (Dempsey et al., 2011; Macaulay et al., 2017). In other plant systems, ICS exists as a single copy gene and encodes multiple splice variants to regulate enzyme activity (Yuan et al., 2009). While *ics2* mutants do not exhibit a reduction in SA, *ics1,2* double mutants enhance the effect of *ics1*, and induced SA was reduced to 4% of wild type. These ICS enzymes mediate nearly all induced SA in *Arabidopsis*, while the small remainder could be produced through alternative means. ICS enzymes have been shown to play a role in SA accumulation in a number of plant species, including *Nicotiana benthamiana* (Catinot et al., 2008), tomato (Uppalapati et al., 2007) and soybean (Shine et al., 2016).

The SA biosynthetic mutant *sid1/eds5*, identified in the mutant screens that isolated *ICS1*, elucidates the subcellular location of SA synthesis, and provides additional support for the ICS pathway in *Arabidopsis*. *EDS5*, a member of the Multidrug and Toxin Extrusion family, is an SA-specific transporter localized to the chloroplast envelope (Nawrath, 2002; Serrano et al., 2013; Yamasaki et al., 2013). Like *ICS1, EDS5* expression is inducible by pathogen inoculation,

and mutants are deficient in SA accumulation, presumably due to product inhibition on synthesis. The transcriptional repressor DEL1 regulates *EDS5* expression, and its impact on accumulation of basal SA is detailed in Chapter 3.

The phenotype of *eds5* also supports that SA is largely derived via the ICS pathway in *Arabidopsis*. Consistent with their role in SA formation, *ICS1* and *ICS2* both localize to the chloroplast stroma (Strawn et al., 2007; Garcion et al., 2008). Further work to characterize *Arabidopsis* PAL enzyme localization is required. Although phenylalanine is produced in the chloroplast, the *Arabidopsis* PAL enzymes lack putative chloroplast-signal peptides. Rather, a phenylalanine chloroplast exporter has been identified in *Petunia hybrida* (Widhalm et al., 2015) that relocates phenylalanine to the cytosol, where, in tobacco, PAL enzymes channel phenylalanine into *p*-coumaric acid via association with cinnamate-4-hydroxylase (Achnine et al., 2004).

Chorismate metabolism is regulated in *Arabidopsis*

Chorismate is a central branch point for synthesis of aromatic amino acids, phylloquinone and folate, so ICS competes for chorismate utilization with three other enzyme types: chorismate mutase (CM, 5.4.99.5), anthranilate synthase (AS, EC 4.1.3.27) and aminodeoxychorismate synthase (ADCS, EC 2.6.1.85) (Figure 1.2). Phenylalanine derivatives can constitute up to 30% of total photosynthetic carbon under certain conditions, and include lignins and other phenylpropanoids, some of which play a role in cell wall architecture, and are strongly induced during a defense response. Additionally, tryptophan derivatives such as the hormone auxin (indole-3-acetic acid), the antimicrobial camalexin and indole glucosinolates constitute major derivatives (Fig. 1.2). Metabolite flux through this pathway is tightly controlled through allosteric regulation; CM1 is the only chorismate-utilizing enzyme known to have both positive and negative allosteric regulation and coordinates flux between tryptophan synthesis and phenylalanine and tyrosine synthesis. CM1 is positively influenced by tryptophan and negatively regulated by its downstream reaction products phenylalanine and tyrosine (Westfall et al., 2014). Tryptophan acts as a negative regulator of ASA1, and downstream accumulation of tryptophan restrains AS activity (Li and Last, 1996). ICS, AS, and ADCS belong to the menaquinone, siderophore or tryptophan biosynthesis (MST) enzyme family and share a similar complex folded α-helical/β-sheet structure. Biochemical characterization of recombinant ICS1 and ICS2 enzymes determined that they possess K_ms for chorismate of 20-40 μM, making them competitive with these other enzymes *in vivo* (See Chapter 2). Both ICS enzymes operate at equilibrium to catalyze the reversible conversion of chorismate to isochorismate (Strawn et al., 2007; Macaulay et al., 2017) but do not produce SA and are thus monofunctional. Since *ICS1* and *2* catalyze a reversible reaction, chorismate concentration can dictate flux to isochorismate and influence SA synthesis.

Bacterial synthesis of SA utilizes ICS and IPL enzymes

Several bacterial genera produce SA as an intermediate in the production of iron-scavenging siderophores: pyochelin in *Pseudomonas aeruginosa* (Cox et al., 1981), yersiniabactin in *Yersinia enterocolitica* (Pelludat et al., 2003)*,* pseudomonine in *Pseudomonas fluorescens* (Mercado-Blanco et al., 2001) and mycobactin in *Mycobacterium tuberculosis* (De Voss et al., 2000). To catalyze formation of SA from chorismate, these bacteria employ either a single-step salicylate synthase (SAS), or sequential conversion using two enzymes, an ICS and an isochorismate pyruvate lyase (IPL, EC 4.2.99.21), which converts isochorismate into SA. The

two *Arabidopsis* ICS share predicted structural homology to both bacterial SAS and ICS enzymes with highly conserved active sites. The mechanisms that dictate SAS and ICS activities are still not fully understood, and may depend on small positional variations in amino acids that coordinate the location of Mg^{2+} ions in the active site (Lamb, 2011; Meneely et al., 2016). Crystal structures have been resolved for SAS Irp9 from *Y. enterocolitica* and MbtI from *M. tuberculosis,* which reveal shared structural homology with bacterial ICS enzymes, and conservation of all but two active site residues (Meneely et al., 2013). However, exchanging these differing active site residues of the two classes of proteins via site-directed mutants reduced reaction efficiency but didn't interchange activity (Kerbarh et al., 2005; Sridharan et al., 2010), and some mutant enzymes also catalyzed promiscuous reactions to create prephenate and phenylpyruvate, two additional derivatives of chorismate (Meneely et al., 2013). Thus it appears computational prediction via comparison of sequence similarity and active site residues is insufficient to accurately predict enzyme function, and instead activities must be determined biochemically.

In SA-producing bacterial species that possess a monofunctional ICS, an IPL enzyme is employed to catalyze conversion of isochorismate to SA and pyruvate. Two examples of such proteins exist: PmsB from *Pseudomonas fluorescens* (Mercado-Blanco et al., 2001) and PchB from *Pseudomonas aeruginosa* (Serino et al., 1995), with PchB being the more studied of the two and the focus of this discussion. *PchB* is co-expressed with the ICS *PchA*, and the two proteins have been shown to be sufficient for production of SA from chorismate in both bacteria and plants (Serino et al., 1995; Mauch et al., 2001). Interestingly, PchB does not share structural homology to the MST family, but instead is structurally highly similar to the AroQ class of CMs, which exhibit an α-helical structure (Fig. 1.3A) (Zaitseva et al., 2006; Lamb, 2011). These CMs use a rare pericyclic reaction to convert chorismate to prephenate for use in phenylalanine and tyrosine synthesis. PchB's active site residues are partially conserved with the CM from *E. coli*, though only exhibits about 20% sequence similarity. PchB possesses IPL activity (κ_{cat}/K_m of 8.48 $\mu M^{-1} min^{-1}$) that is two orders of magnitude greater than a residual CM activity (κ_{cat}/K_m = 0.052 $\mu M^{-1} min^{-1}$), which appears to be its ancestral state (Gaille et al., 2002). The two reactions are performed in the same active site (Gaille et al., 2002) and proceed via the same pericyclic reaction mechanism (Lamb, 2011), in which the transition state intermediate forms a cyclical structure resulting in either rearrangement or elimination of the pyruvate side chain. As seen for MST enzymes, disentangling the CM and IPL activities of PchB by modifying active site residues is not straightforward, and no mutants have been produced with abrogated CM function that retain robust IPL activity. Rather, modification generally affects both activities (Gaille et al., 2002; Künzler et al., 2005; Luo et al., 2009).

Reverse genetic approach identified CM1 as candidate for *Arabidopsis* IPL

All evidence suggests induced SA biosynthesis in *Arabidopsis* occurs from chorismate and necessitates an ICS enzyme. In bacteria, SA is produced utilizing an ICS and IPL enzyme, but no *Arabidopsis* IPL enzyme has been identified computationally, or in forward genetic screens assaying for SA deficiency. There are many possible explanations for this, including genetic redundancy among duplicated isoforms, the fact that these screens were not conducted to saturation, or that genetic disruption causes lethality in an unforeseen way. It also remains possible that SA is converted from isochorismate in a novel manner, but enzymatic conversion is likely. Isochorismate can convert to SA non-enzymatically, though this reaction is 8 times less

A

PchB (dimer)

CM1 (monomer)

B

R229 (R31)

SA

V269 (R53)

Q331(Q90)

pyruvate

K240 (K42)

CM1(PchB) active site residues

C

CM1 (dimer) from above, with allosteric residues marked in purple
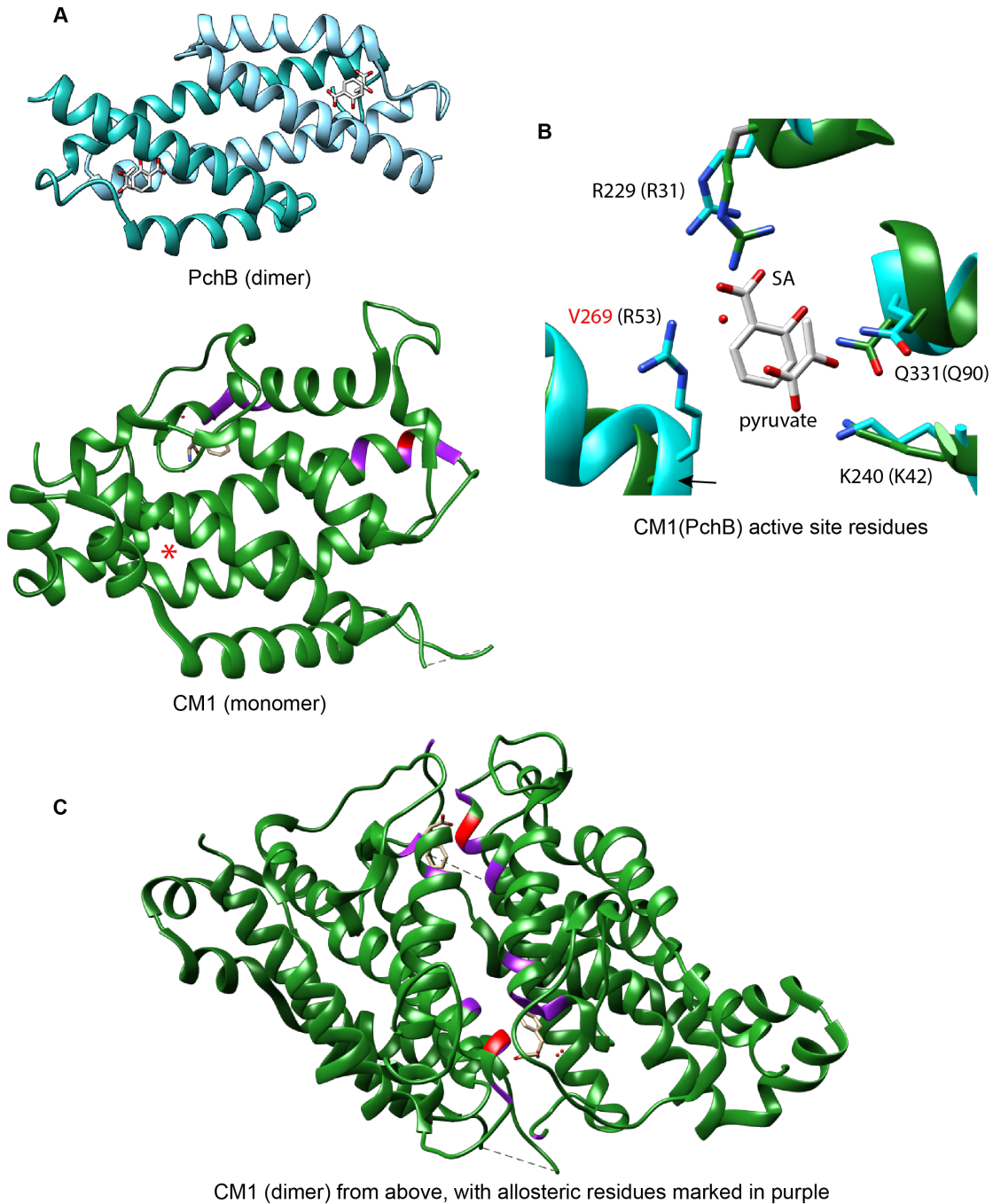
Figure 1.3: Crystal structures reveal structural homology of PchB and CM1
A) PchB (PDB 3REM) functional dimer has 2 active sites, indicated by pyruvate and SA molecules, and displays an α-helical structure. CM1 (PDB 4PPV) monomer has 1 active site, indicated by red asterisk. Purple residues are involved in binding to allosteric effectors; red is G213, a residue critical for allosteric modulation. **B)** Active sites of PchB and CM1 are aligned and residue identity is labeled for CM1, while corresponding PchB residue is in parentheses. **C)** CM1 associates as a dimer, creating an interface where 2 allosteric binding domains are formed, indicated by purple and red residues, with bound phenylalanine.

8

favored than non-enzymatic formation of 3-carboxy-phenylpyruvate (DeClue et al., 2006). Strawn *et al.* determined that *in vitro* under plastid conditions isochorismate decomposition to SA does not occur at a rate sufficient to explain induced SA synthesis. As such, we turned to reverse genetics to identify candidate IPL proteins in *Arabidopsis* informed by the example of PchB. Could a CM protein have convergently evolved promiscuous IPL activity in *Arabidopsis*?

Three AroQ chorismate mutases have been identified in the *Arabidopsis* genome; computational prediction localizes CM1 and CM3 to the plastid, where SA biosynthesis occurs, and CM2 to the cytosol. Phylogenetic analysis reveals that dicots broadly have several copies of putative plastidic CM genes, a condition in which functional redundancy lessens selection pressure and mutation-driven diversification of function is possible (Weng et al., 2012; Tohge et al., 2013). CM1 is transcriptionally responsive to both bacterial and fungal pathogens, and CM2 maintains constant low expression, while the effects on CM3 is less clear (Eberhard et al., 1996; Mobley et al., 1999). Initially reported kinetic parameters suggested that CM1 had a 10-fold higher K_m for chorismate (2.9 mM for CM1, 0.42 mM for CM3), although subsequent work by (Westfall et al., 2014) did not confirm that pattern. I also characterized the kinetics of CM1 and CM3, and this is discussed in more detail in Chapter 2. Preliminary experiments on recombinant CM1, CM2 and CM3 indicated that CM1 possessed low IPL activity *in vitro* (Strawn, 2010).

Crystal Structure Analysis of PchB and CM1

Although overall structural similarity is not predictive of exact chorismate-utilizing activity, structural models can be useful to determine conservation of key catalytic residues and additional potential insights into enzyme function. At the time, crystal structures were not solved for any of the *Arabidopsis* CMs, and it was unknown what degree of structural similarity plant CMs share to those of bacteria. I performed structural protein homology modeling using the predictive software Protein Homology/analogY Recognition Engine (Phyre2) (Kelly et al., 2015) to produce a likely model for CM1 structure. CM1 amino acids 78-340 were aligned to the chorismate mutase from *Saccharomyces cerevisiae* (ScCM, PBD: 5CSM) with 100% confidence (Fig 1.3A) and this homology model was used until the crystal structure for CM1 was published (Westfall et al., 2014). The CM1 monomer is comprised of 8 α-helical regions connected via disordered loops in an arrangement similar to the PchB functional dimer of 6 α-helices (Fig. 1.2A), with some modification. The CM1 monomer has a highly conserved active site (3 of 4 residues) with ScCM, which has one active site per protein (Strater et al., 1996); by contrast bacterial PchB and *E. coli* CMs have 2 active sites that form when the proteins dimerize (Zaitseva et al., 2006). Homology modeling of CM3 with Phyre2 also used the ScCM model.

Next, I used the software UCSF Chimera (Pettersen et al., 2004) to align the published structure of PchB co-crystallized with SA and pyruvate in its active sites (PDB: 3REM, (Olucha et al., 2011)) onto the CM1 structure. One monomer of PchB could be matched to the C-terminal region of CM1, which shared just 16% sequence similarity. Residues of the overlapping CM1 and PchB active site are shown in Fig. 1.3B. Of the five residues that make up the active site of PchB, three are completely conserved with CM1, while Arg53 of PchB corresponds to Val269 in CM1. The final residue PchB Arg14 is located on the second monomer, which was not modeled due to poor overall alignment. Active site residues between CM1 and CM3 are invariant, and are not shown modeled separately. These results show the active site residues between PchB and the plastidic *Arabidopsis* CMs are partially conserved, including Lys42, which has been shown to be important for PchB's IPL activity (Olucha et al., 2011).
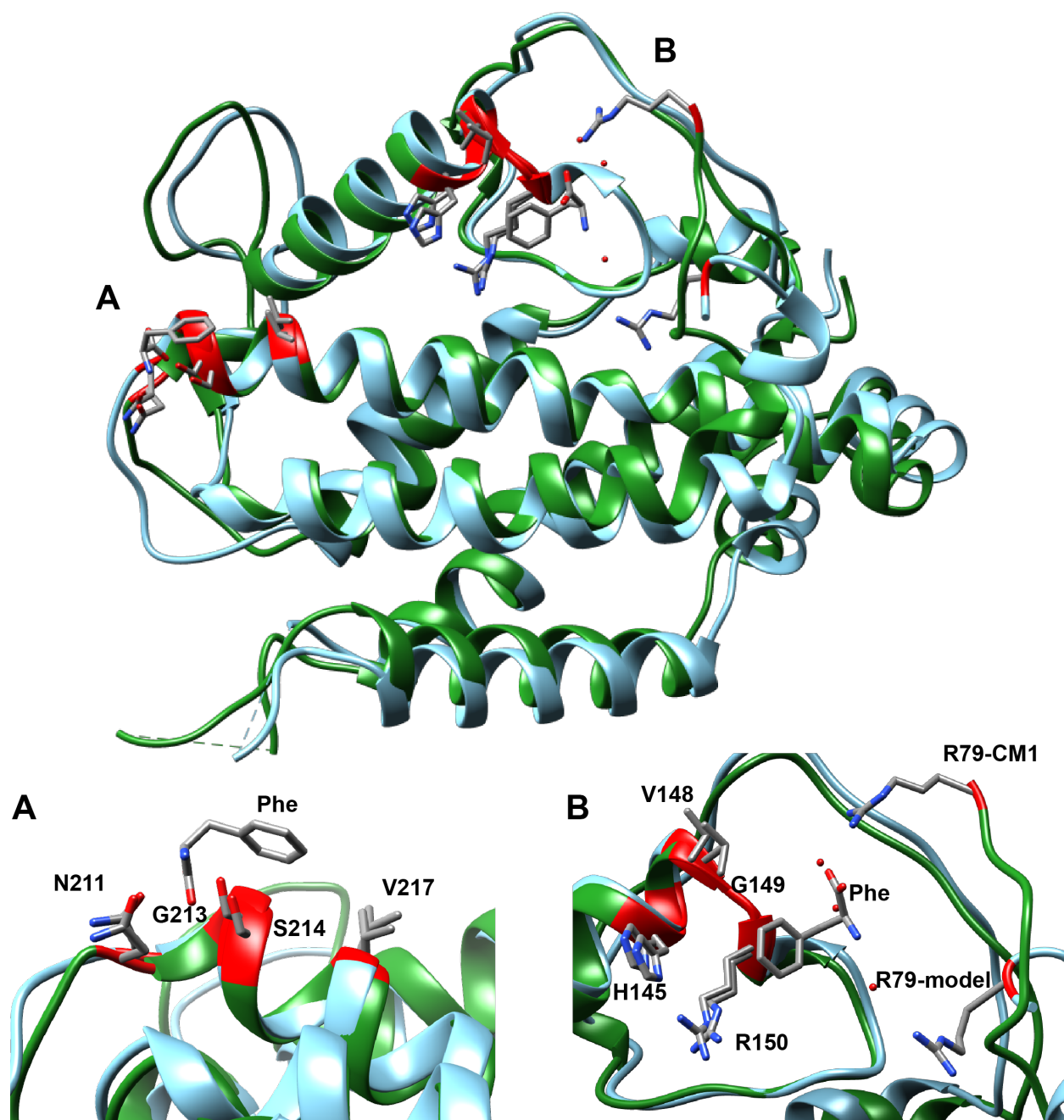
Figure 1.4: Comparison of Phyre2 homology model to CM1 crystal structure with allosteric effector binding residues
Phyre2 generated homology model of CM1 using (PDB 5CSM) in teal is overlaid with experimentally derived CM1 (PDB 4PPV) in green. Predicted binding residues for the allosteric effector phenylalanine overlap, with the exception of R79, which was predicted away from the binding domain.

Allosteric regulation of chorismate mutase activity by aromatic amino acids

Homology modeling to ScCM provided insight on mechanisms of CM1 allosteric regulation by aromatic amino acids, to which PchB is largely insensitive (Gaille et al., 2002). As chorismate is the common precursor to several primary metabolites, organisms have evolved mechanisms to effectively partition it among chorismate-utilizing enzymes. Genes encoding enzymes can be transcriptionally regulated, so that enzyme abundance is responsive to specific conditions, as seen for *ICS1*, or subject to post-translational regulation via allosteric modulation of protein activity. In plants, putative plastidic CM isoforms are responsive to several amino acid allosteric effectors, while the cytosolic CM is insensitive to regulation. CM1 and 3 expressed in yeast extracts exhibited increased activity in the presence of 1 mM tryptophan, and both exhibited a reduction in the presence of phenylalanine and tyrosine, which are downstream metabolites of the CM reaction product prephenate (Eberhard et al., 1996; Mobley et al., 1999). However, subsequent screening of amino acids on purified recombinant CM3 protein by (Westfall et al., 2014) did not find CM3 to be inhibited by phenylalanine or tyrosine at concentrations up to 3.2 mM (Westfall et al., 2014). CM3 exhibited positive allosteric regulation by tryptophan, which increases activity 6-fold, and unexpectedly, cysteine and histidine, which increase activity 3-fold. CM1 exhibited similar activity to previously published results.

The allosteric regulation of ScCM is well studied, and as the proteins are predicted to be structurally similar, ScCM served to inform the mechanism of *Arabidopsis* CM allostery. As shown in Figure 1.3C, CM1 monomers associate along an interface, and residues from each monomer contribute to form two allosteric binding sites, as for ScCM (Strater et al., 1996; Sträter et al., 1997). Both allosteric effectors tryptophan and tyrosine bind to this region in ScCM, causing a 15˚ rotation of the catalytic domains in the active site to enhance or hinder activity, shifting from a relaxed "R" state to a closed "T" state. I identified the corresponding effector binding residues in CM1 as targets for modulating protein activity based on structural alignment, and Westfall *et al*. elaborated on additional residues when publishing the CM1 crystal structure co-crystallized with phenylalanine or tyrosine in the effector binding domain (Fig. 1.4). To examine the accuracy of my Phyre2-generated model, I aligned it to the published CM1 (PBD: 4PPV) and the positions of allosteric binding sites were compared. All residues were accurately positioned with the exception of Arg79, which sits on a disordered loop and is closer to the bound phenylalanine than its predicted position. Mutating the Gly213 position to either alanine or proline abrogated allosteric modulation (Westfall et al., 2014). I use the mutant isoform G213A in Chapter 2 to examine *in planta* activity of CM1 without allosteric inhibition.

Conclusions

In this dissertation, I describe my work to elucidate the governing mechanisms of SA biosynthesis. In Chapter 2, I demonstrate that none of the CM proteins exhibit *in vitro* IPL activity, nor function as an IPL in transient *in planta* expression assays. Instead, genetic knockdowns in *CM1* exhibit elevated pre-infection SA accumulation, which enhanced disease resistance to virulent bacterial pathogens. Alteration of *CM1* expression likely upsets chorismate dynamics to enhance isochorismate synthesis via ICS1 in the uninduced state. The effect largely disappears under robust induced SA synthesis and therefore the enhanced resistance effect of *cm1* silencing likely occurs in the early stages of infection. I identified that expression of SA-related defense response genes are more highly expressed in *cm1#1* upon infection, thus this elevated pre-infection SA primes a quicker response.

Similarly, Chapter 3 details the role the transcriptional repressor DEL1 plays to limit SA synthesis in developing tissue by reducing expression of the SA transporter *EDS5*. *Del1* mutant plants display elevated levels of basal SA that activates gene expression of *ICS1* and *PR-1* in the absence of an inducing agent, thereby enhancing disease resistance, but at a fitness cost to the plant that results in reduced size. In this way, CM1 and DEL1 mutant plants represent a continuum of low-level defense priming by augmenting endogenous SA, and illustrate new approaches for modulating increased disease resistance in plants through influencing metabolic flux of chorismate products. This parallels pathogenic strategies employed by diverse microbes and pests that secrete effectors to manipulate chorismate metabolism, discussed in Chapter 4.

REFERENCES

Achnine L, Blancaflor EB, Rasmussen S, Dixon RA (2004) Colocalization of L-Phenylalanine Ammonia-Lyase and Cinnamate 4-Hydroxylase for Metabolic Channeling in Phenylpropanoid Biosynthesis. Plant Cell **16**: 3098–3109

An C, Mou Z (2011) Salicylic Acid and its Function in Plant Immunity. J Integr Plant Biol **53**: 412–428

Bigeard J, Colcombet J, Hirt H (2015) Signaling mechanisms in pattern-triggered immunity (PTI). Mol Plant **8**: 521–539

Catinot J, Buchala A, Abou-Mansour E, Métraux J-P (2008) Salicylic acid production in response to biotic and abiotic stress depends on isochorismate in *Nicotiana benthamiana*. FEBS Lett **582**: 473–478

Cochrane FC, Davin LB, Lewis NG (2004) The Arabidopsis phenylalanine ammonia lyase gene family: Kinetic characterization of the four PAL isoforms. Phytochemistry **65**: 1557–1564

Cox CD, Rinehart KL, Moore ML, Cook JC (1981) Pyochelin: novel structure of an iron-chelating growth promoter for Pseudomonas aeruginosa. Proc Natl Acad Sci U S A **78**: 4256–4260

Dean J V., Delaney SP (2008) Metabolism of salicylic acid in wild-type, ugt74f1 and ugt74f2 glucosyltransferase mutants of Arabidopsis thaliana. Physiol Plant **132**: 417–425

DeClue MS, Baldridge KK, Kast P, Hilvert D (2006) Experimental and computational investigation of the uncatalyzed rearrangement and elimination reactions of isochorismate. J Am Chem Soc **128**: 2043–2051

Dempsey DA, Vlot AC, Wildermuth MC, Klessig DF (2011) Salicylic Acid Biosynthesis and Metabolism. Arab B **9**: e0156

Dewdney J, Lynne Reuber T, Wildermuth MC, Devoto A, Cui J, Stutius LM, Drummond EP, Ausubel FM (2000) Three unique mutants of Arabidopsis identify eds loci required for limiting growth of a biotrophic fungal pathogen. Plant J **24**: 205–218

Eberhard J, Ehrler TT, Epple P, Felix G, Raesecke H-R, Amrhein N, Schmid J (1996) Cytosolic and plastidic chorismate mutase isozymes from *Arabidopsis thaliana*: molecular characterization and enzymatic properties. Plant J **10**: 815–821

El-Basyouni SZ, Chen D, Ibrahim RK, Neish AC, Towers GHN (1964) The Biosynthesis of Hydroxybenzoic Acids in Higher Plants. Phytochemistry **3**: 485–492

Fu ZQ, Dong X (2013) Systemic Acquired Resistance: Turning Local Infection into Global Defense. Annu Rev Plant Biol **64**: 839–863

Fu ZQ, Yan S, Saleh A, Wang W, Ruble J, Oka N, Mohan R, Spoel SH, Tada Y, Zheng N, et al (2012) NPR3 and NPR4 are receptors for the immune signal salicylic acid in plants. Nature. doi: 10.1038/nature11162

Gaille C, Kast P, Dieter H (2002) Salicylate biosynthesis in Pseudomonas aeruginosa. Purification and characterization of PchB, a novel bifunctional enzyme displaying isochorismate pyruvate-lyase and chorismate mutase activities. J Biol Chem **277**: 21768–21775

Garcion C, Lohmann A, Lamodiere E, Catinot J, Buchala A, Doermann P, Metraux J-P (2008) Characterization and Biological Function of the ISOCHORISMATE SYNTHASE2 Gene of Arabidopsis. Plant Physiol **147**: 1279–1287

George Thompson AM, Iancu C V., Neet KE, Dean J V., Choe J (2017) Differences in salicylic acid glucose conjugations by UGT74F1 and UGT74F2 from Arabidopsis thaliana. Sci Rep **7**: 46629

Huang J, Gu M, Lai Z, Fan B, Shi K, Zhou Y-H, Yu J-Q, Chen Z (2010) Functional Analysis of the Arabidopsis PAL Gene Family in Plant Growth, Development, and Response to Environmental Stress. Plant Physiol **153**: 1526–1538

Jones JDG, Dangl JL (2006) The plant immune system. Nature **444**: 323–329

Kelly LA, Mezulis S, Yates C, Wass M, Sternberg M (2015) The Phyre2 web portal for protein modelling, prediction, and analysis. Nat Protoc **10**: 845–858

Kerbarh O, Ciulli A, Howard NI, Abell C (2005) Salicylate biosynthesis: Overexpression, purification, and characterization of Irp9, a bifunctional salicylate synthase from Yersinia enterocolitica. J Bacteriol **187**: 5061–5066

Künzler DE, Sasso S, Gamper M, Hilvert D, Kast P (2005) Mechanistic insights into the isochorismate pyruvate lyase activity of the catalytically promiscuous PchB from combinatorial mutagenesis and selection. J Biol Chem **280**: 32827–32834

Lamb AL (2011) Pericyclic reactions catalyzed by chorismate-utilizing enzymes. Biochemistry **50**: 7476–7483

León J, Shulaev V, Yalpani N, Raskin L, Lawton MA (1995) lnduction of Benzoic Acid 2-Hydroxylase in Virus-lnoculated Tobacco. PLANT Physiol **92**: 10413–10417

León J, Yalpani N, Raskin L, Lawton MA (1993) lnduction of Benzoic Acid 2-Hydroxylase in Virus-lnoculated Tobacco'. Plant Physiol **103**: 323–328

Li J, Last RL (1996) The Arabidopsis thaliana trp5 Mutant Has a Feedback-Resistant Anthranilate Synthase and Elevated Soluble Tryptophan. Plant Physiol **110**: 51–59

Luo Q, Olucha J, Lamb AL (2009) Structure-function analyses of isochorismate-pyruvate lyase from Pseudomonas aeruginosa suggest differing catalytic mechanisms for the two pericyclic reactions of this bifunctional enzyme. Biochemistry **48**: 5239–5245

Macaulay KM, Heath GA, Ciulli A, Murphy AM, Abell C, Carr JP, Smith AG (2017) The biochemical properties of the two *Arabidopsis thaliana* isochorismate synthases. Biochem J **474**: 1579–1590

Mauch-Mani B, Slusarenko AJ (1996) Production of Salicylic Acid Precursors Is a Major Function of Phenylalanine Ammonia-Lyase in the Resistance of Arabidopsis to Peronospora parasitica. Plant Cell **8**: 203–212

Mauch F, Mauch-Mani B, Gaille C, Kull B, Haas D, Reimmann C (2001) Manipulation of salicylate content in Arabidopsis thaliana by the expression of an engineered bacterial salicylate. Plant J **25**: 67–77

Meneely KM, Luo Q, Lamb AL (2013) Redesign of MST enzymes to target lyase activity instead promotes mutase and dehydratase activities. Arch Biochem Biophys **539**: 70–80

Meneely KM, Sundlov JA, Gulick AM, Moran GR, Lamb AL (2016) An Open and Shut Case: The Interaction of Magnesium with MST Enzymes. J Am Chem Soc **138**: 9277–9293

Mercado-Blanco J, Van Der Drift KMGM, Olsson PE, Thomas-Oates JE, Van Loon LC, Bakker PAHM (2001) Analysis of the pmsCEAB gene cluster involved in biosynthesis of salicylic acid and the siderophore pseudomonine in the biocontrol strain Pseudomonas fluorescens WCS374. J Bacteriol **183**: 1909–1920

Meuwly P, Mölders W, Buchala A, Métraux J (1995) Transport of Salicylic Acid in Tobacco Necrosis Virus-Infected Cucumber Plants. Plant Physiol **109**: 1107–1114

Mobley EM, Kunkel BN, Keith B (1999) Identification, characterization and comparative analysis of a novel chorismate mutase gene in Arabidopsis thaliana. Gene **240**: 115–123

Mou Z, Fan W, Dong X (2003) Inducers of plant systemic acquired resistance Regulate NPR1 function through redox changes. Cell **113**: 935–944

Mustafa NR, Kim HK, Choi YH, Erkelens C, Lefeber AWM, Spijksma G, Heijden R van der, Verpoorte R (2009) Biosynthesis of salicylic acid in fungus elicited Catharanthus roseus cells. Phytochemistry **70**: 532–539

Nawrath C (2002) EDS5, an Essential Component of Salicylic Acid-Dependent Signaling for Disease Resistance in Arabidopsis, Is a Member of the MATE Transporter Family. Plant Cell Online **14**: 275–286

Nawrath C., Metraux J-P (1999) Salicylic Acid InductionDeficient Mutants of Arabidopsis Express PR-2 and PR-5 and Accumulate High Levels of Camalexin after Pathogen Inoculation. Plant Cell Online **11**: 1393–1404

Olsen KM, Lea US, Slimestad R, Verheul M, Lillo C (2008) Differential expression of four Arabidopsis PAL genes; PAL1 and PAL2 have functional specialization in abiotic environmental-triggered flavonoid synthesis. J Plant Physiol **165**: 1491–1499

Olucha J, Ouellette AN, Luo Q, Lamb AL (2011) PH dependence of catalysis by pseudomonas aeruginosa isochorismate - Pyruvate lyase: Implications for transition state stabilization and the role

of lysine 42. Biochemistry **50**: 7198–7207

Pelludat C, Brem D, Heesemann J (2003) Irp9, encoded by the high-pathogenicity island of Yersinia enterocolitica, is able to convert chorismate into salicylate, the precursor of the siderophore yersiniabactin. J Bacteriol **185**: 5648–5653

Pettersen EF, Goddard TD, Huang CC, Couch GS, Greenblatt DM, Meng EC, Ferrin TE (2004) UCSF Chimera - A visualization system for exploratory research and analysis. J Comput Chem **25**: 1605–1612

Rivas-San Vicente M, Plasencia J (2011) Salicylic acid beyond defence: Its role in plant growth and development. J Exp Bot **62**: 3321–3338

Serino L, Reimmann C, Baur H, Beyeler M, Visca P, Haas D (1995) Structural genes for salicylate biosynthesis from chorismate in Pseudomonas aeruginosa. Mgg Mol Gen Genet **249**: 217–228

Serrano M, Wang B, Aryal B, Garcion C, Abou-Mansour E, Heck S, Geisler M, Mauch F, Nawrath C, Metraux J-P (2013) Export of Salicylic Acid from the Chloroplast Requires the Multidrug and Toxin Extrusion-Like Transporter EDS5. Plant Physiol **162**: 1815–1821

Seyfferth C, Tsuda K (2014) Salicylic acid signal transduction: the initiation of biosynthesis, perception and transcriptional reprogramming. Front Plant Sci **5**: 1–10

Shine MB, Yang JW, El-Habbak M, Nagyabhyru P, Fu DQ, Navarre D, Ghabrial S, Kachroo P, Kachroo A (2016) Cooperative functioning between phenylalanine ammonia lyase and isochorismate synthase activities contributes to salicylic acid biosynthesis in soybean. New Phytol **212**: 627–636

Silverman P, Seskar M, Kanter D, Schweizer P, Metraux JP, Raskin I (1995) Salicylic Acid in Rice (Biosynthesis, Conjugation, and Possible Role). Plant Physiol **108**: 633–639

Spoel SH, Mou Z, Tada Y, Spivey NW, Genschik P, Dong X (2009) Proteasome-Mediated Turnover of the Transcription Coactivator NPR1 Plays Dual Roles in Regulating Plant Immunity. Cell **137**: 860–872

Sridharan S, Howard N, Kerbarh O, Błaszczyk M, Abell C, Blundell TL (2010) Crystal Structure of Escherichia coli Enterobactin-specific Isochorismate Synthase (EntC) Bound to its Reaction Product Isochorismate: Implications for the Enzyme Mechanism and Differential Activity of Chorismate-utilizing Enzymes. J Mol Biol **397**: 290–300

Strater N, Hakansson K, Schnappauf G, Braus G, Lipscomb WN (1996) Crystal structure of the T state of allosteric yeast chorismate mutase and comparison with the R state. Proc Natl Acad Sci U S A **93**: 3330–3334

Sträter N, Schnappauf G, Braus G, Lipscomb WN (1997) Mechanisms of catalysis and allosteric regulation of yeast chorismate mutase from crystal structures. Structure **5**: 1437–1452

Strawn MA (2010) Isochorismate Synthase Enzymes in Arabidopsis.

Strawn MA, Marr SK, Inoue K, Inada N, Zubieta C, Wildermuth MC (2007) Arabidopsis isochorismate synthase functional in pathogen-induced salicylate biosynthesis exhibits properties consistent with a role in diverse stress responses. J Biol Chem **282**: 5919–5933

Sun T, Li Y, Zhang Q, Ding Y, Zhang Y, Zhang Y (2015) ChIP-seq reveals broad roles of SARD1 and CBP60g in regulating plant immunity. Nat Commun. doi: 10.1038/ncomms10159

Tohge T, Watanabe M, Hoefgen R, Fernie AR (2013) Shikimate and Phenylalanine Biosynthesis in the Green Lineage. Front Plant Sci **4**: 1–13

Uppalapati SR, Ishiga Y, Wangdi T, Kunkel BN, Anand A, Mysore KS, Bender CL (2007) The phytotoxin coronatine contributes to pathogen fitness and is required for suppression of salicylic acid accumulation in tomato inoculated with Pseudomonas syringae pv. tomato DC3000. Mol Plant Microbe Interact **20**: 955–965

Vlot AC, Dempsey DA, Klessig DF (2009) Salicylic Acid, a Multifaceted Hormone to Combat Disease. Annu Rev Phytopathol **47**: 177–206

De Voss JJ, Rutter K, Schroeder BG, Su H, Zhu Y, Barry CE (2000) The salicylate-derived mycobactin siderophores of Mycobacterium tuberculosis are essential for growth in macrophages. Proc Natl Acad Sci U S A **97**: 1252–1257

Weng J-K, Philippe RN, Noel JP (2012) The Rise of Chemodiversity in Plants. Science (80-) **336**: 1667–1670

Westfall CS, Xu A, Jez JM (2014) Structural evolution of differential amino acid effector regulation in plant chorismate mutases. J Biol Chem **289**: 28619–28628

Widhalm JR, Gutensohn M, Yoo H, Adebesin F, Qian Y, Guo L, Jaini R, Lynch JH, McCoy RM, Shreve JT, et al (2015) Identification of a plastidial phenylalanine exporter that influences flux distribution through the phenylalanine biosynthetic network. Nat Commun **6**: 8142

Wildermuth MC, Dewdney J, Wu G, Ausubel FM (2001) Isochorismate synthase is required to synthesize salicylic acid for plant defence. Nature **414**: 564–571

Wu Y, Zhang D, Chu JY, Boyle P, Wang Y, Brindle ID, De Luca V, Després C (2012) The Arabidopsis NPR1 Protein Is a Receptor for the Plant Defense Hormone Salicylic Acid. Cell Rep **1**: 639–647

Yalpani N, Leon J, Lawton MA, Raskin I (1993) Pathway of Salicylic Acid Biosynthesis in Healthy and Virus-Inoculated Tobacco. Plant Physiol **103**: 315–321

Yamasaki K, Motomura Y, Yagi Y, Nomura H, Kikuchi S, Nakai M, Shiina T (2013) Chloroplast envelope localization of EDS5, an essential factor for salicylic acid biosynthesis in *Arabidopsis thaliana*. Plant Signal Behav **8**: e23603

Yuan Y, Chung J-D, Fu X, Johnson VE, Ranjan P, Booth SL, Harding SA, Tsai C-J (2009) Alternative splicing and gene duplication differentially shaped the regulation of isochorismate synthase in Populus and Arabidopsis. Proc Natl Acad Sci U S A **106**: 22020–22025

Zaitseva J, Lu J, Olechoski KL, Lamb AL (2006) Two crystal structures of the isochorismate pyruvate lyase from Pseudomonas aeruginosa. J Biol Chem **281**: 33441–33449

Zhang X, Chen S, Mou Z (2010) Nuclear localization of NPR1 is required for regulation of salicylate tolerance, isochorismate synthase 1 expression and salicylate accumulation in Arabidopsis. J Plant Physiol **167**: 144–148

Zheng X, Zhou M, Yoo H, Pruneda-Paz JL, Spivey NW, Kay SA, Dong X (2015) Spatial and temporal regulation of biosynthesis of the plant immune signal salicylic acid. Proc Natl Acad Sci **112**: 9166–9173

CHAPTER 2: Plastidic chorismate mutases mediate substrate availability for salicylate synthesis in *Arabidopsis thaliana*

SUMMARY

The hormone salicylate is a key plant immune regulator whose synthesis is induced in response to biotic stress. In *Arabidopsis*, SA synthesis occurs predominantly in the chloroplast via ICS1, which acts at equilibrium to convert the central metabolite chorismate into isochorismate; isochorismate is subsequently converted to SA through an undetermined route. The bacteria *Pseudomonas aeruginosa* produces SA from isochorismate using an isochorismate pyruvate lyase (IPL) that evolved from a chorismate mutase (CM), and still retains low CM activity. *Arabidopsis* contains three CMs, two of which I confirmed are localized to the plastid. Biochemical kinetic assays show CM1 and CM3 exhibit chorismate mutase activity to convert chorismate to prephenate, with K_ms for chorismate of 650 µM and 1,450 µM, respectively. Despite structural similarity with PchB, neither *Arabidopsis* CM exhibited IPL activity *in vitro*, and transient *in planta* expression of these enzymes alone or with ICS1 did not result in increased SA accumulation. Instead, CM1 and CM3 behave more similarly to the yeast AroQ CM, which forms a dimeric complex that can be allosterically regulated by aromatic amino acids. Transient expression of allosteric mutant CM1 G213A or CM3 paired with ICS1 showed reduced SA accumulation *in planta*, suggesting these enzymes redirected chorismate flux away from SA synthesis. Consistent with this hypothesis, knockdown lines with dramatically reduced *CM1* expression exhibited elevated basal SA and showed enhanced resistance to the hemibiotrophic pathogen *Pseudomonas syringae pv maculicola,* whose growth is typically limited by SA-mediated responses. Despite elevated SA, *CM1* knockdown plant lines were similar in size to WT and did not exhibit basal expression of defense genes. Analysis of expression at early infection time points indicate rapid differential activation of MPK3 signaling in the *CM1* knockdown line, suggesting this confers enhanced resistance. These results further elucidate mechanisms governing SA synthesis, and highlight modulation of CM enzymes as an important mechanism for engineering enhanced disease resistance without a growth consequence.

Abbreviations
Enzymes: CM- chorismate mutase; IPL- isochorismate pyruvate lyase; ICS- isochorismate synthase; AS- anthranilate synthase; ADCS- aminodeoxychorismate synthase; PAL- phenylalanine ammonia lyase; DAHPS- 3-deoxy-d-arabino-heptulosonate-7-phosphate synthase
Genes: *ICS1- isochorismate synthase (sid2/eds16-1); EDS5- enhanced disease susceptibility 5 (sid1/eds5); CM1- chorismate mutase 1; CM2- chorismate mutase 2; CM3- chorismate mutase 3; ASA1- anthranilate synthase alpha unit 1; SSI2- suppressor of SA insensitive 2; CPR1- constitutive expresser of PR genes 1; CPR5- constitutive expresser of PR genes 5; DEL1- DP-E2F-Like 1; MAPK3- mitogen activated protein kinase 3; MAPK6- mitogen activated protein kinase 6; WRKY33- WRKY DNA-binding protein 33; CIM6- constitutive immunity 6; FLS2- flagellin sensitive 2; RBOHD- respiratory burst oxidase homologue D.*
Organisms*: Pma ES4326- Pseudomonas syringae pv maculicola ES4326; G. orontii- Golovinomyces orontii* (formerly *Erisyphe orontii).*
Terminology: CFU- colony-forming units; PAMP- pathogen associated molecular pattern; PTI- pattern triggered immunity, ROS- reactive oxygen species

INTRODUCTION

The hormone salicylic acid (SA) mediates plant responses to abiotic stresses (Rivas-San Vicente and Plasencia, 2011) and (hemi)biotrophic pathogens like foliar bacterial, oomycete and fungal pathogens. Unlike many other phytohormones, our knowledge of SA biosynthesis in *Arabidopsis* remains incomplete. As discussed in Chapter 1, two pathways for induced SA synthesis have been proposed, one using the amino acid phenylalanine as a precursor and one that utilizes the central metabolite chorismate. In *Arabidopsis,* SA is made via isochorismate (Wildermuth el al 2001, Garcion et al. 2008). Despite the discovery sixteen years ago that the *sid2/eds16* alleles correspond to *ICS1*, an isochorismate synthase that utilizes chorismate in the plastid (Chapter 1), there has been no subsequent identification of an additional biosynthetic enzyme that performs the predicted isochorismate pyruvate lyase (IPL) activity.

Chorismate is the end product of the shikimate pathway and is a central branch point for synthesis of aromatic amino acids, which are precursors for the hormone auxin, important phenylpropanoids like the cell wall component lignin, and a wide variety of specialized secondary metabolites to mediate stress and defense against pests and pathogens (Tzin and Galili, 2010; Maeda and Dudareva, 2012). Four types of enzymes compete for chorismate utilization in *Arabidopsis*: chorismate mutase (CM), isochorismate synthase (ICS), anthranilate synthase (AS) and aminodeoxychorismate synthase (ADCS) (Fig 2.1). Metabolite flux through the pathway is tightly controlled through allosteric regulation; CM1 activity can be influenced by aromatic amino acids from both branches and thus balances chorismate allocation between synthesis of tryptophan, which positively influences CM1 activity, and phenylalanine and tyrosine, two downstream reaction products that can reduce CM1 activity (Westfall et al., 2014). Another isoform, CM3, is only susceptible to positive allosteric regulation by additional amino acids. Tryptophan acts as a negative regulator of ASA1, and downstream accumulation of tryptophan restrains AS activity (Li and Last, 1996). ICS1 functions at equilibrium to catalyze the reversible conversion of chorismate to isochorismate, and thus chorismate concentration controls the availability of isochorismate.

In the bacteria *Pseudomonas aeruginosa*, the bacterial IPL PchB also exhibits low-level CM activity and shares structural homology to the AroQ class of CM enzymes (Gaille et al., 2002; Zaitseva et al., 2006). Both IPL and CM activities proceed via a rare pericyclic reaction mechanism and occur at the same active site (Lamb, 2011). The three *Arabidopsis* CMs share a degree of structural homology with PchB (Chapter 1). As CM1 exhibited low levels of IPL activity in preliminary results (Strawn, 2010), we hypothesized one or more plastidic CMs might have convergently evolved IPL activity to catalyze the formation of SA.

RESULTS
CM1 and CM3 are plastid-localized proteins

Much of cellular biochemistry is compartmentalized into subcellular locations where chemical conditions and local maxima of substrate concentrations can be tailored for optimal biochemical activity. While PAL enzymes are presumably localized to the cytosol, experimental evidence demonstrates quite strongly that SA biosynthesis in *Arabidopsis* occurs in the chloroplast. Bacterial ICS and IPL transgenes fused with chloroplast signal peptides increased total SA production 10-fold relative to those transgenes targeted to the cytosol in *Arabidopsis* (Mauch et al., 2001) and tobacco (Verberne et al., 2000) SA-overproducing lines. Strawn *et al*. demonstrated ICS1 is imported into the chloroplast, where it is processed into its mature form. The chloroplast membrane-localized protein EDS5, a Multidrug and Toxin Extrusion-like
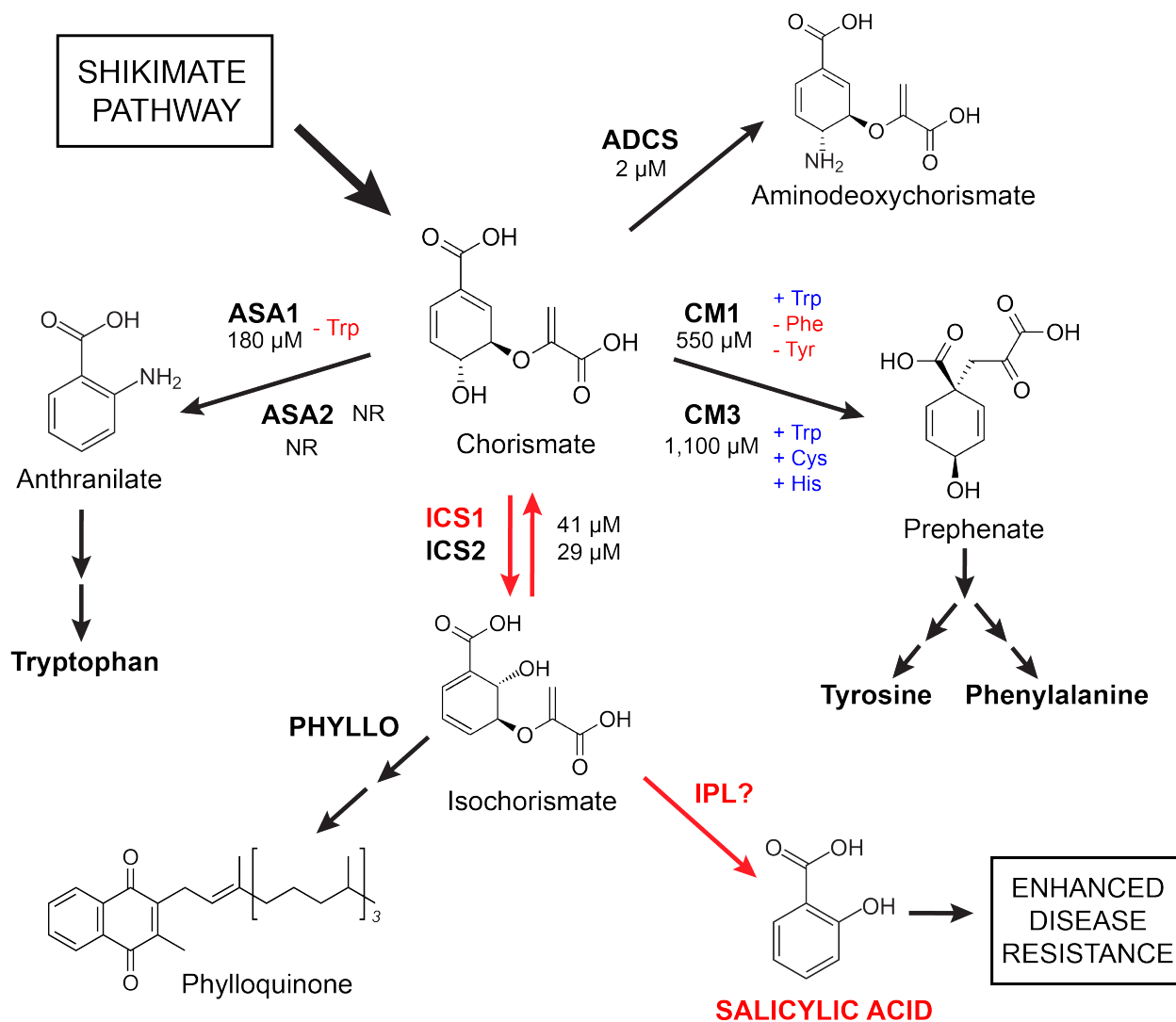
Figure 2.1: Chorismate-utilizing enzymes and salicylic acid biosynthesis in *Arabidopsis*
Chorismate serves as a branching point for synthesis of aromatic amino acids, phylloquinone and salicylic acid, among others. Published K_m values of each enzyme for chorismate are indicated in black: ASA1 (At5g05730; Bernasconi et al., 1994), CM1 and CM3 (At3g29200, At1g69370; Westfall et al., 2014) ICS1 (At1g74710; Strawn et al., 2007), ICS2 (At1g18870; Macaulay et al., 2017), ADCS (At2g28880; Sahr et al., 2006). Allosteric regulation of chorismate-utilizing enzymes by indicated amino acids is marked in either blue (increase in enzyme activity) or red (decrease in enzyme activity). The route for induced salicylic acid biosynthesis is marked with red arrows, and reactions with multiple steps are indicated by double arrows. An IPL enzyme is hypothesized to perform final conversion of isochorismate to chorismate, but has not been identified in *Arabidopsis*. Induced defense compounds, including camalexin and phenylpropanoids are derived from aromatic amino acids (not shown). NR= value not reported.

transporter, specifically exports SA from the chloroplast and is required for robust total SA accumulation (Nawrath, 2002; Serrano et al., 2013; Yamasaki et al., 2013), presumably due to product inhibition in mutant lines. Therefore, any isochorismate pyruvate lyase would likely be plastid localized.

The three Arabidopsis CM proteins show high sequence similarity and many conserved active site residues between them, and to the CM enzyme from *Saccharomyces cerevisiae* (ScCM) (Westfall et al., 2014). However, the N-terminal sequences of both CM1 and CM3 contain additional residues that do not align to the N-termini of CM2 or ScCM. The software TargetP (Emanuelsson et al., 1999; Emanuelsson et al., 2007), was used to predict that CM1 and CM3 contain putative chloroplast transit peptides that are cleaved after residues Arg58, and Arg 47, respectively (seen in Fig. 2.9). CM2 does not contain a putative transit peptide, making it an unlikely candidate as an IPL, and it was not tested. To validate that these proteins localize to the plastid, I transiently expressed *ICS1*, *CM1* and *CM3* fused to c-terminal eCFP driven by the constitutive CaMV 35S promoter in *Nicotiana benthamiana* and examined protein localization by confocal microscopy (Fig 2.2). Chlorophyll autofluorescence served as a marker for the plastid. Consistent with results in (Strawn et al., 2007; Garcion et al., 2008), ICS1::CFP is visible in the plastids of both mesophyll and epidermal cells 48 hours after agroinfiltration. Similarly, both CM1::CFP and CM3::CFP are visible in the chloroplasts. Fluorescent fusion proteins are also visible in stromules, tubular projections of the chloroplast stroma that can be induced by either chloroplast redox conditions or *Agrobacterium* GV3101 (data not shown) (Erickson et al., 2014; Brunkard et al., 2015). These results taken together demonstrate that CM1 and CM3 localize to the stroma of the chloroplast.

Purification and kinetic characterization of CM1 and CM3

Based on structural similarity to the bacterial IPL PchB (Chapter 1), we hypothesized that CM1 or CM3 might possess IPL activity. CM1 and CM3 have previously been shown to exhibit CM activity *in vitro* with recombinant protein purified from yeast (Mobley et al., 1999) and *Escherichia coli* (Eberhard et al., 1996b; Westfall et al., 2014) However, the kinetic parameters of these enzymes reported in the literature vary, with the K_m for chorismate of CM1 and CM3 varying 6- and 3- fold, respectively. Concurrent with (Westfall et al., 2014), I purified CM1 and CM3 protein lacking the predicted chloroplast signal peptide amino acid residues (Figure 2.3) and determined each enzyme's kinetic activity on chorismate with *in vitro* spectrophotometric assays. Velocity versus substrate curves were generated for CM1 and CM3 (Figure 2.4A,B). CM1 was fit to the Michaelis-Menten equation and its V_{max} and K_m were calculated using Prism 7 (GraphPad). CM3 was fitted via an allosteric sigmoidal curve. The enzymes exhibit similar kinetic activity to that reported in (Westfall et al., 2014); I found CM1 exhibits an average K_m of 650 μM, and CM3 exhibits a K_m of 1,450 μM for chorismate, compared to 550 μM and 1,100 μM, respectively in (Westfall et al., 2014). The maximal activity is similar for both proteins, though I found my enzymes had lower V_{max} than reported in (Westfall et al., 2014), likely due to variation in the protein preparations. Recombinant PchB (Strawn et al., 2007) is also functional on chorismate (Figure 2.4C) at much lower V_{max}, and displays a K_m of 95 μM for chorismate, similar to that reported in (Gaille et al., 2002), who found a K_m for chorismate of 150 μM. These results demonstrate that these CM and PchB recombinant proteins are active and display enzyme kinetics consistent with previous reports.
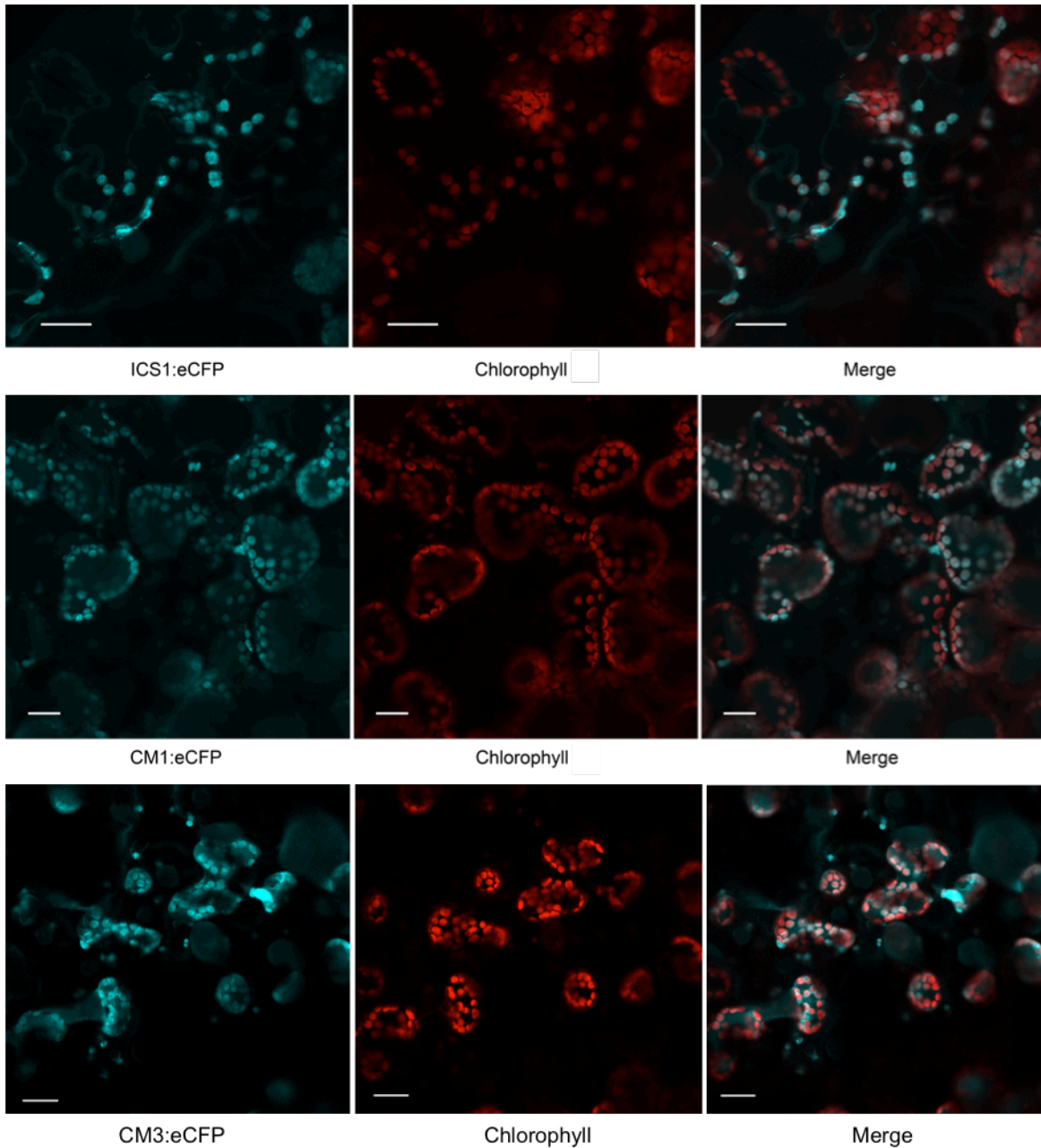
Figure 2.2: CM1- and CM3-CFP fusion proteins localize to the chloroplast under transient expression in *N.benthamiana*

CM1 and CM3 contain N-terminal chloroplast transit peptides, as predicted by the ChloroP localization software. 5-week old *N.benthamiana* were agroinfiltrated with constructs driven by the CaMV 35S promoter expressing c-terminal fusions of eCFP with ICS1, CM1 or CM3. Plants were examined 48 hours post inoculation with a Zeiss 710 confocal microscope (eCFP ex405nm/em454-581nm; chlorophyll ex633nm/em647-701). Fluorescent proteins were visible in both mesophyll and epidermal plastids. Chlorophyll autofluorescence served as a marker for the chloroplast. Scale bar is 20 µm.
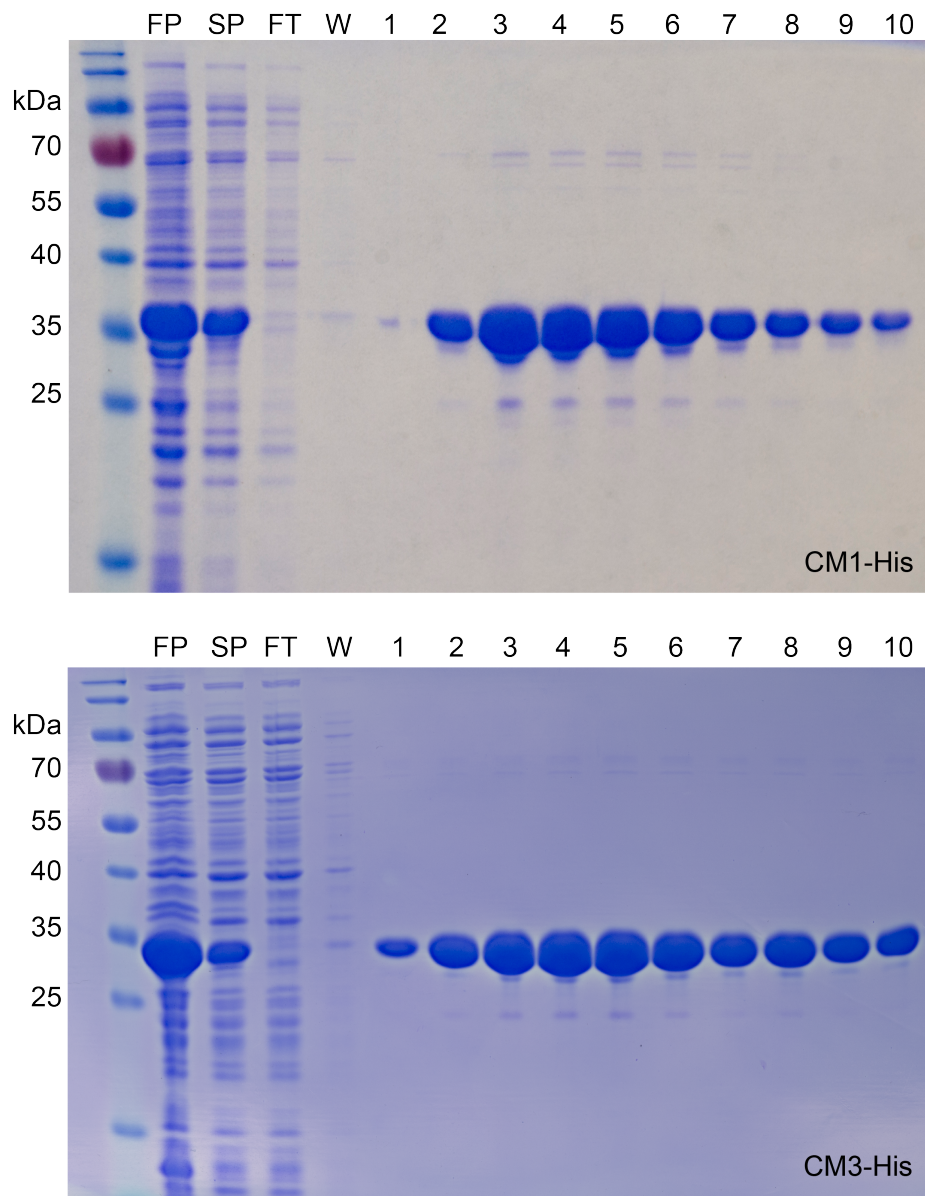
Figure 2.3: Purification of recombinant CM1 and CM3 proteins
Recombinant CM1 and CM3 proteins were purified from *E. coli* and analyzed via a 10%
SDS-PAGE gel stained with Coomassie Blue. Abbreviations used are FP: Induced protein
in *E. coli* cell lysate after French press; SP: total soluble protein after centrifugation of cell
lysate; FT: flow through of unbound proteins after incubation with NiNTA beads; W:
removal of non-specifically bound proteins via wash; Fractions 1-10: Elution of His-tagged
proteins collected in 1 mL volumes in sequential order. Purification yielded between 2-4
mg/mL of protein after aliquots were pooled. Recombinant CM2 was also purified with
similar results (not shown). Ladder on left shows size in kilodaltons (kDa).

A

CM1

B

CM3

C
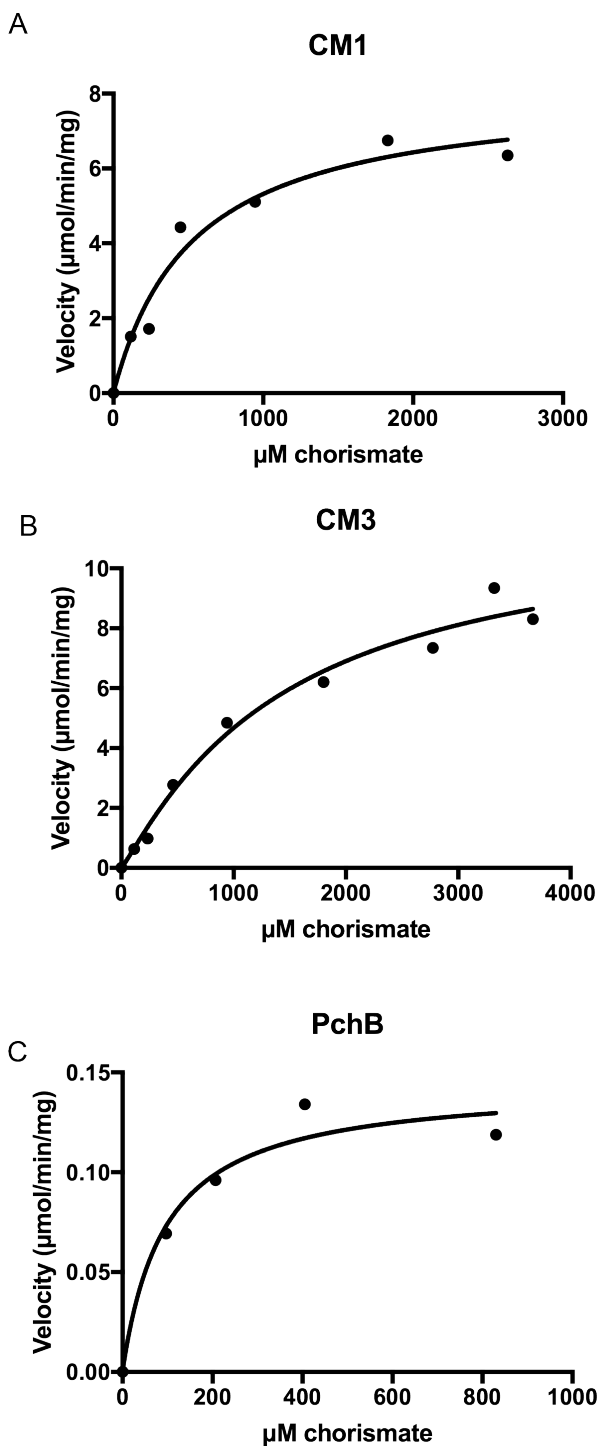
PchB

Figure 2.4: Kinetic characterization of chorismate mutase activity of CM1, CM3 and PchB

Spectrophotometric assays were used to produce velocity versus substrate curves for activity of recombinant CM1, CM3 and PchB on chorismate. Product formation was inferred through disappearance of chorismate, monitored at 10-second intervals over 30 minutes at absorbance A_{274}.

A) CM1 was fit to the Michaelis-Menten equation, and exhibited a V_{max} of 8.078 μmol chorismate/min/mg protein and an average K_m of 650 μM for chorismate (R^2 = 0.9653).

B) CM3 was fit to an allosteric sigmoidal curve, and exhibited a V_{max} of 11.7 μmol/min/mg protein and an average K_m of 1,448 μM for chorismate (R^2 = 0.982).

C) PchB was fit to the Michaelis-Menten equation, and exhibited a V_{max} of 0.144 μmol/min/mg and an average K_m of 95 μM for chorismate. (R^2 = 0.9613). Independent experiments gave similar results.

CM1 and CM3 do not exhibit IPL function *in vitro*

Do CM1 or CM3 also possess IPL activity, converting the substrate isochorismate into SA and pyruvate? Although chorismate was commercially available, it was not possible to purchase purified isochorismate, so a coupled enzyme assay pairing the CM proteins to recombinant ICS1 was employed. ICS1 functions at equilibrium and reversibly converts chorismate to isochorismate (Strawn et al., 2007; Macaulay et al., 2017). The resulting peaks of isochorismate and chorismate are distinct in my HPLC analysis by UV absorbance at A_{280} (Fig. 2.5) in the ICS1 sample incubated with 1 mM chorismate. The isochorismate and chorismate peaks are absent when ICS1 was coupled with the bacterial IPL PchB, and a strong SA peak is present via fluorescence detection. However, when ICS1 is incubated with CM1, CM2 or CM3, the isochorismate and chorismate peaks are absent, but no SA is detected. Under these conditions, no CM enzymes exhibit IPL activity. CM activity was determined via disappearance of chorismate. In this HPLC method, prephenate and phenylpyruvate, which are products of CM activity, could not be detected.

To ensure isochorismate was available for utilization, ICS1 was also incubated with chorismate to create a mixed substrate pool, and ICS1 was removed via filtration; CM1 was then added. HPLC analysis in Figure 2.6 shows that the chorismate peak is absent after incubation with CM1, while the isochorismate peak area is reduced 12%. Again, no increase in SA above the control is detected. Previous work demonstrated that chorismate and isochorismate competitively bound to the same active site on PchB, and chorismate could reduce IPL activity (K_i = 400 µM) (Gaille et al., 2002). To assess the possibility that IPL activity is impeded in a mixed substrate pool at this concentration, isochorismate was isolated following enzymatic conversion with recombinant ICS1, and its purity confirmed via NMR (Fig. 2.7A), for *in vitro* assays. PchB converts all available isochorismate to SA while assays with CM1 or CM3 do not produce elevated SA above the control sample with no added enzyme (Fig. 2.7B).

CM1 and CM3 do not enhance SA synthesis when transiently expressed in *N. benthamiana*

Although CM1 and CM3 did not display IPL activity *in vitro*, I could not rule out that these enzymes behave differently *in planta,* where essential molecular cofactors or other protein interactors would be present. Agroinfiltration of *N. benthamiana* leaves for expression of candidate proteins has long been employed as a model for assessing *Arabidopsis*-microbe protein interactions in a resistance context (Choi et al., 2011) and more recently, to reconstitute biosynthetic pathways *in planta* (Lau and Sattely, 2015). Expression constructs were generated to express ICS1, CM1 and CM3 coding sequence, including chloroplast signal peptides, driven by the constitutive 35S promoter. As a positive control, a chimeric PchB construct was generated that fused the ICS1 chloroplast signal peptide on its N-terminus, similar to (Verberne et al., 2000). Constructs were agroinfiltrated either singly or paired with ICS1 into leaves of 5-week old plants and assessed for total SA (free SA and SA-glucoside) accumulation, as in Figure 2.8A. SA accumulates as glucosylated SA, a readily hydrolysable form stored in the vacuole (Dean and Delaney, 2008; Song et al., 2008; George Thompson et al., 2017) and the combined amount of free and glucosylated SA represent total active SA.

Leaf areas infiltrated with *Agrobacterium* lacking a binary vector showed a significant increase in total SA compared to leaf areas infiltrated with infiltration medium alone (Fig. 2.8B). This elevated SA level demonstrates agroinfiltration stimulated induction of endogenous SA synthesis, which proceeds via an ICS enzyme in this species (Catinot et al., 2008). Therefore, chorismate is likely available for conversion by the transiently expressed proteins and cellular
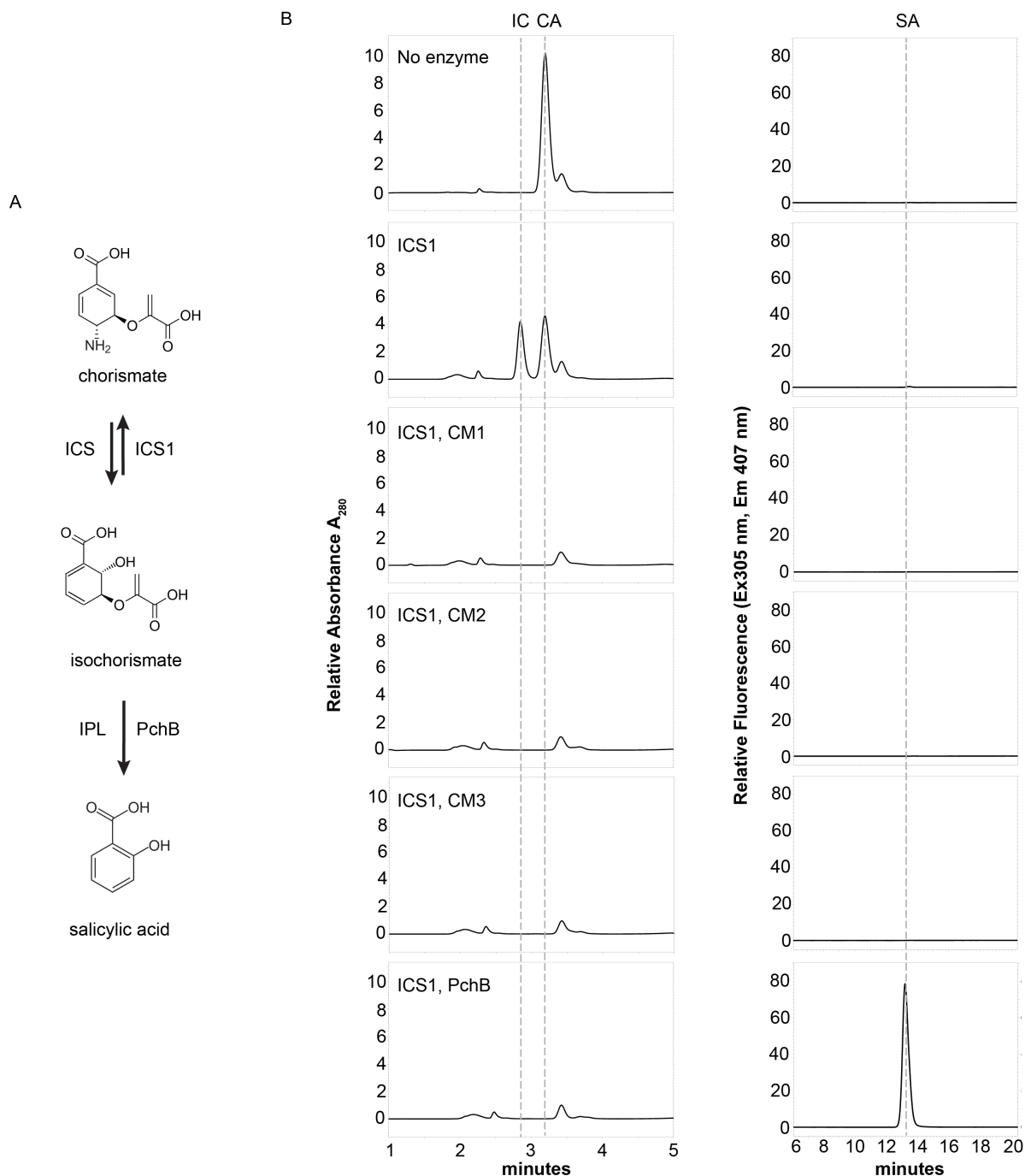
Figure 2.5: Recombinant CM enzymes do not exhibit IPL activity coupled to ICS1 *in vitro*
A) Isochorismate is reversibly produced by ICS1, and converted to SA via an IPL protein, such as the bacterial enzyme PchB.
B) Excess ICS1 was incubated with recombinant CM1, CM2, CM3 or PchB in the presence of 1 mM chorismate for 1 hour at room temperature. Samples were analyzed via reverse-phase HPLC to detect reaction products. Isochorismate (IC) and chorismate (CA) were detected via absorbance at A_{280} and peak identities confirmed with standards and UV spectra profiles. SA was detected via fluorescence in the same run (Excitation at 305 nm, emission detected at 407 nm).
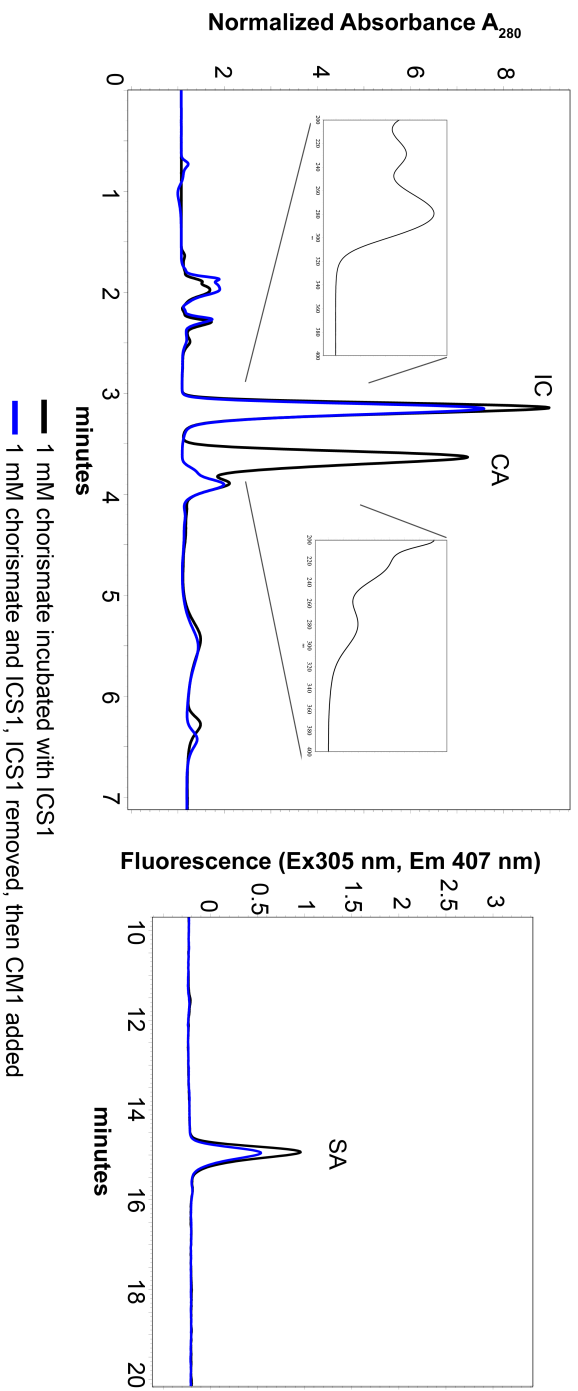
Figure 2.6: Recombinant CM1 utilizes chorismate, but not isochorismate, when incubated in a mixed substrate pool

Isochorismate was produced by recombinant ICS1 *in vitro*, then ICS1 protein was removed (black). Recombinant CM1 was added to ICS1 reaction products for 1 hour at room temperature. Samples were analyzed via reverse-phase HPLC to detect reaction products. Isochorismate (IC) and chorismate (CA) were detected via absorbance at A_{280} and peak identities confirmed with standards and UV spectra profiles (each shown in inset). SA was detected via fluorescence in the same run (Excitation at 305 nm, emission detected at 407 nm).

26
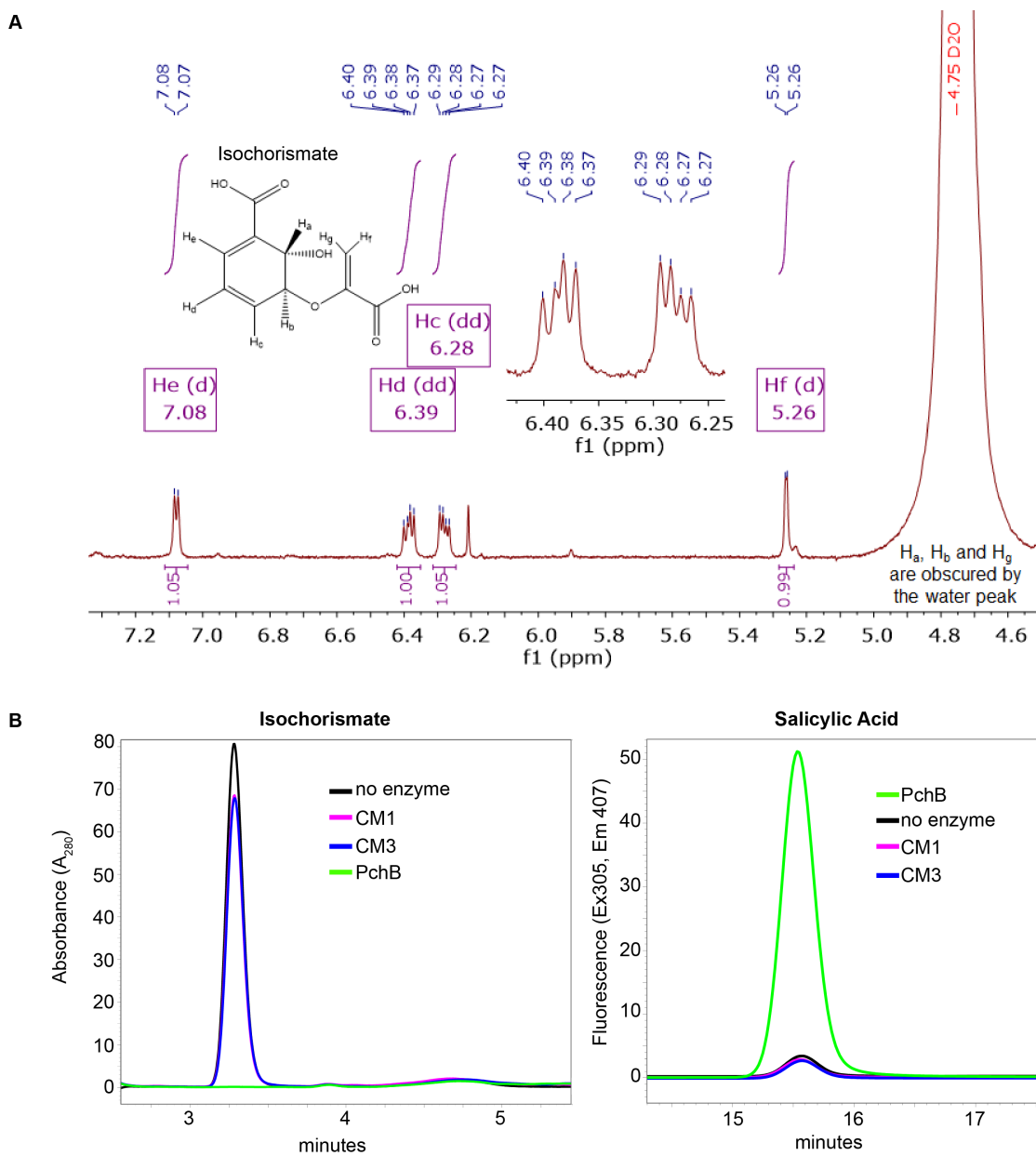
Figure 2.7: CM1 and CM3 do not utilize isochorismate for SA synthesis *in vitro*
A) NMR spectrum obtained from isochorismate prep confirms purity.
B) 75 μM isochorismate was incubated with CM1, CM3 or PchB for one hour, then reactions were assayed via reverse-phase HPLC. Isochorismate was detected via absorbance at A_{280}. SA was detected via fluorescence in the same run (Excitation at 305 nm, emission detected at 407 nm).
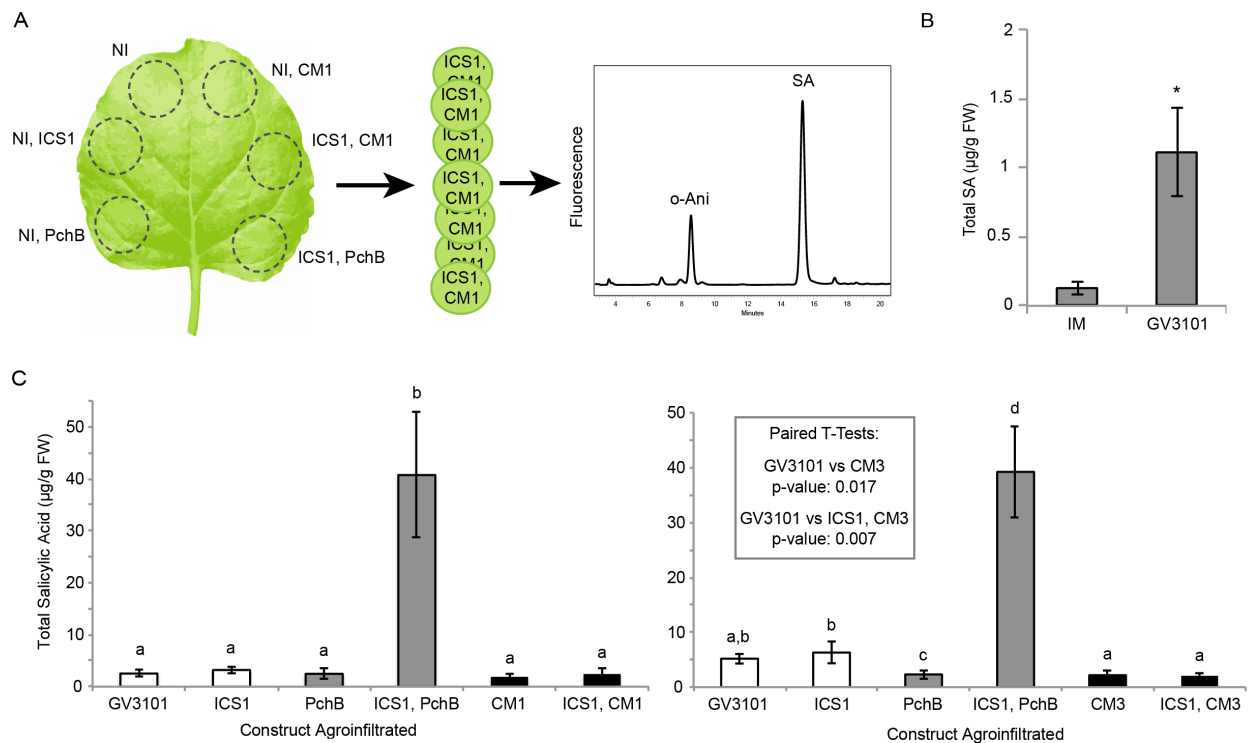
Figure 2.8: CM1 and CM3 do not enhance SA synthesis in *N.benthamiana* transient expression assay

A) Each construct (coding sequence with chloroplast signal peptide driven by 35S CaMV promoter) is infiltrated onto each *N. benthamiana* leaf with either GV3101 *Agrobacterium* lacking a binary vector insert (NI) or p35S:ICS1. NI was combined to normalize total number of *Agrobacterium* infiltrated in sectors expressing a single construct. 7-8 leaf punches of each construct were pooled from 7-8 leaves for SA extraction. SA was quantified via HPLC with fluorescence detection (Ex305, Em407) normalized by *o*-anisic acid (*o*-Ani) internal standard for extraction efficiency (Ex305/Em365). Each bar represents the average of three replicates of pooled leaf punches ± standard deviation.
B) Total SA quantified from leaves 2 days after treatment with either infiltration medium (IM) alone or GV3101 *Agrobacterium*. Asterisk indicates difference by paired t-test (p-value <0.05).
C) Total SA quantified from CM1 and CM3 transient expression in *N. benthamiana* 2 days after infiltration with listed constructs. Significant difference was detected for each sample by two-way ANOVA with Tukey post-hoc test (p-value < 0.05). Inset: paired t-test results shown for samples that are within 0.01 of significance threshold with ANOVA post-hoc test.

conditions are amenable to SA synthesis. Expression of CM1 alone or co-inoculated with ICS1 does not show a statistically significant enhancement of SA synthesis above the GV3101 treatment (Fig. 2.8C). Interestingly, CM3 expressed either alone or paired with ICS1 shows a reduction in total SA relative to GV3101 or ICS1 alone (Fig. 2.8D). In both experiments, pairing ICS1 with the bacterial IPL PchB generates an average of 40 µg/g FW total SA. This represents an 8-fold increase from control samples with bacteria harboring no insert, demonstrating the positive control is able to make SA in this assay. Taken together, these results suggest that in this context neither CM1 nor CM3 plays a positive role in SA production and do not have IPL activity.

Arabidopsis CM1 knockdown line has elevated basal total SA, while *cm3* does not differ from wild type

I attempted to isolate homozygous T-DNA insertion mutants for *CM1* and *CM3* to assess whether there was any impact on the level of SA in the absence of these enzymes *in planta.* Four potential T-DNA insertion mutants were listed for *CM1* on T-DNA Express and available from the Arabidopsis Biological Resource Center and GABI-Kat. No publications have detailed use of these lines. I was unsuccessful in isolating homozygous knockout mutants from any of the collections, as summarized in Table 2.1. Two isolated homozygous lines SALK_002696 and GABI_536F05 contain confirmed insertions upstream of *CM1* coding sequence, but expression analysis determined that neither exhibits reduced *CM1* transcript. Two lines, SK14921 and GT_3_111149, do not appear to have insertions in *CM1*, as no PCR product spanning regions of the *CM1* gene and T-DNA insertion could be produced despite multiple PCR strategies. However, a homozygous *cm3* mutant line was identified from the SALK collection detailed in (Alonso et al., 2003) and the insertion site confirmed via sequencing (Fig. 2.9A).

As no *cm1* knockout line was available, I created a transgenic knockdown line, named *cm1 #1*, using an artificial microRNA for *CM1* calculated by the Web MicroRNA Designer tool (Ossowski et al., 2008) (Figure 2.9A). This amiRNA has no predicted mRNA off-targets reported in the Web MicroRNA Designer tool or using a BLAST search against the NCBI *Arabidopsis* reference transcript database. The target site in *CM2* and *CM3* mRNA differs by eight and six bases, respectively, with seven and three of those bases in the mismatch sensitive 5' region of the amiRNA. SiteFinding-PCR (Tan et al., 2005) was used to identify the insertion site of the T-DNA in this line, and quantitative RT-PCR of the two neighboring genes show their expression is not significantly impacted (Fig. 2.10). Transformation of this same amiRNA construct into *cm3* did not yield any transformants that displayed significant levels of *CM1* silencing (data not shown), suggesting a *cm1,3* line may not be viable.

CM1 and *CM3* expression was assayed by quantitative RT-PCR in wild type, *cm1 #1*, *cm3* and *ics1* 4-week old plants (Fig. 2.9B). The amiRNA reduces *CM1* expression to 95% of wild type and is specific to *CM1*, as *CM3* expression remains unaltered. This reduction in *CM1* expression was seen in multiple independent insertion events of the amiRNA. *CM3* transcript is nearly undetectable in *cm3*. Neither gene's expression differs between wild type and *ics1*. Plastid total protein was isolated for comparison of CM activity in the *CM1* silenced line, *cm3* and wild type, yet thus far attempts at *in vitro* assays are unable to detect activity in extracts from any genotype. CMs may represent a small fraction of total protein and thus below the threshold of detection for activity in current protein preparations.

Basal levels of total SA were quantified, and surprisingly, *cm1 #1* has a three-fold increase (Fig. 2.9C) from Col-0. Preliminary results showed a second independent insertion of

CMI At3g29200 T-DNA insertion mutant summary

T-DNA ID	Putative location	Reference for insertion collection	Ecotype	Germination	PCR Genotyping	*CMI* expression in homozygous?
SALK_002696	promoter	Alonso *et al*, 2001	Col-0	yes	homozygous isolated	no change (RT-PCR)
SK14921	intron 2	Robinson *et al*, 2009	Col-4	yes	T-DNA not detected in CMI, 2nd insertion elsewhere	no change (RT-PCR)
GT_3_111149	exon 1	Sundaresen *et al*, 1995	Ler-0	poor	no homozygous isolated with multiple primers	ND
GABI_536F05	promoter	Kleinboelting *et al*, 2012	Col-0	poor	homozygous isolated	no change (qPCR)

Table 2.1. *CMI* **T-DNA insertion lines tested for gene disruption**
See Table 2.4 for genotyping primers.

A

CM1 CDS 5' GA GCC AAG TAC TGT TAC AAT G **3'**
miRNA 3' CT CGG TGC ATG ACA ATG TTA T **5'**

CM1
At3g29200

SALK_147350

CM3
At1g69370

predicted chloroplast
signal peptide

chorismate mutase AroQ class domain IPR008238

B Expression Relative to *Actin 2* — Genotype (Col-0, *cm1 #1*, *cm3*, *ics1*)

C Basal Total SA (µg/g FW) — Genotype (Col-0, *cm1 #1*, *cm3*, *ics1*)
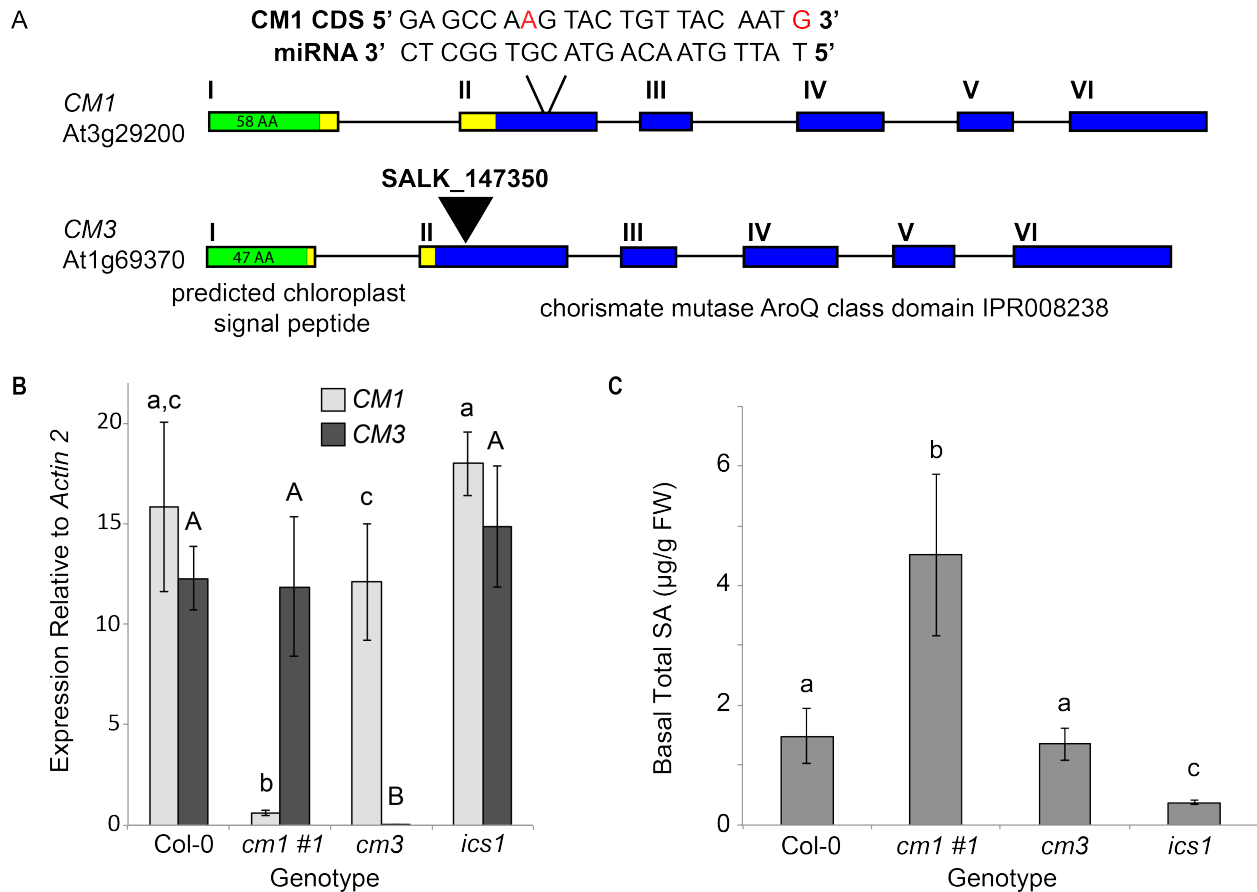
Figure 2.9: *CM1* **silenced line reduces** *CM1* **expression, but not** *CM3***.** *Cm1 #1* **exhibits elevated basal SA, while** *CM3* **insertion mutant does not**
A) Exon structure for *CM1* and *CM3*. *CM1* coding sequence and its complementary amiRNA sequence is indicated. Bases that do not pair to *CM1* are in red. T-DNA insertion into second exon of *cm3* is indicated.
B) Quantitative RT-PCR analysis of *CM1* and *CM3* expression in indicated genotypes. Bars represent the average of 4 biological replicates (3 leaves per plant pooled) ± standard deviation.
C) Basal total SA (SA + SAG) was quantified via HPLC from 4-week old plants infiltrated with 10 mM $MgSO_4$ and collected 48 hours later. Bars represent the average of 3 biological replicates ± standard deviation. Significance was determined for each genotype via two-way ANOVA with Tukey Post-Hoc test, ($p < 0.05$). An independent experiment gave similar results.

A)

p35S:amiRNA CM1 326bp
T-DNA insertion 48 bp from 3' UTR

At5g47820
FRAGILE FIBER 1

3' UTR

579 bp

3' UTR

At5g47830
hypothetical protein

B)
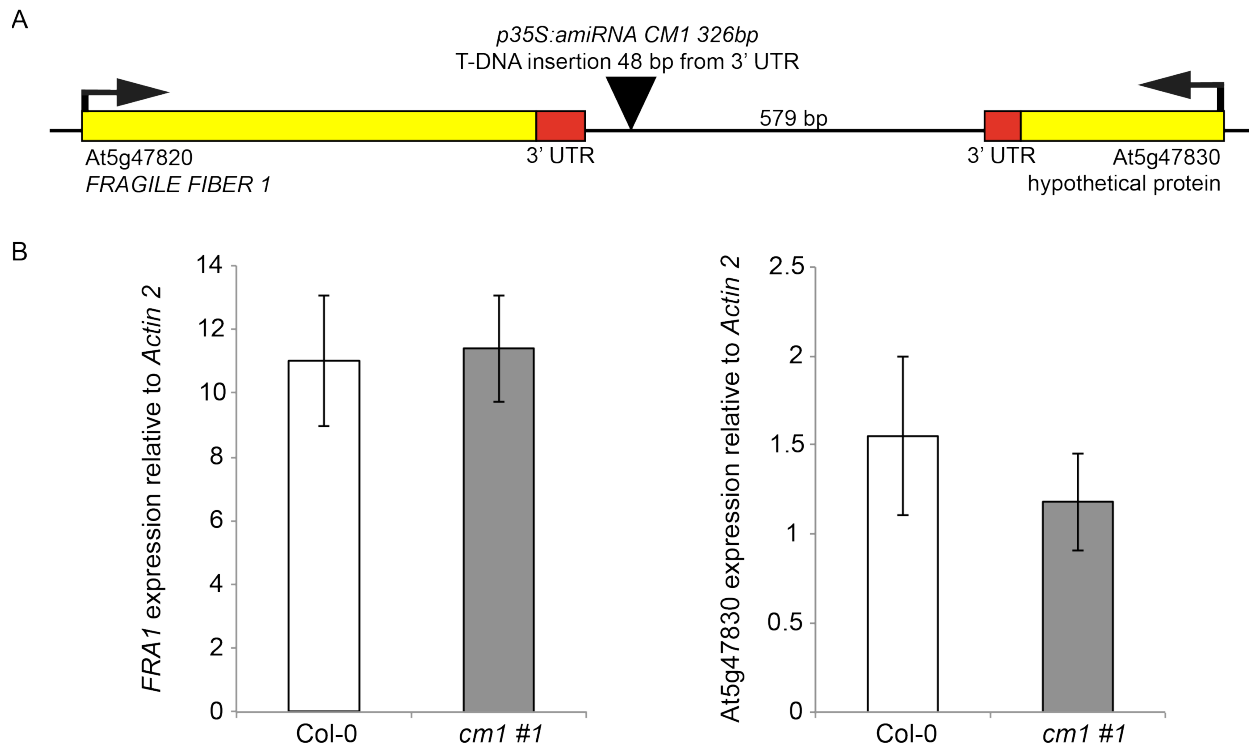
Fig. 2.10: Insertion of *CM1* amiRNA T-DNA does not disrupt neighboring gene expression
A) Sequencing identified T-DNA insertion carrying amiRNA inserted into chromosome 5 between At5g47820 (*FRA1*) and At5g47830.
B) Quantitative RT-PCR on cDNA from 4-week old leaves for *FRA1* and At5G47830. Bars represent the average of 4 biological replicates ± standard deviation. Neither gene displays a significant difference in expression in *cm1 #1* as determined by paired t-test (p <0.05). An independent experiment gave similar results.

the *CM1* amiRNA construct exhibited an intermediate increase in basal levels of total SA (data not shown). Total SA is not significantly altered in c*m3*, while the SA biosynthetic mutant *ics1* exhibits 20% of basal total SA level relative to wild type, consistent with previously published results that show *ics1* has lowered basal total SA (Wildermuth et al., 2001; Garcion et al., 2008; Chandran et al., 2014).

Chorismate mutase mutants are similar in size to wild type

The elevated basal SA in *cm1 #1* shows that silencing of *CM1* enhanced SA synthesis. This is likely to be via *ICS1*, as ICS1 contributes 80% of basal SA (Fig. 2.9C). However, *cm1 #1*'s phenotype does not appear to be due to elevated *ICS1* transcript, as basal levels are similar between both *CM* mutant lines and wild type (Fig. 2.11A). Furthermore, there is no indication of SA-responsive *PR-1* expression (Fig. 2.11B), which upon infection by (hemi)biotrophic pathogens can increase by as much as 100-fold. Additionally, these single CM mutants displayed no deficiency in plant size, as average rosette diameters of 4-week old plants are similar to wild type (Fig. 2.11C).

Transient overexpression of allosteric mutant CM1 lowers induced SA in *N. benthamiana*

As chorismate is a key metabolite in primary and secondary metabolism, chorismate-utilizing enzymes are allosterically (*ie* CM1,3 and ASA1) and/or transcriptionally (*ie* ICS1) regulated, ensuring chorismate partitioning is responsive to cellular conditions. I hypothesized that disruption of *CM* expression could upset this balance, resulting in atypical flux to chorismate derivatives, including SA. Unlike CM1, CM3 is not negatively affected by allosteric effectors, but its activity can be increased by tryptophan, cysteine and histidine. Plants lacking *cm3* do not exhibit elevated basal SA (Fig. 2.9C), but interestingly, transient overexpression of CM3 in *N. benthamiana* reduces total SA accumulation (Fig. 2.8C). This suggests that overexpression of CM3 causes redirection of chorismate away from SA synthesis. The same result is not seen upon overexpression of CM1, which can be negatively regulated via tyrosine and phenylalanine at micromolar concentrations (Eberhard et al., 1996b; Westfall et al., 2014). Informed by my structural modeling that identified CM1's possible aromatic amino acid allosteric effector binding residues (Chapter 1), confirmed in (Westfall et al., 2014), I generated and transiently expressed an allosteric-insensitive *CM1* mutant (CM1 G213A) in *N. benthamiana* as before. Average induced SA accumulation with CM1 G213A is reduced 50% relative to leaves infiltrated with GV3101 alone (Fig. 2.12), indicating that overexpression of CM3 or a non-allosteric CM1 could interfere with SA synthesis, likely by competing with the endogenous ICS for chorismate.

Elevated basal SA in *cm1 #1* confers enhanced resistance to *Pma* ES4326

Many mutants have been identified with elevated levels of basal total SA up to 20-fold greater than wild type (*ie ssi2*, *cpr1*, *cpr5, del1*), though both the mechanisms underlying the phenotype and effective fold-increase in total SA vary. The elevated SA in these mutants results in heightened pathogenesis-related gene expression (*ie PR-1*), sometimes accompanied by spontaneous leaf necrosis or reduced plant growth, and enhanced disease resistance to a broad-spectrum of pathogens (Bowling, 1994; Bowling et al., 1997; Kachroo et al., 2003; Chandran et al., 2014). Does the elevated level of pre-infection total SA in *cm1 #1* have a similar impact on the outcome of (hemi)biotrophic pathogen-plant interactions? To assess this question, 4-week old plants were inoculated with either virulent bacterial hemi-biotrophic pathogen *Pseudomonas*

A

B

C

Genotype	Rosette diameter	p-value
Col-0	4.5 ± 0.6	NA
cm1 #1	4.5 ±0.55	0.98
cm3	4.3 ±0.6	0.94
ics1	4.4 ±0.6	0.92
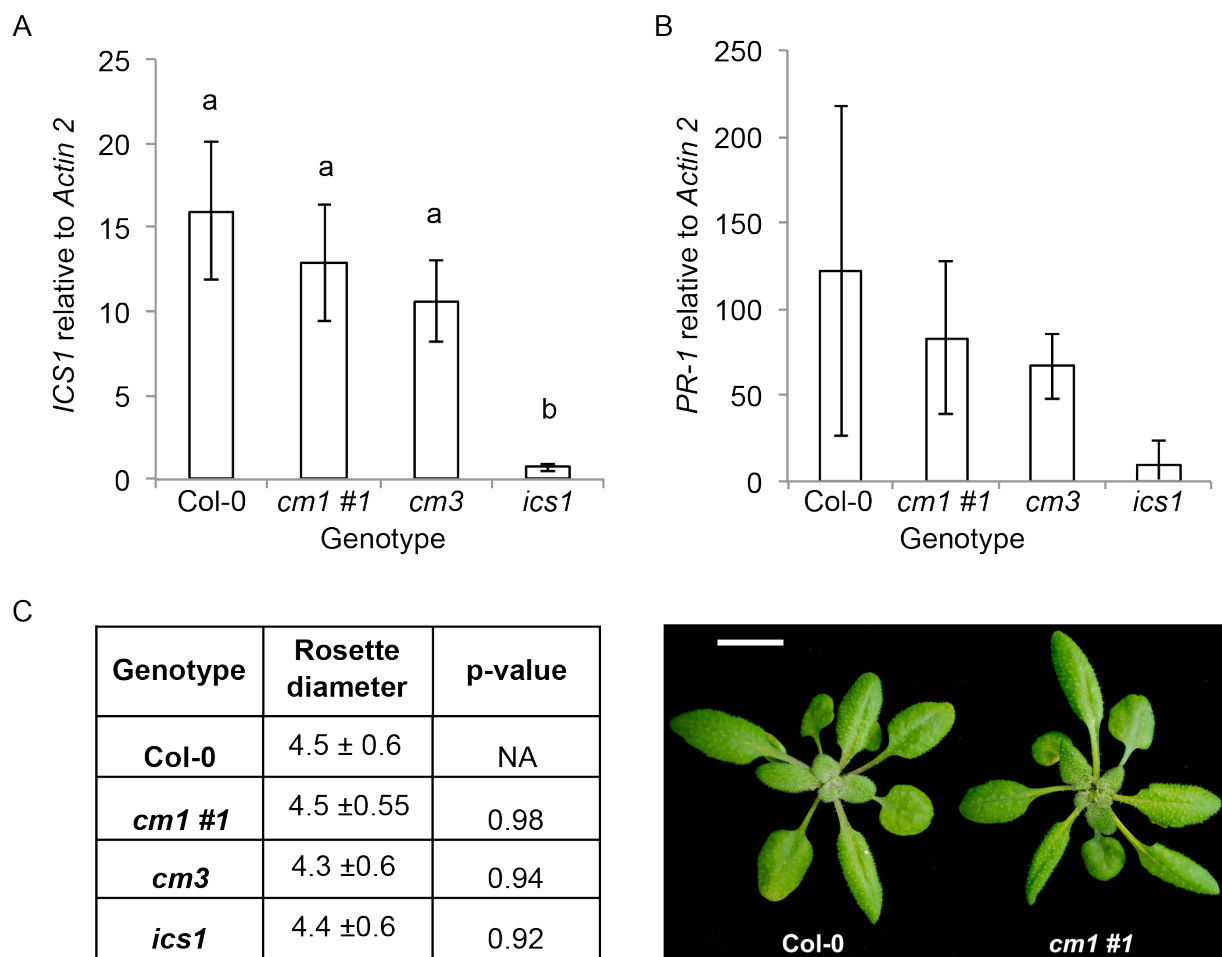
Figure 2.11: *cm1 #1* **does not exhibit elevated basal expression of SA-responsive genes or differ in rosette growth**
Quantitative RT-PCR was performed on cDNA from 4-week old plants. Bars are the average of 4 biological replicates ± standard deviation. Basal expression of **A)** *ICS1* expression was only significantly altered in *ics1*. **B)** *PR-1* is not significantly different between any genotypes. **C)** *cm1 #1* does not exhibit any altered growth phenotype. Rosette diameter was measured for the longest distance across leaves. N= 12 for Col-0, *cm1 #1* and *cm3*, and 9 for *ics1*. Significance was determined with two-way ANOVA with Tukey post-hoc test. Scale bar on image is 1 cm. Another experiment gave similar results.
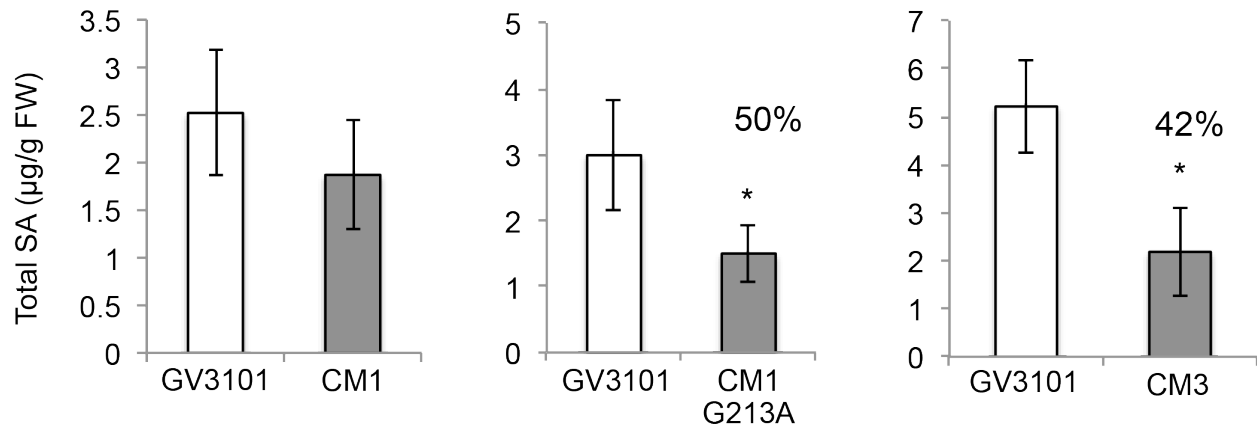
Figure 2.12: Transient expression of CM3 and allosteric insensitive mutant CM1 G213A reduce SA accumulation in *N. benthamiana*
CM1 and CM3 from Figure 2.8 are reproduced here for ease of comparison. p35S:CM1 G213A was transiently expressed in *N. benthamiana* as described earlier and total SA quantified. Bars represent 3 biological replicates of 8 pooled leaf punches ± standard deviation. Percent reduction from GV3101 treatment is marked. Statistical significance ($p<0.05$) determined by paired t-test in each experiment.

syringae pv *maculicola* ES4326 (*Pma* ES4326*)* (Dong et al., 1991) or the obligate fungal biotroph *Golovinomyces orontii* (Plotnikova et al., 1998) and assayed for pathogen fitness.

As seen in Fig. 2.13A, *cm1 #1* displays enhanced disease resistance to *Pma* ES4326, as bacterial growth in the leaf was an average of one-half $\log_{10}$ (three-fold) less relative to wild type. This is not true for *cm3*, which supports growth equal to that on wild-type plants. Consistent with previous reports and SA's key role in resistance to (hemi)biotrophic pathogens, *ics1* plants are more susceptible to *Pma* ES4326, supporting a 2.5-log fold increase (300-fold greater) in bacteria. Upon pathogen challenge, *ICS1* is transcriptionally upregulated and plants accumulate increased amounts of total SA (Wildermuth et al., 2001; Zheng et al., 2015) that is broadly correlative with a robust defense response. At two days post infection, total induced SA is similar between *cm1 #1* and wild type (Fig. 13B). Accordingly, expression of *ICS1* and *PR-1* is similar between wild type and the *CM* mutants (Fig. 13C). A significant reduction in induced total SA, *ICS1* and *PR-1* expression is seen in *ics1*. Thus, knockdown of *CM1* conferred greater resistance, through responses coordinated via its elevated pre-infection total SA or possibly an SA-independent effect, such as altering concentrations of chorismate derivatives.

Induced SA biosynthesis is elevated in *cm1 #1* upon *G. orontii* inoculation, yet exhibits inconsistent infection phenotype

G. orontii is an obligate biotroph and obtains all nutrients from its host. Fungal reproduction has been used as a metric of fitness, and is shown to be highly responsive to SA-mediated responses in the host plant (Lynne Reuber et al., 1998; Chandran et al., 2014), which restrict reproductive output. *G. orontii* growth and reproductive fitness can be assessed at multiple stages during its infection and asexual lifecycle, allowing researchers to distinguish plant resistance mechanisms that occur during (callose deposition and spore penetrative attempts/successes) and post-penetration (hyphal growth quantitation, reproductive structures per fungal colony, total spore counts). We quantified powdery mildew fitness via total reproductive output per gram leaf weight, a metric that encompasses both penetration and post-penetration resistance responses to give a holistic view of the infection. Each genotype was assayed multiple times, inoculated in parallel with wild type to ensure inoculum dosage between the pair is similar. Spore quantification for each mutant (leaves from 5 pooled plants) was normalized to its corresponding wild type, and averages for each genotype are displayed in Fig. 2.14A. The amount of spores produced by *G. orontii* infecting *cm1#1* is inconsistent; less spores were produced relative to wild type in 5 of 8 independent infections, on average a 25% reduction, while the other 3 supported a 15% average increase in spore production. Taking those results together, *cm1 #1* supports an overall average 15% reduction in asexual spores, although this result is not statistically different from wild type. By contrast, *cm3* and *ics1* boasted consistent increases in spore production of 30% and 75%, respectively.

Similar to *Pma* ES4326 infection, I quantified the level of induced SA in infected and mock-treated plants to determine if induced SA synthesis is also impacted in this knockdown line. The scale and timeframe of SA accumulation in wild type differs for each pathogen, as *Pma* ES4326 inoculation induces total SA 10-fold in wild type over a 48-hour period, while *G. orontii* induces total SA by 2.5-fold over a 7-day period. Interestingly, *cm#1* had twice the induced total SA of wild type in response to *G. orontii* infection (Fig. 2.14B). Although *cm3* supported greater production of asexual spores, this phenotype is not due to reduced total SA, which was identical in the mutant and wild type. Despite *cm1#1*'s increased SA induced by *G. orontii*, analysis of

ICS1 and *PR-1* transcripts at this stage of the *G. orontii* infection showed no difference between mutants and wild type (Fig. 2.14C, D).

With our extraction protocol, we can separately quantify total SA and the free form of SA localized in the plastid and cytosol, which is typically much lower, even under inducing conditions. As shown in Fig. 2.15A and B, induced free SA is not significantly altered from wild type in either *cm1 #1* or *cm3*. However, *cm1 #1* does show a consistent increase in pre-infection free SA, though it cannot always be resolved to statistical significance due to low number of biological replicates. Synthesis of the antimicrobial camalexin is induced in response to *Pma* ES4326 (Tsuji et al., 1992; Glazebrook and Ausubel, 1994; Zhou et al., 1999), and was quantified via HPLC. Induced levels of camalexin elicited by *Pma* ES4326 and *G. orontii* does not differ between CM mutants and WT, though statistically elevated levels are seen in *ics1* (Fig. 15.C,D). SA is clearly a larger player in *Arabidopsis* resistance to *Pma* ES4326 than camalexin, as *ics1* plants are more susceptible to infection by *Pma* ES4326 despite possessing a 4-fold increase in camalexin.

Differential activation of *MPK3* and *PR-1* in *cm1 #1* suggest early activation of PTI responses

As total SA levels and defense gene expression were similar between *cm1 #1* and wild type at tested late-stage infection time points for *Pma* ES4326, I hypothesized that *cm1 #1*'s enhanced resistance might arise from early mobilization of responses upon pathogen challenge influenced by basal SA. Wild type and *cm1 #1* plants were treated with a low-level of *Pma* ES4326 inoculum, and leaves were collected immediately upon inoculation, at 9 hours and 18 hours post inoculation (hpi). Select gene expression was analyzed via quantitative RT-PCR (Fig. 2.15). Although *PR-1* reaches similar expression between wild type and *cm1 #1* by 48 hpi in our previous infection assays (Fig. 13D), *cm1 #1* boasts increased expression at 18 hpi. Examination of *ICS1* did not reveal any differential expression in *cm1#1* from wild type at any time point.

The earliest responses to inoculation occur upon pathogen perception. Plant cells employ transmembrane receptor proteins on the cell surface to recognize conserved molecular signatures of microbial pathogens, like the flagellin receptor FLS2 (Gómez-Gómez and Boller, 2000), which trigger a signal cascade that phosphorylates, among others, mitogen-activated protein kinases (MPK) 3 and 6 (Asai et al., 2002). *MPK3* and *MPK6* expression can be upregulated via exogenous application of salicylic acid or its functional analog benzothiadiazole as a molecular mechanism of priming (Beckers et al., 2009). I quantified expression of *MPK3* and *MPK6*, and found that *MPK3* was induced 3-fold relative to wild type in *cm1 #1* immediately after inoculation with *Pma* ES4326 (Figure 16A). *MPK6* expression increased over time post inoculation, but remained similar to wild type. The transcription factor WRKY33 is one of the phosphorylation targets of MPK3, and auto-activation of the MPK3/MPK6 signaling node upregulates *WRKY33* transcription by as much as 8-fold (Wan et al., 2004; Mao et al., 2011). I found that *WKRY33* expression is induced 3-fold in *cm1 #1* relative to wild type just after inoculation, consistent with the enhanced expression of *MPK3* (Fig. 16B). However, expression of transcription factor *WRKY29*, previously shown to be responsive to the FLS2/MPK3/MPK6 signaling cascade (Asai et al., 2002), is not altered in *cm1 #1*(Figure 15B).

Similar to the downstream signaling components, *FLS2* expression increases with application of exogenous SA (Yi et al., 2014) and basal expression is reduced in the *ics1* background. I examined whether *FLS2* was upregulated in *cm1 #1* relative to wild type at early time points of infection. I found that variation in one of the mutant replicates rendered the result
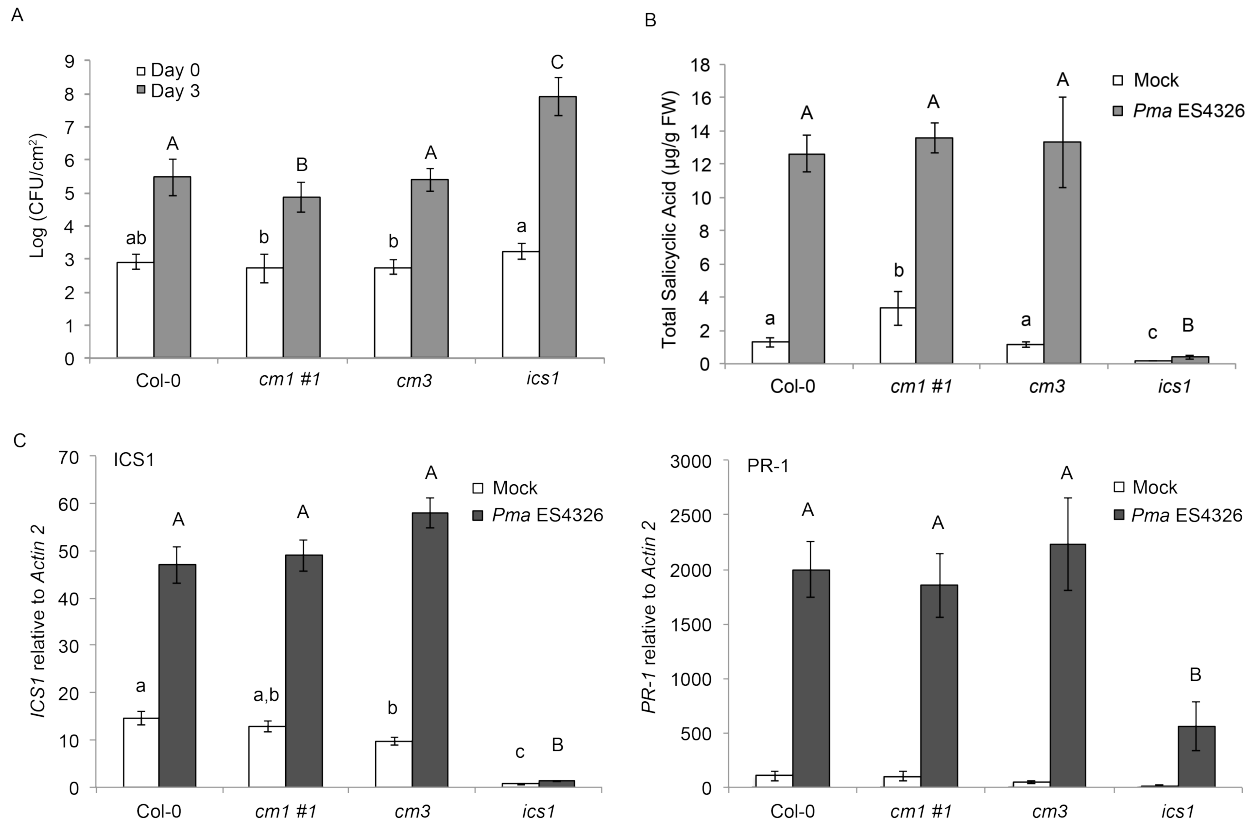
Figure 2.13: *cm1 #1* **exhibits enhanced disease resistance to bacterial pathogen, but total induced SA and SA-mediated gene expression are not significantly different at 2 dpi.**
A) *Pma* ES4326 growth at 0 and 3 days post inoculation with 10^3 colony forming units (CFU)(OD_{600} =0.0002) in 4-week old plants, n = 12 per genotype. **B)** Total SA in untreated and plants inoculated with *Pma* ES4326 and collected 2 dpi. Bars are average of 3 biological pools ± standard deviation. **C)** Only *ics1* shows significantly altered expression of *ICS1* and *PR-1* upon infection with *Pma* ES4326. In mock samples, *cm3* shows slightly reduced expression from wild type, but not *cm1 #1*. Bars represent the average of 2 independent experiments ± standard error (n=8). Significance was determined by two-way ANOVA with Tukey post-hoc test ($p<0.05$) for each condition and bars lacking groupings were not significantly different.
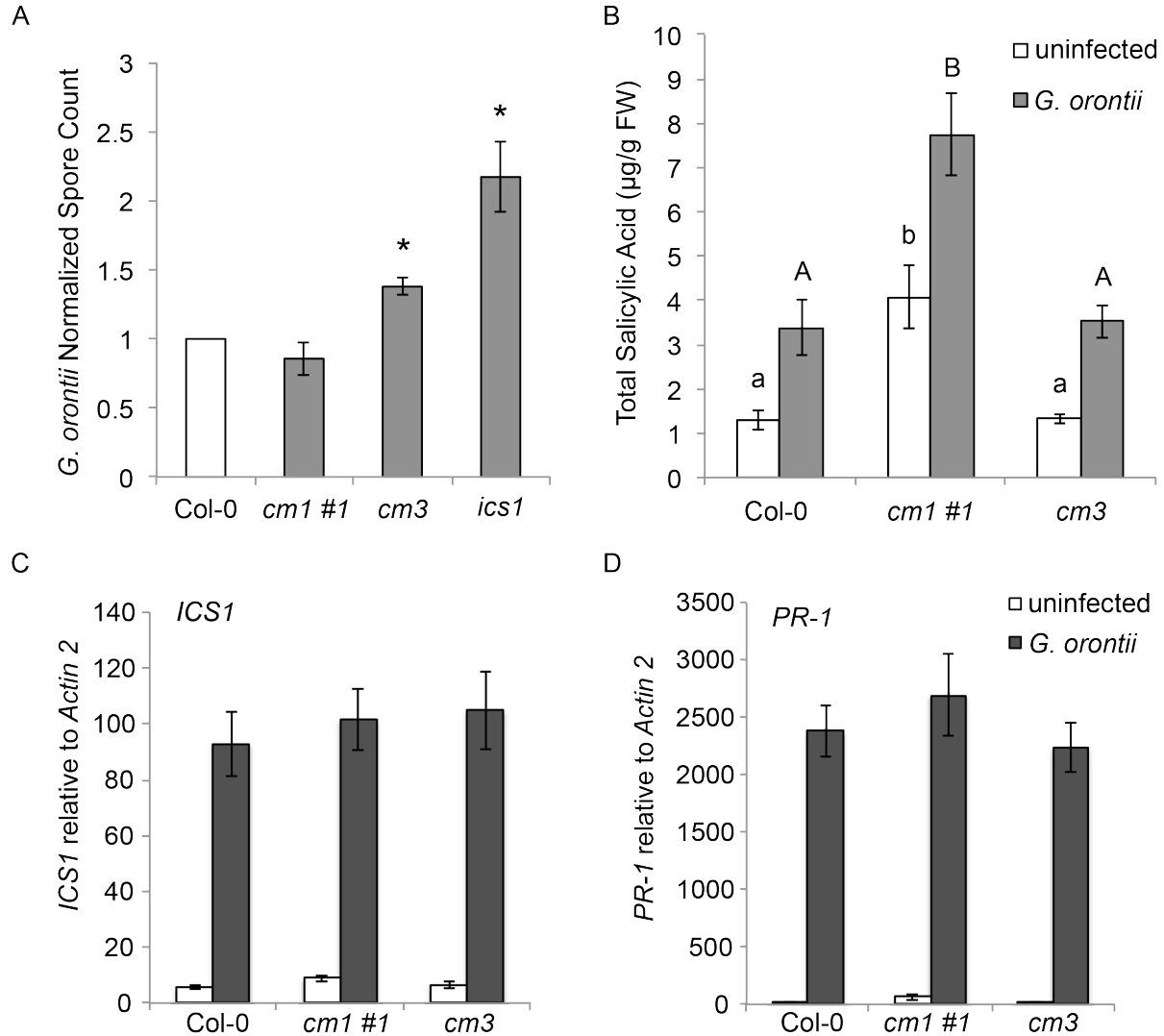
Figure 2.14: *cm1 #1* **exhibits indeterminate resistance to** *G. orontii,* **despite elevated induced levels of total SA**

A) Spore output of *cm3* and *ics1* were statistically elevated from Col-0 wild type, while *cm1 #1* showed inconsistent results. In 5 of 8 independent experiments, *cm1#1* supported reduced spore growth, while 3 of 8 spore amounts were elevated or same as wild type. Bars represent normalized average of independent experiments (each experiment is the pooled spores from 5 plants of wild type and 5 of the mutant co-inoculated), ± standard error (n= 8 for *cm1 #1, 6* for *ics1* and 4 for *cm3*). Statistical difference from wild type was determined via paired t-test (p<0.01). **B)** *cm1 #1* exhibits both elevated pre- and post-infection total SA (leaves collected at 7 dpi). Statistical significance determined via ANOVA with Tukey post-hoc test (p<0.05). An independent experiment gave similar results. **C)** Expression of *ICS1* and **D)** *PR-1* in *cm1 #1* does not differ in *G. orontii* infected tissue at 7 dpi, despite elevated total SA. Bars are the average of 2 independent experiments (n=8) ± standard error. There was no statistical significance using two-way ANOVA with Tukey post-hoc test between genotypes.
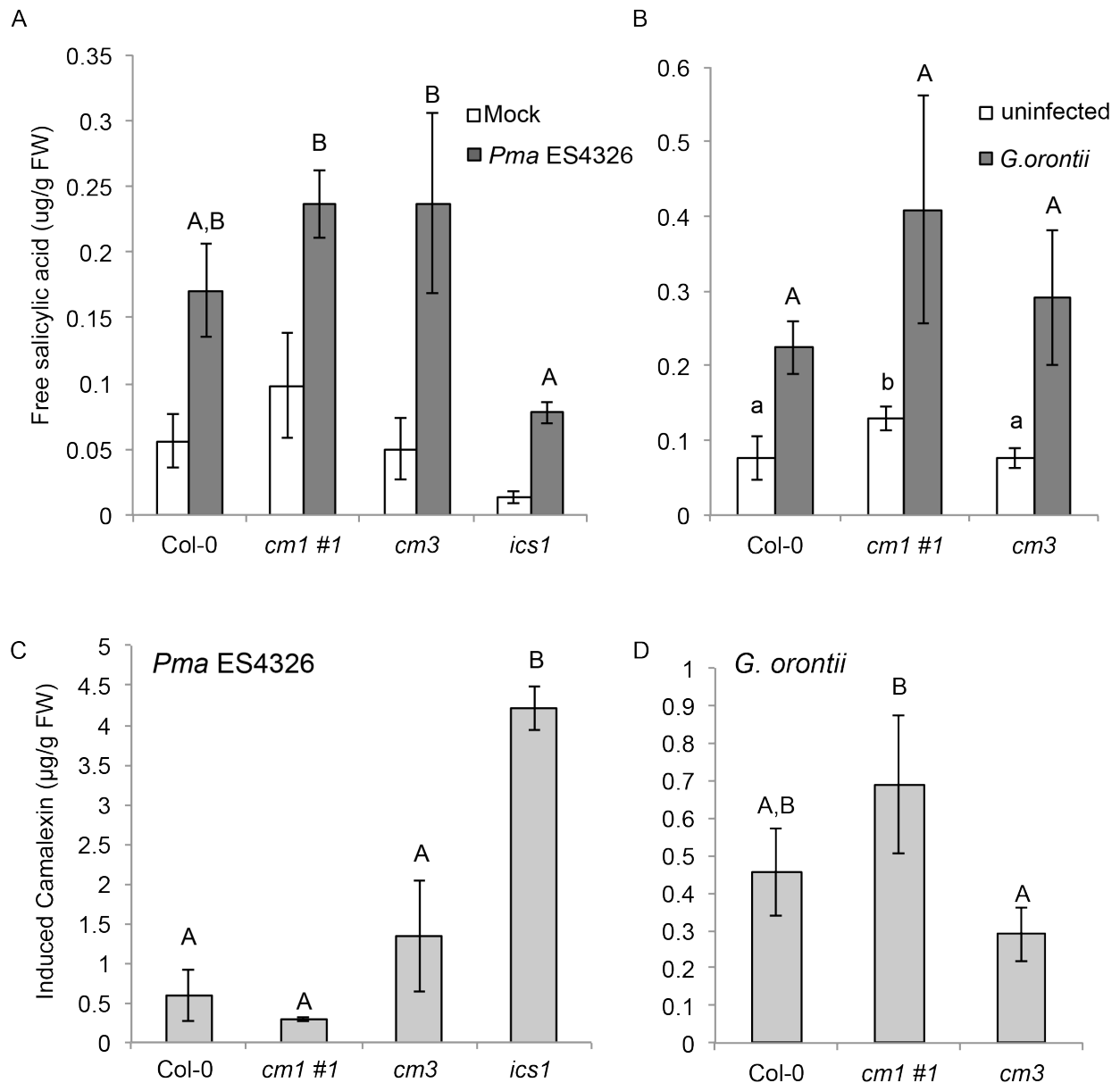
Figure 2.15: Free SA is elevated in pre-infected leaves, but not upon infection with *Pma* ES4326 or *G. orontii*

A) Untreated leaves show elevated free SA levels that are not always statistically significant. Induced free SA is not significantly altered relative to *cm1 #1* by *Pma* ES4326 (inoculated with 10^3 CFU) at 2 dpi or **B)** *G. orontii* (inoculated with moderate dose) at 7 dpi. **C)** Induced camalexin does not differ between Col-0, *cm1 #1* or *cm3* with *Pma* ES4326 or **D)** *G. orontii* treatment. *ics1* exhibited elevated induced camalexin in response to *Pma* ES4326, but was not tested for *G. orontii*. Bars represent the average of 3 biological replicates ± standard deviation. Statistical groupings determined by two-way ANOVA with Tukey post-hoc test. An independent experiment gave similar results.
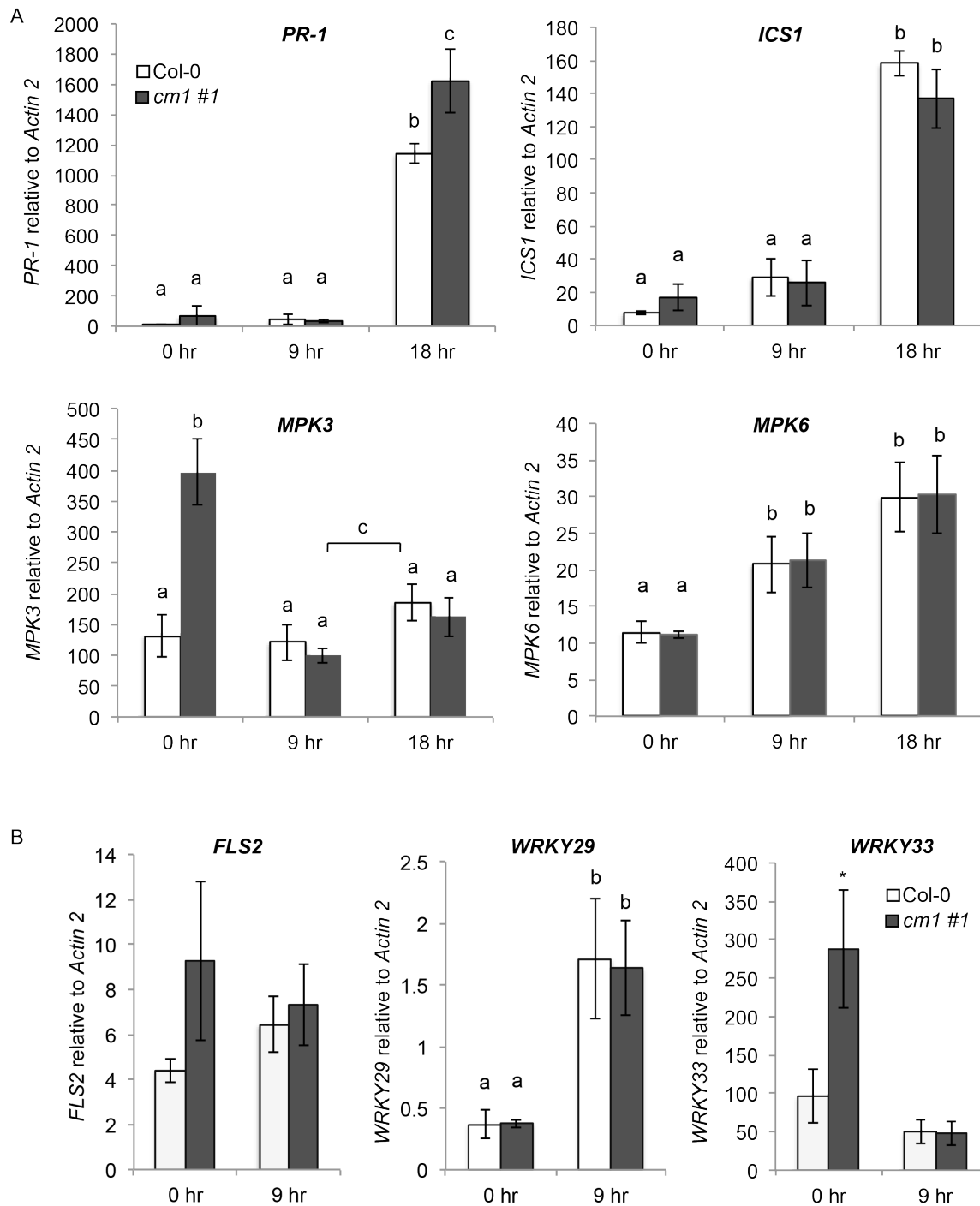
Figure 2.16: Expression time course of *Pma* ES4326 infection reveals differentially expressed genes involved in SA-mediated defense responses
A) Quantitative RT-PCR of indicated genes involved in defense response. **B)** Quantitative RT-PCR of genes associated with MPK3 signaling. For both, plants were inoculated with 10^3 CFU *Pma* ES4326 and collected either immediately after infiltration (0 hr) or 9 and 18 hours after. Bars are the average of 3 biological replicates of inoculated leaves from 2-3 plants, ± standard deviation. Statistical grouping determined by two-way ANOVA with Tukey post-hoc test (p<0.05).

statistically not significant, but further experimentation could determine whether *FLS2* is also upregulated at this early infection time point. Taken together, my results indicate that *cm1 #1* enhanced resistance might arise through early and/or stronger induced activation of MPK3/6-mediated signaling mechanisms in response to *Pma* ES4326.

DISCUSSION

SA has long been known to be a key mediator of initial plant defense responses upon pathogen infection and the sustained primed state of systemic acquired resistance in distal plant tissues that follows (Gaffney et al., 2000; Wildermuth et al., 2001; Vlot et al., 2009). While *ICS1* has been demonstrated to be a major contributor to induced SA synthesis, no *Arabidopsis* enzyme has been identified to perform subsequent conversion of isochorismate to SA. Building on initial structural modeling detailed in Chapter 1, I sought to determine whether Arabidopsis chorismate mutases, long considered as candidates for IPL function (Strawn et al., 2007; Dempsey et al., 2011), play a direct role in SA biosynthesis. I instead found that modulation of CM activity through altered expression has an indirect impact on SA accumulation, likely due to the dynamics of chorismate-utilizing enzymes and their downstream biosynthetic pathways.

***Arabidopsis* chorismate mutases do not exhibit IPL activity**

In vitro assays and transient expression experiments strongly indicate that neither plastidic CM protein catalyzes the conversion of isochorismate to SA. Reactions were conducted under conditions in which ICS1/2 and the bacterial ICS EntC were characterized (Strawn et al., 2007; Sridharan et al., 2010; Macaulay et al., 2017), as an IPL likely functions under similar cellular conditions. Consistent with previous results, ICS1 incubated with chorismate reached equilibrium between isochorismate and chorismate, but did not exhibit detectable salicylate synthase activity (Fig. 2.3). When coupled with either CM1, 2 or 3, neither chorismate, isochorismate nor SA were detected by HPLC. There was no difference among the other peaks present in both control and enzyme runs, indicating no other detectable product was made. ICS1 functions at equilibrium, and thus two scenarios were possible for this result: ICS1 produced isochorismate but CM directed flux to prephenate and drew down the isochorismate pool, or the CM enzyme outcompeted ICS1 for chorismate and thus little isochorismate was produced. PchB produced SA; its K_m for isochorismate is 12.5 μM, and thus low concentrations of isochorismate are sufficient for SA synthesis. As the enzyme is bifunctional, prephenate was likely also generated.

I produced and purified isochorismate, and assays were repeated, this time directly supplying this substrate to CMs (Fig. 2.7) in the absence of ICS1. Again, no SA was produced by CM1 or CM3, and these results confirmed that CM enzymes do not convert isochorismate into SA *in vitro*. A small amount of SA (44 ng/50 μL sample) was present in this control, likely a byproduct of the spontaneous pyruvate side chain elimination reaction of isochorismate during the multi-day purification process (DeClue et al., 2006; Hubrich et al., 2014). Strawn *et al.* found isochorismate degradation to SA in assay conditions and timeframe was negligible (<0.1%). CM protein was removed prior to HPLC quantification, and isochorismate peak area decreased 10% after incubation with CM1 and 3, suggesting these enzymes may bind isochorismate. Further investigation could determine whether isochorismate acts as a competitive inhibitor, similar to (Gaille et al., 2002) who determined chorismate inhibits PchB's IPL activity.

In vitro assays have limitations, chief among them that the assay may not reflect cell physiology. "Known unknowns," like chemical cofactors, chaperone proteins and multi-protein

complexes, are difficult to anticipate or challenging to replicate outside a living cell. Many chorismate-utilizing enzymes, including ICS1, have a requirement for Mg^{2+} for function (Strawn et al., 2007), as it coordinates the carboxylic residues of chorismate in the active site (Zwahlen et al., 2007). Yet greater context can be key for enzyme activity, as demonstrated by bacterial salicylate synthase Mbt1, an ICS1 structural homolog that converts chorismate to either isochorismate or salicylic acid as dictated by pH; it exhibits promiscuous chorismate mutase activity in the absence of Mg^{2+} (Zwahlen et al., 2007). Additionally, protein-protein interactions may be required to channel reaction intermediates for efficient production of final products (Castellana et al., 2014), and unknown interactors may be needed to bring ICS1 into proximity with an IPL. Therefore a negative result does not definitively disprove an enzyme is unable to perform the reaction under another condition.

To circumvent the restraints of *in vitro* assays, transient overexpression of these enzymes in *N. benthamiana* coupled with ICS1 was employed to test for IPL activity in cellular conditions with the necessary metabolites and accessory proteins. Salicylic acid biosynthesis in *N. benthamiana* proceeds through an ICS enzyme (Catinot et al., 2008) and the chorismate binding domain of NbICS is nearly identical to ICS1. As such, endogenous *N. benthamiana* proteins would likely associate similarly to ICS1 as in *Arabidopsis*. Equivalent approaches were successfully used to identify enzymes composing an indole glucosinolate pathway from *Arabidopsis* (Pfalz et al., 2011) and podophyllotoxin pathway from mayapple (Lau and Sattely, 2015).

Co-expression of ICS1 and chloroplast-localized PchB generated substantial total SA in line with previously seen values under expression of a bacterial IPL (Verberne et al., 2000), while expression of CM3 and allosteric-insensitive mutant CM1 G213A reduced SA production by roughly 50%. This result strongly suggests that CM1 and CM3 protein do not possess IPL activity. Instead, overexpression of CM1 G213A and CM3 lacking negative allosteric regulation likely increases competition for substrate between CM and ICS.

Alteration of chorismate usage impacts SA accumulation

Introduction of allosterically unregulated biosynthesis genes into the phenylalanine/tyrosine branch in *Arabidopsis* has been demonstrated to cause large metabolic shifts in aromatic amino acids and have second-order effects on downstream products. Increasing shikimate synthesis by expression of AroG, a bacterial feedback-insensitive DAHPS enzyme, increased metabolites derived from all aromatic amino acids and elevated levels of SA-glucosides (Tzin et al., 2012), demonstrating that DAHPS activity and subsequent chorismate concentration govern total metabolic output of this pathway. Perturbation of chorismate utilization via expression of feedback-insensitive *E. coli PheA* chorismate mutase/prephenate dehydratase increased phenylalanine synthesis, consequently reducing not only tryptophan biosynthesis but also the accumulation of tryptophan-derived secondary metabolites (Tzin et al., 2009).

ICS1 catalyzes a reversible reaction and functions at equilibrium. Introduction of abundant CM to convert chorismate to prephenate could deplete the chorismate pool and stimulate ICS1 to redirect isochorismate back into chorismate. This would ultimately reduce isochorismate flux to SA synthesis in this *N. benthamiana* transient assay, as seen in Fig. 2.12. This mirrors the effect seen in *cm1 #1*, in which silencing *CM1* likely increases available chorismate that is utilized by ICS1. A similar SA phenotype was seen in *Arabidopsis* plants expressing a feedback-insensitive form of *Arogenate Dehydratase 2* (*padt2-1D*) that

accumulated 80-fold greater phenylalanine than wild type (Huang et al., 2010). Among many pleiotropic effects, SA levels were elevated 4-fold, likely due to excess phenylalanine inhibiting CM1 activity, and basal *PR-1* expression was upregulated. This level of phenylalanine is atypical, and while this SA could be synthesized through an ICS-independent route, this is unlikely given that ICS accounts for nearly all induced SA synthesis in *Arabidopsis* (Garcion et al., 2008). Other phenylalanine derivatives in *padt2-1D* were not statistically different from wild type, suggesting that export from the chloroplast or PAL enzymes are rate-limiting steps.

Interestingly, the effect of silencing *CM1* in *Arabidopsis* appears to only augment low rates of synthesis, such as basal accumulation of 1-2 μg/g FW or the lower 4 μg/g FW total SA induced in response to *G. orontii* in wild type. Total SA accumulation two days after inoculation with *Pma* ES4326 is 3-fold higher than induced by *G. orontii* and reaches similar levels in both *cm1 #1* and wild type. *DAHP1* expression increases within hours of treatment with virulent and avirulent *Pma* ES4326 or *Pseudomonas syringae* pv *tomato* (Keith et al., 1991; Eberhard et al., 1996a), likely increasing chorismate concentration, as this enzyme is seen as a key regulatory step in chorismate synthesis (Tzin et al., 2012). This additional metabolic flux in the entire pathway appears to outweigh any effect of reduced CM protein on chorismate partitioning. Accordingly, there was no increase in induced camalexin in *cm1 #1* (Fig. 2.14). Metabolite profiling could reveal the extent to which chorismate metabolism is altered in this silenced line and *cm3* under both mock and inoculated plants.

Do CM1 and CM3 have different roles in primary and secondary metabolism?

Phenylalanine derivatives such as lignins and other phenylpropanoids can constitute up to 30% of total photosynthetic carbon under certain conditions (Weber and Linka, 2011). Although CM1 and CM3 both exhibit chorismate mutase activities, differential allosteric regulation and genetic phenotypes indicate they may play separate overlapping roles in chorismate metabolism. Chorismate flux to prephenate is thought to be stronger than flux of chorismate to anthranilate (Tzin and Galili, 2010). In *Arabidopsis*, CM1 is the only chorismate-utilizing enzyme to respond to allosteric modulation from the three major aromatic amino acid products of this pathway, and the only CM to experience inhibition from some of these products. This suggests it is responsible for the majority of flux to phenylalanine and tyrosine, and its activity can be indirectly affected via aromatic amino acid export from the plastid, as in petunia (Widhalm et al., 2015). CM1 has a 5- and 10-fold higher K_m for chorismate relative to ASA1 and ICS1/2, respectively (Fig. 2.1), so these enzymes likely remain competitive for chorismate at lower substrate concentrations. CM3 has an even higher K_m for chorismate, exhibits no negative allosteric regulation, and likely is responsible for a basal flux into prephenate under typical growth in leaves. As CM3 is positively regulated by histidine, cysteine and tryptophan (Westfall et al., 2014), it may serve to augment CM1 activity to increase flux to phenylalanine for use in phenylpropanoid metabolism under specific conditions or cell types. In *Arabidopsis*, silencing *cm1* had a large effect on basal total SA accumulation, but a similar impact on SA was not seen in a null *cm3* (Fig. 2.9). Total SA was reduced when CM3 was overexpressed in *N. benthamiana* (Fig. 2.8, 2.12), indicating CM3 is capable of altering chorismate flux and its function in *Arabidopsis* is likely governed by protein abundance and kinetics. To see a comparable reduction of SA in *N. benthamiana,* an allosteric-insensitive CM1 G213A was needed. This confirms that the differential allosteric regulation observed *in vitro* governs the activity of the two CMs *in planta*.

While increase in SA may enhance disease resistance, alteration of flux to phenylpropanoid production might increase the susceptibility of the host plant to filamentous

pathogens that penetrate the cell wall (Naoumkina et al., 2010). Phenylpropanoids are induced in response to the oomycete pathogen *Hyaloperonospora arabidopsidis (Hpa)* for cell wall lignification (Mauch-Mani and Slusarenko, 1996) and others may play an antimicrobial role against oomycete pathogens and powdery mildews (Shetty et al., 2011; König et al., 2014). CM3 was identified via yeast-two hybrid screening as a putative effector target of *Hpa* (Weßling et al., 2014), and though no cognate *G. orontii* effector was identified in this screen, I found that *cm3* supported powdery mildew growth with a 30% increase in spore output (Fig. 2.12) relative to wild type. Transient silencing of the plastidic CM in barley increased the penetration rate and hyphal growth of the powdery mildew *Blumeria graminis* f.sp *hordei*, indicating loss of CM-mediated phenylpropanoids likely resulted in cell wall changes or responses that advantaged fungal infection (Hu et al., 2009). Proportional contribution of CM1 and CM3 to induced and basal phenylpropanoids has not been shown for *Arabidopsis*, which makes comparison to species with only one plastidic isoform more difficult. It is possible that both *cm1 #1* and *cm3* are more susceptible to fungal penetration than wild type, but enhanced SA-mediated resistance of *cm1 #1* masks a susceptibility phenotype similar to *cm3*. This may account for the more variable spore quantification results seen in *cm1 #1*. Disruption of chorismate metabolism could also alter metabolites required by the fungus that influence spore output. The *G. orontii* spore-count metric encompasses all stages of infection, but specific analysis of penetration resistance and hyphal colony growth in *cm1 #1* and *cm3* may elucidate the difference in the two phenotypes.

Given the difficulty in isolating null *CM1* T-DNA insertion lines, it was suspected that CM1 and CM3 might have non-redundant roles, particularly in seed development. Germination rates were low for several independent T-DNA lines (Table 2.1) maintained in different collections, suggesting some level of *CM1* is necessary for seed viability. All tested T_2 *cm1*-silenced lines in wild type background had at least a 70% reduction of *CM1* expression, but that same amiRNA transformed into *cm3* did not yield *CM1* silencing in any recovered transformants confirmed to carry the transgene. Thus, while *cm3* is dispensable for seed set, plastidic CM activity appears essential. *CM1* and *CM3* are expressed at roughly equivalent levels in 4-week old leaf tissue (Fig. 2.9C), consistent with microarray data of *CM1* and *CM3* expression (Schmid et al., 2005) on the Arabidopsis E-FP browser (Winter et al., 2007; Bassel et al., 2008) that shows expression of the two genes is relatively equal (<1.5 fold difference) in most vegetative tissues. However, there is high differential expression in the developing seed (Fig. 2.17). *CM1* has higher overall seed expression in the data deposited by (Le et al., 2010) relative to *CM3*, and its transcript is most abundant in the developing seed coat, endosperm and maturing embryo. *CM3* is expressed most abundantly in the endosperm and is nearly absent in the maturing embryo. True *cm1* knockouts may be stunted during embryo development, which could be explored in future work using gene-editing tools to fully characterize this phenotype.

Elevated basal SA of *cm1 #1* increases disease resistance through early expression of resistance signaling

The phenotype identified in *cm1 #1* represents a unique class of SA-synthesis mutant: one with elevated basal SA that remains below the threshold of defense gene activation, yet primes the plant for a degree of resistance to (hemi)biotrophic bacteria. The term "priming" has many definitions (Conrath et al., 2015); for the purpose of this dissertation, it refers to any increase in resistance conferred by pre-infection SA. Basal total SA in mutants *ssi2*, *cpr1* or *cpr5*, which each have an increase of SA in excess of 20-fold relative to wild type, show pleiotropic phenotypes, including activated defense gene expression (*ie PR-1*) in the absence of a

CM1

Seed Development

Pre-globular   Globular   Heart   Linear Cotyledon   Maturation Green

Absolute
670.11
603.09
536.08
469.07
402.06
335.05
268.04
201.03
134.02
67.01
0.0
Masked

CM3

Absolute
292.58
263.32
234.06
204.8
175.54
146.28
117.03
87.77
58.51
29.25
0.0
Masked

Peripheral endosperm — General seed coat
Embryo proper —
Suspensor — Chalazal Endosperm
Micropylar endosperm — Chalazal seed coat

- Developing seeds from Ws plants were isolated from continuous light-grown plants and the indicated parts were excised by laser-capture microdissection.
- RNA was extracted and amplified, before hybridization to the ATH1 GeneChip.

Data provided by the Goldberg and Harada Labs. Images adapted from images drawn by Meryl Hashimoto. Data published in Le *et al.* 2010.

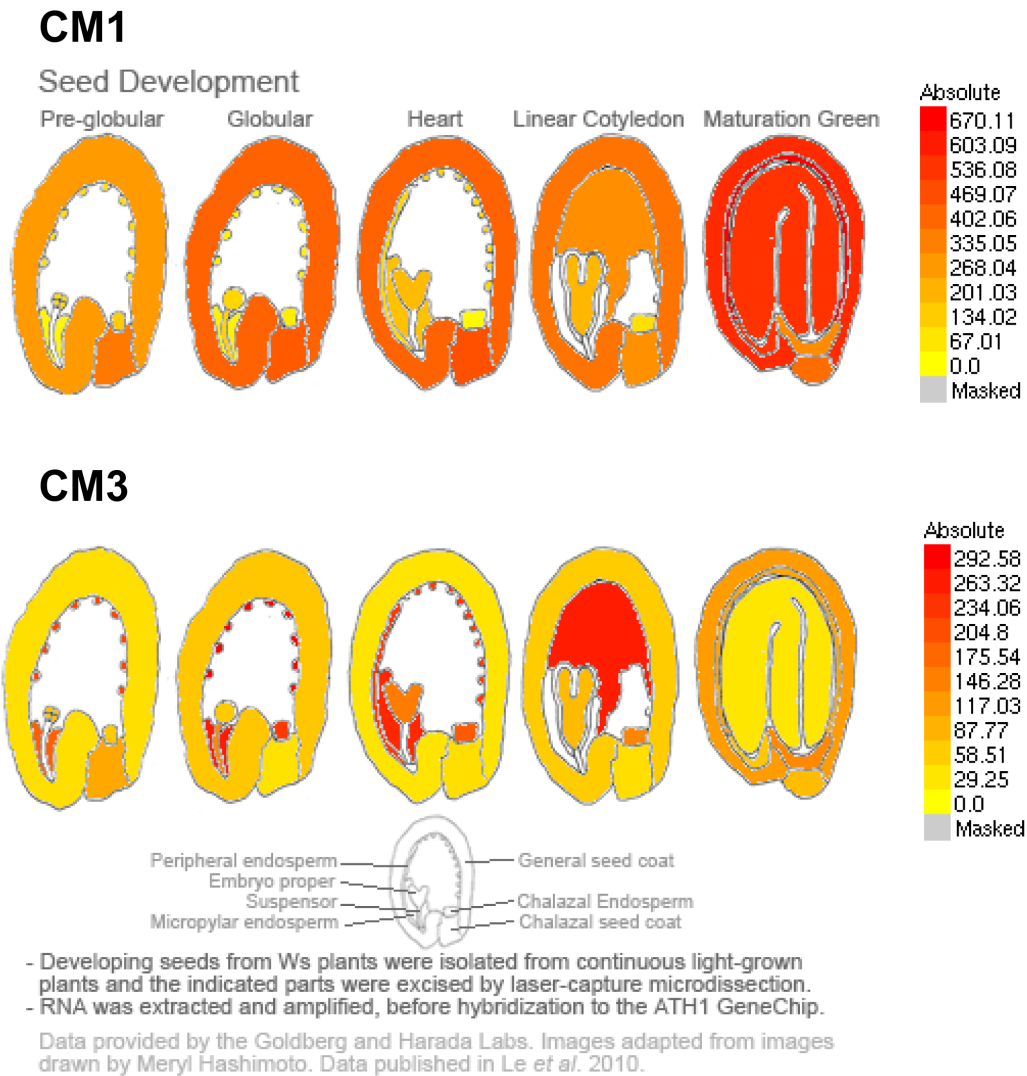**Figure 2.17: Developing-seed microarray quantification of *CM1* and *CM3* gene expression reveals differential expression in maturing embryo**
Developing seed tissue-specific expression data from Le *et al,* 2010 shows *CM1* is more highly expressed in maturing embryo and has higher expression than *CM3* overall in these tissues. *CM3* is typically lowly expressed in the developing seed, with the exception of endosperm.

pathogen elicitor, and very reduced rosette growth. Auto-active MPK3 transgenic plants show similar SA accumulation, accompanied by generation of reactive oxygen species, camalexin and spontaneous cell death (Genot et al., 2017), all of which were at least partially dependent on SA. Rather, *cm1 #1* SA accumulation is more similar to that of the atypical E2F transcriptional repressor *del1* mutant (Chapter 3, Chandran et al., 2014)), which has a 2-fold increase in SA over wild type, and also to transgenic lines expressing a cytosolic bacterial ICS and IPL fusion (c-SAS), which produce 3-fold more basal SA than wild type (Mauch et al., 2001). Still, both of these lines show a degree of elevated SA-responsive *ICS1* and/or *PR-1* expression, and *del1* plants have an SA-dependent reduction in rosette diameter. As *cm1 #1* rosettes grow normally and have no increase in basal *ICS1* (Fig. 11), this silenced line has can be used to dissect events mediated by the basal levels of SA in host-pathogen interactions prior to *de novo* SA synthesis.

Among the early responses in PTI is the accumulation of reactive oxygen species (ROS) and Ca^{2+}, which coincide with increase in SA synthesis and activation of MAP kinase phosphorylation signaling cascades (Herrera-Vásquez et al., 2015). The stress-induced MPK3/6 protein kinases were specifically phosphorylated in the kinase cascade mediated by MAPKKK ANP1 in the presence of H_2O_2 (Kovtun et al., 2000), and also via the FLS2 signaling cascade (Asai et al., 2002) and are therefore responsive to both ROS and PAMP signals. Upon infiltration with *Pma* ES4326, preliminary results show *cm1 #1* exhibits an increase in *MPK3* expression, which also corresponded to an increase in the expression of *WRKY33*, whose protein is phosphorylated by MPK3 (Mao et al., 2011) and promotes its own expression. Additional experiments are still needed to confirm this pattern, but these results suggest that elevated basal SA may activate initial responses quicker and faster than wild type.

How might this altered expression arise in *cm1 #1*? The buildup of extracellular ROS has been shown to be independent of MPK3/6 activation (Xu et al., 2014), and requires the NADPH oxidase RBOHD, which associates with components of FLS2-mediated signaling at the plasma membrane (Kadota et al., 2014). The oxidative burst associated with PTI is also influenced by basal SA; the ROS response was stronger and peaked sooner in a mutant with elevated SA and constitutive defense gene induction (*cim6,* Maleck et al., 2002) while it was similarly timed and greatly reduced in SA-deficient *ics1* upon flg22 treatment (Yi et al., 2014). It is possible that basal SA augments formation of ROS after FLS2 perception of flagellin. Intracellular ROS is thought to be generated in the chloroplast and peroxisomes, although an additional mitochondrial origin has been identified that is receptive to SA at concentrations as low as 30 μM (Belt et al., 2017).

Conclusions and resources for future characterization:
I sought to determine whether one or both of the plastid-localized chorismate mutases possessed IPL activity, catalyzing the formation of salicylic acid in *Arabidopsis*. *In vitro* and *in planta* assays did not support this hypothesis, but rather suggested that modulation of chorismate flux to prephenate can have an indirect influence on basal SA, which accumulates 3-fold compared to wild type. Interestingly, this phenotype confers a degree of disease resistance, and represents a potential route for modulating SA levels (See Chapter 4 for more discussion on this topic).

To further expand upon the work characterized here, several additional lines of inquiry should be investigated. First, further experiments should be performed to confirm relative protein levels and activity *in planta*. Although the silencing of *cm1 #1* is consistently low between individual plant replicates, its effect on SA accumulation has a degree of stochasticity, as the

standard deviation in pooled *cm1 #1* samples is greater than other genotypes (Fig. 2.9C). This could stem from biological variation in translation of the small amount of *CM1* mRNA, CM1 protein stability or CM1 modulated activity. In petunia, RNAi silencing of the plastidic *PhCM1* by 80% led to a proportional decrease in CM total activity in petal protein extracts (Colquhoun et al., 2010). The lack of an available antibody for CM1 prevented me from directly assaying protein amounts in *cm1 #1*, so I have identified a variable region in CM1 and CM3 protein that could serve as an epitope for an antibody. Crystal structure confirms that this region is in an accessible external part of the proteins. As greater resolution of the specific RNA/enzyme correlation in *cm1 #1* is informative, visualization and protein quantification should be performed.

As *in planta* function is most relevant context for studying enzyme dynamics, I've created additional genetic resources for future study of CM function and its impact on *Arabidopsis* metabolism. First, as an additional confirmation that silencing of *CM1* is responsible for the SA phenotype in *cm1 #1*, I'm developing complemented lines with modified sequence that abolishes amiRNA binding, with and without the G213A mutation, driven by a leaf-specific promoter to avoid any ill effects in embryo development. Transgenic plants have been generated and are being evaluated for expression of the transgene and restoration of wild type SA levels. Second, CM1 and CM1 G213A overexpression lines in a wild type background are similarly being generated and evaluated. These genetic complements and overexpression lines should be compared with *cm1 #1* and wild type with metabolite profiling to elucidate CM1's role in aromatic amino acid biosynthesis. Third, I've generated *cm1 #1* x *ics1* crossed plants, which can clarify that this induced basal SA and subsequent enhanced resistance is *ICS1*-dependent.

MATERIALS AND METHODS

Plants and growth conditions

Arabidopsis thaliana ecotype Col-0 were grown in Sunshine MVP in Percival growth chambers at 50% relative humidity under a 12-hour light/dark cycle at 22˚C, with 100-150 µmol m^{-2} s^{-1} of photosynthetically active light. T-DNA insertion lines were obtained from ABRC (Sundaresan et al., 1995; Alonso et al., 2003; Robinson et al., 2009) and GABI-Kat (Kleinboelting et al., 2012). Fully expanded mature leaves of 4-week old rosettes were used for all experiments, unless otherwise specified. Genotyping primers are specified in primer table 2.3.

4-5 week old plants of *N.benthamiana* were grown in Sunshine #4 mix (lacking the RESiLIENCE soil amendment) in greenhouse conditions with supplemented light for a 16-hour light/8-hour dark cycle. Plants were used prior to full development of first emerging flowers.

Production of recombinant chorismate-utilizing proteins

Cloning of expression constructs for mature ICS1-His (pSM157) and His-PchB (pSM147-1) were described previously (Strawn et al., 2007). Sharon Marr generated the CM expression vectors by cloning CM coding sequences into the NdeI and XhoI sites of pET28c (Novagen) to generate CM1-His (pSM157-4) and CM3-His (pSM157-13). Coding sequence for CM2 was cloned into pMTAC (pET28c with a lac promoter) to create CM2-His (pSM165-13). Coding sequence was truncated to exclude stop codons, and predicted chloroplast transit peptides (for

CM1 and CM3). All constructs were transformed into BL21-Codon+(DE3)-RIL *E.coli* (Agilent) for protein expression for *in vitro* assays.

Cells were grown in one liter of Terrific Broth supplemented with 0.2% glucose, 50 µg/mL chloramphenicol and 50 µg/mL kanamycin shaking at 200 rpm at 37°C, until mid-log phase (OD$_{600}$ of 0.5-0.9). Lactose-inducible recombinant protein expression was stimulated by addition of 0.1 mM IPTG (isopropyl β-D-1-thiogalactopyranoside) and cultures were transferred to 20°C for protein accumulation for 16 hours. Cells were then collected via centrifugation (8,000 g, 20 min, 4°C) and resuspended in binding buffer (300mM NaCl, 50 mM sodium phosphate buffer pH 8, 10mM imidazole, 10% glycerol) with 2 mM phenylmethylsulfynyl fluoride, 10 µM leupeptin and 10 µg/mL DNase added prior to lysis. At 4°C, cells were passed twice through a French pressure cell at 18,000 psi, centrifuged and the supernatant incubated with Ni-NTA beads (Novagen) to bind His-tagged proteins. Proteins were washed in wash buffer (300mM NaCl, 50 mM sodium phosphate pH 8, 25 mM imidazole), then eluted from the column into one-milliliter fractions with elution buffer (300 mM NaCl, 50 mM sodium phosphate buffer pH8, 250 mM imidazole) and dialyzed overnight into 50 mM TRIS-HCl pH 7.7, 10% glycerol and 1 mM dithiothreitol. Protein fractions were visualized via an 8% SDS-PAGE gel with PageRuler Protein ladder (Thermo Fischer Scientific), pooled, and quantified via the Bradford method with Coomassie Blue G-250 (EM Biosciences). Bovine serum albumin served as a standard. Purified proteins were aliquoted into 150 µL volumes and stored at -80°C until use.

Purification of isochorismate

Tristan de Rond (UC Berkeley, Dept of Chemistry) performed isochorismate isolation as described in (Hubrich et al., 2014) using barium chorismate from Sigma-Aldrich (#C1259, 70% pure) with omission of the chorismatase FKBO, as isochorismate and chorismate were sufficiently separated for fraction collection in our prep-HPLC. Briefly, chorismate was converted to isochorismate in 100 mM Tris-HCl pH 8.0, 10mM MgCl$_2$ with 5 milligrams of recombinant ICS1-His (Strawn et al., 2007) for 1 hour at room temperature. Protein was removed with a 3KDa NMWL Centriprep filter (Millipore Sigma #4303) and the solution was lyophilized for 2 days and stored at -80°C until run on the prep-HPLC. Compounds were separated in a prep-HPLC with a C18 column over an isocratic run of 8% acetonitrile and 0.1% trifluoroacetic acid. Isochorismate fractions were collected and lyophilized for 3 days to dry sample, then purity of isochorismate was assessed via NMR. Concentration of resuspended isochorismate was assayed via UV absorbance at A_{275} in a Tecan M1000 microplate reader using its molar extinction coefficient of 8,830 M^{-1} cm^{-1}.

CM and IPL *in vitro* assays with recombinant protein

Chorismate mutase activity was observed via endpoint assay as detailed in (Gilchrist and Connelly, 1987) to confirm recombinant CM proteins were active on chorismate and produced prephenate. Subsequent kinetic characterization was done by spectrophotometric assay of chorismate disappearance using a Tecan M1000 microplate reader similar to (Westfall et al., 2014). 100 ng of CM protein was incubated in 100 µL of 50 mM TRIS-HCl pH 7.7, 10 mM MgCl$_2$ and reactions were initiated by addition of varying concentrations of chorismate (reaction concentration of 0 µM, 125 µM, 250 µM, 500 µM, 1 mM, 1.5 mM, 2 mM and 3 mM). Reactions were performed in a UV-Star 96-well microplate (Grenier #655801) and pathlength was corrected via measurements at A_{975} and A_{900}, and calculations with measured K-factor of reaction buffer. Chorismate disappearance was measured at A_{274} at 10-second intervals over 30

minutes and concentration calculated using its molar extinction coefficient of 2630 M^{-1} cm^{-1}. Each reaction was run in triplicate and normalized to a no-enzyme control to account for non-enzymatic degradation of chorismate. Non-linear velocity versus substrate curves and estimates of kinetic parameters were determined using GraphPad Prism 7 (GraphPad Software, Inc).

IPL activity was determined in kinetic assays via fluorescence and via HPLC. For coupled enzyme assays, 10 µg of recombinant ICS1 was incubated alone or with 10 µg of recombinant CM1, CM2, CM3 or PchB for 3 minutes in 50 mM TRIS-HCl pH 7.7, 10 mM $MgCl_2$. Reactions were initiated with addition of chorismate to a final concentration of 1 mM and incubated for 1 hour at room temperature. A no-enzyme control with 1 mM chorismate was included. Proteins were removed from the mixture by filtration through a 3 kDa MWCO filter (Amicon #UFC500308) at 4°C and the reaction was acidified by addition of HCl to a final concentration of 3 mM, pH 1.5. 50 µL of filtered sample were loaded onto a Shimadzu HPLC system (SCL-10A system controller, SPD-M10A UV-vis photodiode array detector and RF-10AXL fluorescence detector). Compounds were separated with a Supelcosil ABZ+ reverse phase column (# 59196, 5 µm particle size, 15 cm x 4.6 mm) equilibrated in 25 mM KH_2PO_4 buffer pH 2.5 and 15% acetonitrile running at 1 mL/minute. Elution protocol was as follows: acetonitrile concentration increased linearly over 10 minutes to 20%, a linear increase over 12 minutes to 43%, a linear increase over 2 minutes up to 60%, held isocratic for five minutes and reduced linearly over 5 minutes to 15%. SPD-M10A collected spectra data from 200-400 nm. Isochorismate (retention time of 2.8 min) and chorismate (retention time of 3.2 min) were detected at A_{280} and each peak identified via UV spectra compared to standards. SA (retention time of 13.2 min) was detected via fluorescence (excitation at 305 nm and emission at 407 nm).

For kinetic IPL assay, 5µg of CM1, CM3 or PchB were incubated in reaction buffer with varying concentrations of purified isochorismate (25 µM, 50 µM, 75 µM, 150 µM). Reaction was monitored for SA production via fluorescence on a Tecan M1000 (excitation 305 nm, emission 407 nm, 5 nm band) at 10 second intervals over 30 min at room temperature. These reactions were also analyzed via HPLC, as above, 1 hour after reaction initiation.

Generation of *CM1*-silencing and transient expression constructs
Artificial miRNA and complemented CM1 for Arabidopsis
The Web miRNA Designer tool (Ossowski et al.; Ossowski et al., 2008) was used to generate an amiRNA sequence that targets *CM1*, annealing at base pairs 326-346 of the CDS. The amiRNA construct was created using primers listed in Table 2.2 using pRS300 (Detlef Weigel) as template, and attB1 and attB2 Gateway-compatible sites were added to the 5' and 3' ends, respectively, by PCR. This DNA fragment was recombined into pDONR221 (Invitrogen) using BP Clonase II (Thermo Fisher Scientific #11789020) and recombined via LR Clonase II (Thermo Fisher Scientific #11791100) into pGWB2 (Nakagawa et al., 2007), a plant-expression vector for constitutive expression of this amiRNA via the CaMV 35S promoter.
To create constructs for *CM1* complements, *CM1* coding sequence was amplified from Col-0 cDNA and Gateway-compatible sites were added to the 5' and 3' ends, omitting the stop codon. This sequence was recombined into pAUL1 and pAUL7 expression vectors (Lyska et al., 2013), and insert sequences confirmed using pHCF136 5'-CCGACGAAACAAGAAAGAGG3', p35S 5'-CGCACAATCCCACTATCCTT-3', and c-HA 5'-CGTAAGGGTAAGCGTAATCCG-3'. The Q5 Site-Directed Mutagenesis kit (NEB, #E0554S) and primers 5'-

TTGCTTTAACGCTGATACTTATGATCCTAC-3' and 5'-
AATTTTGCCCTCTCCAATAGCCCAAATATAATG-3' were used to alter nine base pairs of
the amiRNA binding site in CM1 to evade miRNA silencing.

Expression constructs for N.benthamiana assays
Coding sequences of CM1, CM3 and ICS1 were amplified from Arabidopsis Col-0 cDNA with
primers to append Gateway-cloning compatible attB1 and attB2 sites to the 5' and 3' ends,
respectively. Stop codons were omitted and CDS kept in frame for downstream fusions in
expression constructs. To create a chloroplast-localized PchB expression construct, the first 135
bases of ICS1 cDNA or first 174 bases of CM1 cDNA (predicted CTP domains) were fused to
PchB coding sequence amplified from pSM147-1 via PCR, and attB1 and 2 tags added. PCR
fragments were recombined via BP Clonase II into pDONR221. The resulting pDONR221
constructs were linearized by digestion with PvuI, and inserts recombined into pGWB14
((Nakagawa et al., 2007) and pEarleyGate102 (Earley et al., 2006) to create –HA and –CFP c-
terminal expression constructs. Primers 5'-TGGTAACTACGCCTCAACAGCTG-3' and 5'-
TCATCGCCTTTCTTCACAAG-3' were used to generate CM1 G213A expression constructs
using site-directed mutagenesis as above. Sequences were confirmed using primers 5'-CCACCC
ACGAGGAGCATC-3' and 5'-GCAATTGTTTGTTATTGTGG-3', which flank the insertion
site.

All constructs were transformed via electroporation into *Agrobacterium tumefaciens* GV3101.

Generation of transgenic *Arabidopsis* plant lines
Arabidopsis plants were transformed via floral dip method adapted from (Clough and Bent,
1998). Briefly, flowers of Col-0 plants were cut back one time to increase number of flowers,
then utilized a week later. *Agrobacterium tumefaciens* GV3101 harboring miRNA-silencing or
transgene binary vectors were grown overnight in LB liquid culture at 28°C, collected via
centrifugation and resuspended in a 5% sucrose, 10 mM $MgCl_2$ 0.03% Silwet-77 solution, to an
OD_{600} of 0.8. Flowers were swished in bacterial suspension for 1 minute, and then covered for 24
hours before returning to growth lights. T_1 seed were surface sterilized for 8 minutes in a 50%
bleach, 0.1% Triton-X solution and selected on 1% sucrose plates supplemented with 1/2X
Murashige and Skoog salts and appropriate antibiotics as in (Harrison et al., 2006). For amiRNA
lines, 50 µg/mL hygromycin and carbenicillin were used. 50 µg/mL hygromycin and 20 µg/mL
glufosinate were used for *cm1#1* transformed with pAUL1 or 7 carrying miRNA-resistant *CM1*.
T_1 plants were moved to soil and T-DNA insertion confirmed via genotyping. T_2 seed were sown
on selection to analyze segregation ratios and screened via qRT-PCR for reduced *CM1*
expression relative to Col-0 using primers in 2.1. Experiments on *cm1#1* were performed on T_4
homozygous lines.

Transient expression in *N. benthamiana*
Agrobacterium tumefaciens GV3101 strains carrying binary vectors (modified pGWB14 or
pEarleyGate102 detailed above) were inoculated into 30 mL cultures of LB supplemented with
50 µg/mL each of kanamycin, gentamycin and rifampicin and grown overnight at 28°C shaking
at 220 rpm until cultures appeared dense. GV3101 with no binary vector served as a control, and
was grown as above in LB supplemented with 50 µg/mL each of gentamycin and rifampicin.
Cells were collected via centrifugation at 3,000 rpm for 10 minutes, then resuspended in
induction medium (10 mM $MgCl_2$, 10 mM MES-K pH5.6, 150 µM acetosyringone (Acros

Organics, #115540010) and incubated for 3 hours with gentle rocking at room temperature before use. For fluorescent protein expression in localization experiments, bacteria were resuspended to an OD_{600} of 0.5. For experiments assessing SA levels, bacteria were resuspended to an OD_{600} of 0.8, then mixed 1:1 with either GV3101 with no insert or bacteria harboring other expression constructs just prior to leaf infiltration, for an effective OD_{600} of 0.4 for each bacteria strain.

Leaves 2, 3 and 4, as specified in (Ma et al., 2012), were used for agroinfiltration. A needle was used to make a small incision into the abaxial surface of the leaf, and bacterial suspensions were infiltrated with a needless syringe to create a 2.5 cm diameter sector of apoplastic infiltration. Each leaf was inoculated with all constructs in non-overlapping regions. After agroinfiltration, plants were returned to light, and assayed after 48 hours.

Confocal microscopy of *N.benthamiana* leaves
Leaf samples were examined for presence and subcellular location of cyan-fluorescent fusion proteins with a Zeiss LSM710 laser scanning confocal microscope (NIH Grant: 1S10RR026866-01) 48 hours after agroinfiltration. Freshly cut leaf portions were mounted on slides with 50% glycerol and excited with a 405 nm laser. Two channels were used to detect CFP emission at 454-581 nm and chlorophyll autofluorescence at 647-721 nm. Scale bars were added to images using the software ImageJ (NIH).

Plant pathogen inoculation and disease susceptibility quantification
Pseudomonas syringae pv maculicola ES4326
Virulent bacteria (Dong et al., 1991) were grown overnight in King's Broth supplemented with 50 µg/mL of streptomycin shaking at 200 rpm at 28°C. Cultures in mid-log phase (OD_{600} 0.5-0.9) were collected via brief centrifugation (1 minute x 10,000g), washed twice with sterile 10 mM $MgSO_4$ and resuspended to an OD_{600} 0.0002 (10^3 CFU/cm^2). 4-week old plants were inoculated via infiltration with a needless syringe with *Pma* ES4326 or mock treated with 10 mM $MgSO_4$. Leaves 7, 8 and 9 were used from each plant, counting from first true leaves. Leaves were collected for SA quantification 2 days post inoculation, and for RNA at indicated time points.

To assess disease susceptibility, bacterial quantification was performed on plants infected as described above and assessed at the time of inoculation, and three days later. For 12 leaves per genotype, two punches per leaf were collected via cork borer (0.5 cm diameter), rinsed in sterile water, and ground via bead beating with glass beads in 1 mL of 10 mM $MgSO_4$. Serial dilutions of this suspension were plated on King's broth medium with streptomycin and colonies were counted when visible. Two dilutions and two technical replicates per leaf were used to calculate colony-forming units, presented on a log_{10} scale. Growth assays were performed three times with similar results.

Powdery mildew G. orontii
4-week old plants were infected with *G.orontii* (MGH isolate (Plotnikova et al., 1998)) via the settling tower method described in (Chandran et al., 2009) with a moderate dose of inoculum propagated for 14 days. Plants to be utilized for RNA or induced SA assays were planted with Col-0 and all mutant genotypes in each box (12 plants total) in an alternating pattern for even

inoculation. Infected leaves for RNA and SA were collected at 7 days post infection alongside uninfected plants and frozen at -80˚C until processing.

Fungal spore output was used as an indicator of powdery mildew fitness. Quantification was performed by Amanda McRae. Col-0 and a single mutant genotype per box were sown for spore quantification in an alternating pattern, six plants each. Spore quantification assays were performed on adult plants similar to (Weßling and Panstruga, 2012), with some modification. Briefly, PM-covered leaves of five plants (3 leaves per plant) of each genotype were collected and pooled (~1 g fresh weight) 10 days after infection. Leaves were vortexed in 15 mL of 0.01% Tween-80 detergent to wash spores into suspension, then filtered through 50 µm mesh to remove large debris. Spores were concentrated via centrifugation, resuspended in 200 µL and 10 µL was loaded onto a hemacytometer (AO Bright-Line). For each sample, spores were counted from nine 1 mm^2 chambers, normalized to leaf weight and results were averaged. Experiments with Col-0 spore counts equal to or greater than 100,000 spores/g fresh weight were used. Multiple boxes were quantified per mutant in a given experiment. Independent experiments were also performed.

cDNA synthesis and quantitative RT-PCR
For each replicate, 2-3 fully expanded leaves from Arabidopsis rosettes at 4 weeks were frozen in liquid nitrogen at indicated time points and ground with two 3-mm diameter glass beads in a bead beater for 1.5 minutes. RNA was extracted using the Spectrum Plant Total RNA Kit (Sigma-Aldrich, cat# STRN50-1KT). Two µg of total RNA was treated with DNAse, then converted into cDNA using the High Capacity cDNA Reverse Transcription Kit (Applied Biosystems, cat #4368814) and diluted 1:5 with nuclease-free water. For selected genes, each sample was assayed in triplicate using 40 ng of cDNA, 500 nM of appropriate primers and iTaq Universal SYBR Green Supermix (Bio-Rad, cat# 1725124) in a 20-µL reaction, with a Bio-Rad CFX Connect Real Time PCR Detection system. Gene expression was normalized to endogenous controls Actin 2 (At3g18780). Primers used are detailed in Table 2.4.

SA and SA-glucoside extraction and quantification
SA and SA-glucosides were extracted from leaf tissue as described in (Nobuta et al., 2007), with modifications. Briefly, frozen Arabidopsis leaf samples (3 leaves each from 3 plants) or frozen *N. benthamiana* (7-8 leaf punches using a cork borer (2 cm diameter) from individual leaves) weighing between 0.2-0.5 grams fresh weight were ground in pre-chilled mortar and pestles using liquid nitrogen. Leaf material was transferred to a glass tube and 800 ng of *o*-anisic acid (Sigma Aldrich #169987) was added as an internal standard. Samples were extracted twice in 2.5 mL of 90% methanol and divided into tubes of free SA and total SA and evaporated under dry vacuum at 3 Torr. For total SA, 500 µL of 80 U/mL of β-glucosidase (Sigma-Aldrich #49290) in 100 mM Sodium Acetate (pH 5.2) was added and incubated at 37˚C for 1.5 hours. 2.5 mL of 5% trichloroacetic acid was added to both total and free SA tubes and phase extracted twice with a 1:1 mixture of cyclopentane and ethyl acetate. Organic phases were collected and evaporated under dry vacuum as before. Evaporated samples were resuspended in 150 µL of 20% methanol and passed through a 0.2 µm polytetrafluoroethylene filter (Millipore Millex-LG #SLLGR04NL). All solutions were made with HPLC-grade solvents and water.

Leaf extracts were separated using the HPLC elution program detailed previously for IPL *in vitro* assays. SA, *o*-anisic acid and camalexin were quantified via fluorescence: *o*-anisic acid was detected via excitation at 305 nm and emission at 365 nm, while SA and camalexin were detected via excitation at 305 nm and emission at 407 nm. A standard curve for each compound was generated with chemicals procured from Sigma-Aldrich (*o*-anisic acid: #169987, SA: #S-5922, Camalexin: #SML1016) and exhibited linear detection in the relevant range ($R^2 = 0.999$).

Primer tables on next page.

Primers for insert construction (5'-3')			
Name	**Purpose**	**Primer**	**Reference**
CM1 I-miR-s	amiRNA construct	GATATTGTAACAGTACGTGGCTCCTCTCTTTTGTATTCCA	This study
CM1 II-miR-a	amiRNA construct	AGGAGCCACGTACTGTTACAATATCAAAGAGAATCAATGA	This study
CM1 III miR*s	amiRNA construct	AGGAACCACGTACTGATACAATTTCACAGGTCGTGATATG	This study
CM1 IV miR*a	amiRNA construct	GAAATTGTATCAGTACGTGGTTCCTACATATATATTCCTA	This study
Oligo A	amiRNA construct	CTGCAAGGCGATTAAGTTGGGTAAC	Web MiRNA Designer
Oligo B	amiRNA construct	GCGGATAACAATTTCACACAGGAAACAG	Web MiRNA Designer
Oligo A + AttB1	For Gateway-insertion	GGGGACAAGTTTGTACAAAAAAGCAGGCTCTGCAAGGCGAT	This study
Oligo B +BttB2	For Gateway-insertion	GGGGACCACTTTGTACAAGAAAGCTGGGTCGCGGATAACAAT	This study
AttB1 with ICS1 5' F	ICS1 CTP::PchB fusion	GGGGACAAGTTTGTACAAAAAAGCAGGCTGGATGGCTTCACTTCAATTTTCTTCT	This study
ICS1 CTP 3' fused PchB 5' ATG R	ICS1 CTP::PchB fusion	CGGGAGTTTTCATCGAACATGACTCATACTTCTTG	This study
ICS1 CTP 3 ' fused PchB ATG F	ICS1 CTP::PchB fusion	CAAGAAGTATGAGTCATGTTCGATGAAAACTCCCG	This study
PchB 3' with AttB2 R	ICS1 CTP::PchB fusion	GGGGACCACTTTGTACAAGAAAGCTGGGTCTGCGGCACCCCGTGTCTGGCG	This study

Table 2.2: Primers for construction of miRNA insert and PchB expression construct

Arabidopsis Genotyping Primers (5'-3')		
Salk T-DNA LbB1.3	GATTTTGCCGATTTCGGAACC	Alonso *et al*, 2003
CM1 gene specific SK14921 R	GGCAGATAGCGTCACAGACA	This study
CM1 gene specific SK14921 F	AGCTCTGTTCACGCCGTTAT	This study
pSKI015-GW-LB2	GTTGGGCGGGTCCAGGGCGAATT TTGC	Robinson *et al*, 2009
CM1 SALK_002696 gene specific	CGCTACGCTGGGATATTTTC	This study
CM1 SALK_002696 gene specific	AGCACACATTCCATAGACCTC	This study
CM1 SALK_002696 gene specific	CTTCACCCTTGGCGATTTAC	This study
CM1 SALK_002696 gene specific	AGCACACATTCCATAGACCTC	This study
CM1 GT_3_111149 gene specific	TCGCCAAGGGTGAAGAGTAT	This study
CM1 GT_3_111149 gene specific	GCTCTCTCCAATAGCCCAAA	This study
CM1 536F05 gene specific	AATTTGAAAATATCCCAGCGTAG C	This study
GABKI KAT T-DNA	ATAATAACGCTGCGGACATCTAC ATTTT	Kleinboelting *et al*, 2012
CM3 gene specific F	CCTCTTTTGATTCTCCGATGG	This study
CM3 gene specific R	TAGGCAGCAGGATTTTCACG	This study
BASTA primer for SK14921 F	ACCCACGTCATGCCAGTT	This study
BASTA primer for SK14921 R	AAGCACGGTCAACTTCCGTA	This study
GUS primer for GT_3_111149 F	GCAACTGGACAAGGCACTAGC	This study
GUS primer for GT_3_111149 R	CGTAATAACGGTTCAGGCACA	This study
Nos promoter out of RB for pGWB2	CCAAACGTAAAACGGCTTGT	This study
FRA1 GS 1	GGGAGACTTTGGAGGTGGAA	This study
At5g47830 GS	TGCCATTACAGAAGCACAGC	This study

Table 2.3- Genotyping primers for CM T-DNA mutants and *cm1 #1*

Locus	Name	Primer	Reference
At3g62250	*UBQ5* qPCR-F	GAAGACTTACACCAAGCCGAA	Chandran *et a*l, 2014
	UBQ5 qPCR-R	TTCTGGTAAACGTAGGTGAGT	
At3g18780	Actin2 qPCR	GGTAACATTGTGCTCAGTGGTGG	Li *et a*l, 2011
	Actin2 qPCR	AACGACCTTAATCTTCATGCTGC	
At1g74710	*ICS1* qPCR-F	GAATTTGCAGTCGGGATCAG	Chandran *et a*l, 2014
	ICS1 qPCR-R	AATTAATCGCCTGTAGAGATGTTG	
At3g29200	*CM1* qPCR-F	TTTGATCCGTCAAGAGGACAG	This study
	CM1 qPCR-R	TGCAACACCTTTGGGTACTG	
At1g69370	*CM3* qPCR-F	TTCTCCCCAGACTGGTCAAG	This study
	CM3 qPCR-R	AGCTGTGTCCGGTCTTGTTC	
At2g14610	*PR-1* qPCR-F	GAAAACTTAGCCTGGGGTAGC	Chandran *et a*l, 2014
	PR-1 qPCR-R	TTCATTAGTATGGCTTCTCGTT	
At5g47820	*FRA1* qPCR-F	GCTTTGCTAGGGCTTCATCGTTG	Zhu *et al*, 2015
	FRA1 qPCR-R	CGACCACGGTTTGTAAAAGCACG	
At5g47830	qPCR -F	CAAGCTCTCCAAGCGGTCGTG	This study
	qPCR-R	GCAAGAGGCTGTGCTTCTGT	
At3g45640	*MPK3* qPCR-F	TGACGTTTGACCCCAACAGA	Beckers *et al,* 2009
	MPK3 qPCR-R	CTGTTCCTCATCCAGAGGCTG	
At2g43790	*MPK6* qPCR-F	CCGACAGTGCATCCTTTAGCT	Beckers *et al,* 2009
	MPK6 qPCR-R	TGGGCCAATGCGTCTAAAAC	
At4g23550	*WRKY29* qPCR-F	GCGTAAATACGGGCAGAAAC	Trujillo *et al*, 2008
	WRKY29 qPCR-R	GGTTTGGGTTGGGAAGTTTT	
At2g38470	*WRKY33* qPCR-F	GTGATATTGACATTCTTGACGA	Mao *et al,* 2011
	WRKY33 qPCR-R	GATGGTTGTGCACTTGTAGTA	
At5g46330	*FLS2* qPCR-F	ACTCTCCTCCAGGGGCTAAGGAT	Boutrot *et al*, 2010
	FLS2 qPCR-R	AGCTAACAGCTCTCCAGGGATGG	

Table 2.4: qRT-PCR primers used in this study

REFERENCES

Alonso JM, Stepanova AN, Leisse TJ, Kim CJ, Chen H, Shinn P, Stevenson DK, Zimmerman J, Barajas P, Cheuk R, et al (2003) Genome-Wide Insertional Mutagenesis of Arabidopsis thaliana. Science (80-) **301**: 653 LP-657

Asai T, Tena G, Plotnikova J, Willmann MR, Chiu W-L, Gomez-Gomez L, Boller T, Ausubel FM, Sheen J (2002) MAP kinase signalling cascade in Arabidopsis innate immunity. Nature **415**: 977–983

Bassel GW, Fung P, Chow T -f. F, Foong JA, Provart NJ, Cutler SR (2008) Elucidating the Germination Transcriptional Program Using Small Molecules. Plant Physiol **147**: 143–155

Beckers GJM, Jaskiewicz M, Liu Y, Underwood WR, He SY, Zhang S, Conrath U (2009) Mitogen-Activated Protein Kinases 3 and 6 Are Required for Full Priming of Stress Responses in Arabidopsis thaliana. Plant Cell Online **21**: 944–953

Belt K, Huang S, Thatcher LF, Casarotto H, Singh KB, Van Aken O, Millar AH (2017) Salicylic Acid-Dependent Plant Stress Signaling via Mitochondrial Succinate Dehydrogenase. Plant Physiol **173**: 2029–2040

Bowling SA (1994) A Mutation in Arabidopsis That Leads to Constitutive Expression of Systemic Acquired Resistance. Plant Cell Online **6**: 1845–1857

Bowling SA, Clarke JD, Liu Y, Klessig DF, Dongag2 X (1997) The cpr5 Mutant of Arabidopsis Expresses Both NPRl -Dependent and NPRl -1ndependent Resistance. Plant Cell Am Soc Plant Physiol **9**: 1573–1584

Brunkard JO, Runkel AM, Zambryski PC (2015) Chloroplasts extend stromules independently and in response to internal redox signals. Proc Natl Acad Sci **112**: 10044–10049

Castellana M, Wilson MZ, Xu Y, Joshi P, Cristea IM, Rabinowitz JD, Gitai Z, Wingreen NS (2014) Enzyme clustering accelerates processing of intermediates through metabolic channeling. Nat Biotechnol **32**: 1011–1018

Catinot J, Buchala A, Abou-Mansour E, Métraux J-P (2008) Salicylic acid production in response to biotic and abiotic stress depends on isochorismate in *Nicotiana benthamiana*. FEBS Lett **582**: 473–478

Chandran D, Rickert J, Huang Y, Steinwand MA, Marr SK, Wildermuth MC (2014) Atypical E2F transcriptional repressor DEL1 acts at the intersection of plant growth and immunity by controlling the hormone salicylic acid. Cell Host Microbe **15**: 506–513

Chandran D, Tai YC, Hather G, Dewdney J, Denoux C, Burgess DG, Ausubel FM, Speed TP, Wildermuth MC (2009) Temporal Global Expression Data Reveal Known and Novel Salicylate-Impacted Processes and Regulators Mediating Powdery Mildew Growth and Reproduction on Arabidopsis. Plant Physiol **149**: 1435–1451

Choi HW, Kim YJ, Hwang BK (2011) The hypersensitive induced reaction and leucine-rich repeat proteins regulate plant cell death associated with disease and plant immunity. Mol Plant-Microbe Interact **24**: 68–78

Clough SJ, Bent AF (1998) Floral dip: A simplified method for Agrobacterium-mediated transformation of Arabidopsis thaliana. Plant J **16**: 735–743

Colquhoun TA, Schimmel BCJ, Kim JY, Reinhardt D, Cline K, Clark DG (2010) A petunia chorismate mutase specialized for the production of floral volatiles. Plant J **61**: 145–155

Conrath U, Beckers GJM, Langenbach CJG, Jaskiewicz MR (2015) Priming for Enhanced Defense. Annu Rev Phytopathol **53**: 97–119

Dean J V., Delaney SP (2008) Metabolism of salicylic acid in wild-type, ugt74f1 and ugt74f2 glucosyltransferase mutants of Arabidopsis thaliana. Physiol Plant **132**: 417–425

DeClue MS, Baldridge KK, Kast P, Hilvert D (2006) Experimental and computational investigation of the uncatalyzed rearrangement and elimination reactions of isochorismate. J Am Chem Soc **128**: 2043–2051

Dempsey DA, Vlot AC, Wildermuth MC, Klessig DF (2011) Salicylic Acid Biosynthesis and Metabolism. Arab B **9**: e0156

Dong X, Mindrinos M, Keith RD, Ausubel FM (1991) lnduction of Arabídopsís Defense Genes by Virulent and Avirulent Pseudomonas syrngae Strains and by a Cloned Avirulence Gene. Plant Cell **3**: 61–72

Earley KW, Haag JR, Pontes O, Opper K, Juehne T, Song K, Pikaard CS (2006) Gateway-compatible vectors for plant functional genomics and proteomics. Plant J **45**: 616–629

Eberhard J, Bischoff M, Raesecke HR, Amrhein N, Schmid J (1996a) Isolation of a cDNA from tomato coding for an unregulated, cytosolic chorismate mutase. Plant Mol Biol **31**: 917–22

Eberhard J, Ehrler TT, Epple P, Felix G, Raesecke H-R, Amrhein N, Schmid J (1996b) Cytosolic and plastidic chorismate mutase isozymes from *Arabidopsis thaliana*: molecular characterization and enzymatic properties. Plant J **10**: 815–821

Emanuelsson O, Brunak S, von Heijne G, Nielsen H (2007) Locating proteins in the cell using TargetP, SignalP and related tools. Nat Protoc **2**: 953–971

Emanuelsson O, Nielsen H, Heijne G Von (1999) ChloroP, a neural network-based method for predicting chloroplast transit peptides and their cleavage sites. Protein Sci **8**: 978–984

Erickson JL, Ziegler J, Guevara D, Abel S, Klösgen RB, Mathur J, Rothstein SJ, Schattat MH (2014) Agrobacterium-derived cytokinin influences plastid morphology and starch accumulation in Nicotiana benthamiana during transient assays. BMC Plant Biol **14**: 127

Gaffney T, Friedrich L, Vernooij B, Negrotto D, Nye G, Uknes S, Ward E, Kessmann H, Ryals J (2000) Requirement of Salicylic Acid for the Induction of Systemic Acquired Resistance. Science (80-) **261**: 12–14

Gaille C, Kast P, Dieter H (2002) Salicylate biosynthesis in Pseudomonas aeruginosa. Purification and characterization of PchB, a novel bifunctional enzyme displaying isochorismate pyruvate-lyase and chorismate mutase activities. J Biol Chem **277**: 21768–21775

Garcion C, Lohmann A, Lamodiere E, Catinot J, Buchala A, Doermann P, Metraux J-P (2008) Characterization and Biological Function of the ISOCHORISMATE SYNTHASE2 Gene of Arabidopsis. Plant Physiol **147**: 1279–1287

Genot B, Lang J, Berriri S, Garmier M, Gilard F, Pateyron S, Haustraete K, Van Der Streaten D, Hirt H, Colcombet J (2017) Constitutively Active Arabidopsis MAP Kinase 3 Triggers Defense Responses Involving Salicylic Acid and SUMM2 Resistance Protein. Plant Physiol **174**: 1238–1249

George Thompson AM, Iancu C V., Neet KE, Dean J V., Choe J (2017) Differences in salicylic acid glucose conjugations by UGT74F1 and UGT74F2 from Arabidopsis thaliana. Sci Rep **7**: 46629

Gilchrist DG, Connelly JA (1987) Chorismate Mutase from Mung Bean and Sorghum. Methods Enzymol **142**: 450–463

Glazebrook J, Ausubel FM (1994) Isolation of phytoalexin-deficient mutants of Arabidopsis thaliana and characterization of their interactions with bacterial pathogens. Proc Natl Acad

Sci USA **91**: 8955–8959

Gómez-Gómez L, Boller T (2000) Fls2. Mol Cell **5**: 1003–1011

Harrison SJ, Mott EK, Parsley K, Aspinall S, Gray JC, Cottage A (2006) A rapid and robust method of identifying transformed Arabidopsis thaliana seedlings following floral dip transformation. Plant Methods **2**: 19

Herrera-Vázquez A, Salinas P, Holuigue L (2015) Salicylic acid and reactive oxygen species interplay in the transcriptional control of defense genes expression. Front Plant Sci **6**: 1–9

Hu P, Meng Y, Wise RP (2009) Functional contribution of chorismate synthase, anthranilate synthase, and chorismate mutase to penetration resistance in barley-powdery mildew interactions. Mol Plant Microbe Interact **22**: 311–320

Huang T, Tohge T, Lytovchenko A, Fernie AR, Jander G (2010) Pleiotropic physiological consequences of feedback-insensitive phenylalanine biosynthesis in Arabidopsis thaliana. Plant J **63**: 823–835

Hubrich F, Müller M, Andexer JN (2014) In vitro production and purification of isochorismate using a two-enzyme cascade. J Biotechnol **191**: 93–98

Kachroo A, Lapchyk L, Fukushige H, Hildebrand D, Klessig D (2003) Plastidial Fatty Acid Signaling Modulates Salicylic Acid – and Jasmonic Acid – Mediated Defense Pathways in the Arabidopsis ssi2 Mutant. Plant Cell … **15**: 2952–2965

Kadota Y, Sklenar J, Derbyshire P, Stransfeld L, Asai S, Ntoukakis V, Jones JD, Shirasu K, Menke F, Jones A, et al (2014) Direct Regulation of the NADPH Oxidase RBOHD by the PRR-Associated Kinase BIK1 during Plant Immunity. Mol Cell **54**: 43–55

Keith B, Dongt X, Ausubelt FM, Fink GR (1991) Differential induction of 3-deoxy-D-arabino-heptulosonate 7-phosphate synthase genes in Arabidopsis thaliana by wounding and pathogenic attack. Plant Biol **88**: 8821–8825

Kleinboelting N, Huep G, Kloetgen A, Viehoever P, Weisshaar B (2012) GABI-Kat SimpleSearch: New features of the Arabidopsis thaliana T-DNA mutant database. Nucleic Acids Res **40**: 1211–1215

König S, Feussner K, Kaever A, Landesfeind M, Thurow C, Karlovsky P, Gatz C, Polle A, Feussner I (2014) Soluble phenylpropanoids are involved in the defense response of Arabidopsis against Verticillium longisporum. New Phytol **202**: 823–837

Kovtun Y, Chiu W-L, Tena G, Sheen J (2000) Functional analysis of oxidative stress-activated mitogen-activated protein kinase cascade in plants. Proc Natl Acad Sci **97**: 2940–2945

Lamb AL (2011) Pericyclic reactions catalyzed by chorismate-utilizing enzymes. Biochemistry **50**: 7476–7483

Lau W, Sattely ES (2015) Six enzymes from mayapple that complete the biosynthetic pathway to the etoposide aglycone. Science (80-) **349**: 1224–1228

Le BH, Cheng C, Bui AQ, Wagmaister JA, Henry KF, Pelletier J, Kwong L, Belmonte M, Kirkbride R, Horvath S, et al (2010) Global analysis of gene activity during Arabidopsis seed development and identification of seed-specific transcription factors. Proc Natl Acad Sci **107**: 8063–8070

Li J, Last RL (1996) The Arabidopsis thaliana trp5 Mutant Has a Feedback-Resistant Anthranilate Synthase and Elevated Soluble Tryptophan. Plant Physiol **110**: 51–59

Lynne Reuber T, Plotnikova JM, Dewdney J, Rogers EE, William Wood B, Ausubel FM (1998) Correlation of defense gene induction defects with powdery mildew susceptibility in Arabidopsis enhanced disease susceptibility mutants. Plant J **16**: 473–485

Lyska D, Engelmann K, Meierhoff K, Westhoff P (2013) pAUL: A Gateway-Based Vector

System for Adaptive Expression and Flexible Tagging of Proteins in Arabidopsis. PLoS One **8**: 1–12

Ma L, Lukasik E, Gawehns F, Takken FLW (2012) Plant Fungal Pathogens. **835**: 61–74

Macaulay KM, Heath GA, Ciulli A, Murphy AM, Abell C, Carr JP, Smith AG (2017) The biochemical properties of the two *Arabidopsis thaliana* isochorismate synthases. Biochem J **474**: 1579–1590

Maeda H, Dudareva N (2012) The Shikimate Pathway and Aromatic Amino Acid Biosynthesis in Plants. Annu Rev Plant Biol **63**: 73–105

Maleck K, Neuenschwander U, Cade RM, Dietrich RA, Dangl JL, Ryals JA (2002) Isolation and characterization of broad-spectrum disease-resistant Arabidopsis mutants. Genetics **160**: 1661–1671

Mao G, Meng X, Liu Y, Zheng Z, Chen Z, Zhang S (2011) Phosphorylation of a WRKY Transcription Factor by Two Pathogen-Responsive MAPKs Drives Phytoalexin Biosynthesis in *Arabidopsis*. Plant Cell **23**: 1639–1653

Mauch-Mani B, Slusarenko AJ (1996) Production of Salicylic Acid Precursors Is a Major Function of Phenylalanine Ammonia-Lyase in the Resistance of Arabidopsis to Peronospora parasitica. Plant Cell **8**: 203–212

Mauch F, Mauch-Mani B, Gaille C, Kull B, Haas D, Reimmann C (2001) Manipulation of salicylate content in Arabidopsis thaliana by the expression of an engineered bacterial salicylate. Plant J **25**: 67–77

Mobley EM, Kunkel BN, Keith B (1999) Identification, characterization and comparative analysis of a novel chorismate mutase gene in Arabidopsis thaliana. Gene **240**: 115–123

Nakagawa T, Kurose T, Hino T, Tanaka K, Kawamukai M, Niwa Y, Toyooka K, Matsuoka K, Jinbo T, Kimura T (2007) Development of series of gateway binary vectors, pGWBs, for realizing efficient construction of fusion genes for plant transformation. J Biosci Bioeng **104**: 34–41

Naoumkina MA, Zhao Q, Gallego-Giraldo L, Dai X, Zhao PX, Dixon RA (2010) Genome-wide analysis of phenylpropanoid defence pathways. Mol Plant Pathol **11**: 829–846

Nawrath C (2002) EDS5, an Essential Component of Salicylic Acid-Dependent Signaling for Disease Resistance in Arabidopsis, Is a Member of the MATE Transporter Family. Plant Cell Online **14**: 275–286

Nobuta K, Okrent RA, Stoutemyer M, Rodibaugh N, Kempema L, Wildermuth MC, Innes RW (2007) The GH3 Acyl Adenylase Family Member PBS3 Regulates Salicylic Acid-Dependent Defense Responses in Arabidopsis. Plant Physiol **144**: 1144–1156

Ossowski S, Fitz J, Rebecca S, Markus R, Detlef W Personal Communication.

Ossowski S, Schwab R, Weigel D (2008) Gene silencing in plants using artificial microRNAs and other small RNAs. Plant J **53**: 674–690

Pfalz M, Mikkelsen MD, Bednarek P, Olsen CE, Halkier BA, Kroymann J (2011) Metabolic Engineering in *Nicotiana benthamiana* Reveals Key Enzyme Functions in *Arabidopsis* Indole Glucosinolate Modification. Plant Cell **23**: 716–729

Plotnikova JM, Reuber TL, Ausubel FM, Pfister DH (1998) Powdery Mildew Pathogenesis of Arabidopsis thaliana. Mycologia **90**: 1009–1016

Rivas-San Vicente M, Plasencia J (2011) Salicylic acid beyond defence: Its role in plant growth and development. J Exp Bot **62**: 3321–3338

Robinson SJ, Tang LH, Mooney BA, McKay SJ, Clarke WE, Links MG, Karcz S, Regan S, Wu Y-Y, Gruber MY, et al (2009) An archived activation tagged population of

Arabidopsis thaliana to facilitate forward genetics approaches. BMC Plant Biol **9**: 101

Schmid M, Davison TS, Henz SR, Pape UJ, Demar M, Vingron M, Schölkopf B, Weigel D, Lohmann JU (2005) A gene expression map of Arabidopsis thaliana development. Nat Genet **37**: 501–506

Serrano M, Wang B, Aryal B, Garcion C, Abou-Mansour E, Heck S, Geisler M, Mauch F, Nawrath C, Metraux J-P (2013) Export of Salicylic Acid from the Chloroplast Requires the Multidrug and Toxin Extrusion-Like Transporter EDS5. Plant Physiol **162**: 1815–1821

Shetty R, Frette X, Jensen B, Shetty NP, Jensen JD, Jorgensen HJL, Newman M-A, Christensen LP (2011) Silicon-Induced Changes in Antifungal Phenolic Acids, Flavonoids, and Key Phenylpropanoid Pathway Genes during the Interaction between Miniature Roses and the Biotrophic Pathogen Podosphaera pannosa. Plant Physiol **157**: 2194–2205

Song JT, Koo YJ, Seo HS, Kim MC, Choi Y Do, Kim JH (2008) Overexpression of AtSGT1, an Arabidopsis salicylic acid glucosyltransferase, leads to increased susceptibility to Pseudomonas syringae. Phytochemistry **69**: 1128–1134

Sridharan S, Howard N, Kerbarh O, Błaszczyk M, Abell C, Blundell TL (2010) Crystal Structure of Escherichia coli Enterobactin-specific Isochorismate Synthase (EntC) Bound to its Reaction Product Isochorismate: Implications for the Enzyme Mechanism and Differential Activity of Chorismate-utilizing Enzymes. J Mol Biol **397**: 290–300

Strawn MA (2010) Isochorismate Synthase Enzymes in Arabidopsis.

Strawn MA, Marr SK, Inoue K, Inada N, Zubieta C, Wildermuth MC (2007) Arabidopsis isochorismate synthase functional in pathogen-induced salicylate biosynthesis exhibits properties consistent with a role in diverse stress responses. J Biol Chem **282**: 5919–5933

Sundaresan V, Springer P, Volpe T, Haward S, Jones JDG, Dean C, Ma H, Martienssen R (1995) Patterns of gene action in plant development revealed by enhancer trap and gene trap transposable elements. Genes Dev **9**: 1797–1810

Tan G, Gao Y, Shi M, Zhang X, He S, Chen Z, An C (2005) SiteFinding-PCR: A simple and efficient PCR method for chromosome walking. Nucleic Acids Res **33**: 1–7

Tsuji J, Jackson EP, Gage DA, Hammerschmidt R, Somerville SC (1992) Phytoalexin Accumulation in Arabidopsis thaliana during the Hypersensitive Reaction to Pseudomonas syringae pv. syringae. Plant Physiol **98**: 1304–1309

Tzin V, Galili G (2010) The Biosynthetic Pathways for Shikimate and Aromatic Amino Acids in *Arabidopsis thaliana*. Arab B **8**: e0132

Tzin V, Malitsky S, Aharoni A, Galili G (2009) Expression of a bacterial bi-functional chorismate mutase/prephenate dehydratase modulates primary and secondary metabolism associated with aromatic amino acids in Arabidopsis. Plant J **60**: 156–167

Tzin V, Malitsky S, Zvi MM Ben, Bedair M, Sumner L, Aharoni A, Galili G (2012) Expression of a bacterial feedback-insensitive 3-deoxy-d-arabino-heptulosonate 7-phosphate synthase of the shikimate pathway in Arabidopsis elucidates potential metabolic bottlenecks between primary and secondary metabolism. New Phytol **194**: 430–439

Verberne MC, Verpoorte R, Bol JF, Mercado-Blanco J, Linthorst HJ (2000) Overproduction of salicylic acid in plants by bacterial transgenes enhances pathogen resistance. Nat Biotechnol **18**: 779–783

Vlot AC, Dempsey DA, Klessig DF (2009) Salicylic Acid, a Multifaceted Hormone to Combat Disease. Annu Rev Phytopathol **47**: 177–206

Wan J, Zhang S, Stacey G (2004) Activation of a mitogen-activated protein kinase pathway in

Arabidopsis by chitin. Mol Plant Pathol **5**: 125–135

Weber APM, Linka N (2011) Connecting the Plastid: Transporters of the Plastid Envelope and Their Role in Linking Plastidial with Cytosolic Metabolism. Annu Rev Plant Biol **62**: 53–77

Weßling R, Epple P, Altmann S, He Y, Yang L, Henz SR, McDonald N, Wiley K, Bader KC, Gläßer C, et al (2014) Convergent targeting of a common host protein-network by pathogen effectors from three kingdoms of life. Cell Host Microbe **16**: 364–375

Weßling R, Panstruga R (2012) Rapid quantification of plant-powdery mildew interactions by qPCR and conidiospore counts. Plant Methods **8**: 35

Westfall CS, Xu A, Jez JM (2014) Structural evolution of differential amino acid effector regulation in plant chorismate mutases. J Biol Chem **289**: 28619–28628

Widhalm JR, Gutensohn M, Yoo H, Adebesin F, Qian Y, Guo L, Jaini R, Lynch JH, McCoy RM, Shreve JT, et al (2015) Identification of a plastidial phenylalanine exporter that influences flux distribution through the phenylalanine biosynthetic network. Nat Commun **6**: 8142

Wildermuth MC, Dewdney J, Wu G, Ausubel FM (2001) Isochorismate synthase is required to synthesize salicylic acid for plant defence. Nature **414**: 564–571

Winter D, Vinegar B, Nahal H, Ammar R, Wilson G V., Provart NJ (2007) An "electronic fluorescent pictograph" Browser for exploring and analyzing large-scale biological data sets. PLoS One **2**: 1–12

Xu J, Xie J, Yan C, Zou X, Ren D, Zhang S (2014) A chemical genetic approach demonstrates that MPK3/MPK6 activation and NADPH oxidase-mediated oxidative burst are two independent signaling events in plant immunity. Plant J **77**: 222–234

Yamasaki K, Motomura Y, Yagi Y, Nomura H, Kikuchi S, Nakai M, Shiina T (2013) Chloroplast envelope localization of EDS5, an essential factor for salicylic acid biosynthesis in *Arabidopsis thaliana*. Plant Signal Behav **8**: e23603

Yi SY, Shirasu K, Moon JS, Lee SG, Kwon SY (2014) The activated SA and JA signaling pathways have an influence on flg22-triggered oxidative burst and callose deposition. PLoS One **9**: e88951

Zaitseva J, Lu J, Olechoski KL, Lamb AL (2006) Two crystal structures of the isochorismate pyruvate lyase from Pseudomonas aeruginosa. J Biol Chem **281**: 33441–33449

Zheng X, Zhou M, Yoo H, Pruneda-Paz JL, Spivey NW, Kay SA, Dong X (2015) Spatial and temporal regulation of biosynthesis of the plant immune signal salicylic acid. Proc Natl Acad Sci **112**: 9166–9173

Zhou N, Tootle TL, Glazebrook J (1999) a Gene Required for Camalexin Biosynthesis, Encodes a Putative Cytochrome P450 Monooxygenase. Plant Cell **11**: 2419–2428

Zwahlen J, Kolappan S, Zhou R, Kisker C, Tonge PJ (2007) Structure and mechanism of MbtI, the salicylate synthase from Mycobacterium tuberculosis. Biochemistry **46**: 954–964

CHAPTER 3: The Atypical E2F DEL1 Acts At The Intersection of Plant Growth and Immunity By Controlling The Hormone Salicylic Acid
PREFACE
The material presented here was previously published in:

SUMMARY

In eukaryotes, transcriptional control of cell fate is governed by E2Fs and MYB3R proteins. Atypical E2Fs act as transcriptional repressors by selective inhibition of subsets of E2F-activated genes. The *Arabidopsis thaliana* atypical E2F DEL1 is known to promote cell proliferation through inhibition of endocycle onset in growing tissue. We find DEL1 represses accumulation of the hormone salicylic acid (SA), an established regulator of plant immunity. *DEL1* knockout plants are more resistant to pathogens and slightly smaller than wild type. Microarray, ploidy, hormone, and genetic analyses indicate resistance and size phenotypes are not due to an impact on cell ploidy, but to induction of SA and immunity in the absence of pathogen challenge. Moreover, *Enhanced Disease Susceptibility 5* (*EDS5*), required for elevated SA and immunity, is a direct target of DEL1. Together, these findings indicate DEL1 acts via the hormone SA to mediate the competition between growth and immunity in developing leaves.

INTRODUCTION

E2F and MYB3R transcription factors are evolutionarily conserved proteins that act in concert to regulate the eukaryotic cell cycle (Berckmans and De Veylder, 2009). Classical E2F transcription factors contain one E2F DNA binding domain and require a dimerization partner (DP) with a DNA binding domain for high-affinity binding to the E2F cis-acting regulatory element. The atypical E2Fs contain two DNA binding domains negating the need for a DP (Lammens et al., 2009). Atypical E2Fs can compete with classical activating E2F-DPs to preferentially repress the expression of subsets of genes. Of particular interest, both mammalian and plant atypical E2Fs have been shown to play crucial roles in endocycle control (Lammens et al., 2009). The endocycle is a variant of the cell cycle in which replication occurs without mitosis, resulting in a doubling of cellular DNA ploidy with each endocycle round.

Endoreduplication occurs as a part of development in cells of tissue that supports high metabolic activity (Nagl, 1976; Lee et al. 2009). In plants, endoploidy is a common component of development used to support cell growth in a variety of tissue, with endoreduplication preceding cell expansion and/or differentiation. Endoreduplication can also be induced by certain stressors, such as genotoxic stress, to reduce sensitivity to deleterious mutations and support growth under those conditions. In addition, symbiotic and pathogenic biotrophs that establish a sustained site of nutrient acquisition can induce localized host endoreduplication that appears to fuel the growth and reproduction of the biotroph (Wildermuth, 2010).

While mammalian atypical E2Fs, E2F7 and E2F8, maintain endocycle progression during development by preventing mitosis (Chen et al., 2012), the *Arabidopsis thaliana* atypical DP-E2F-like 1 (DEL1) protein promotes proliferation by repressing genes required for endoreduplication onset, such as the anaphase promoting complex/cyclosome (APC/C) activator *CCS52A2*, a homolog of mammalian *CDH1* (Vlieghe et al., 2005; Lammens et al., 2008). In addition, DEL1 can restrain the stress-induced switch from mitosis to the endocycle in dividing cells exposed to UV-B (Radziejwoski et al., 2011) or osmotic stress (Cookson et al., 2006) and repress expression of genes involved in DNA damage repair (Radziejwoski et al., 2011). By contrast, E2F7 and E2F8 are reported to promote DNA damage repair (Carvajal et al., 2012; Zalmas et al., 2008).

We previously showed that the obligate biotrophic powdery mildew fungus *Golovinomyces orontii* induces endoreduplication in *A. thaliana* leaf mesophyll cells directly underlying the fungal feeding structure at 5 days post inoculation (dpi) (Chandran et al. 2010; 2013). This promotes the sustained growth and reproduction of the fungus, presumably by increasing nutrient availability (Wildermuth, 2010). Furthermore, (induced) host mesophyll ploidy acts as a powdery mildew susceptibility determinant (Chandran et al., 2013) in contrast to known powdery mildew resistance determinants such as defense responses controlled by the hormone salicylic acid (SA) (e.g. Chandran et al., 2009; Wildermuth et al., 2001).

SA is induced in response to microbe-associated molecular patterns and (hemi-) biotrophic pathogens including *G. orontii* and *Pseudomonas syringae pv. maculicola* (*Pma*) (Dempsey et al., 2011; Spoel and Dong 2012). In *A. thaliana*, induced SA is synthesized in the plastid via Isochorismate Synthase 1 (ICS1) (Wildermuth et al., 2001) and exported to the cytosol by the MATE transporter Enhanced Disease Susceptibility 5 (EDS5) (Nawrath et al., 2002; Serrano et al., 2013). When sufficient SA accumulates in the cytosol, it can be converted to SA glucosides (SAG) which are readily hydrolyzed back to SA; elevated total SA (free SA plus SAG) has been correlated with the robust induction of defense gene expression and enhanced resistance (in Dempsey et al., 2011).

Herein, we find misexpression of *DEL1* has a dramatic impact on *G. orontii* growth and reproduction. However, this impact is not due to altered ploidy levels as anticipated. Instead, it results from the repression of basal SA-dependent immune responses by DEL1. *del1-1* knockout plants are smaller, have elevated basal SA and SA-dependent defense gene expression, and are more resistant to pathogens; these phenotypes are dependent on SA. Furthermore, we determine *EDS5*, an SA transporter required for robust SA accumulation, to be a direct target of DEL1. *EDS5* expression increases as *DEL1* expression is reduced, both during leaf development and in the *del1-1* knockout, consistent with DEL1 repression of SA synthesis and defense during leaf development. Although it has long been known that there is a fitness cost (i.e. reduced growth) associated with SA-controlled plant immunity, knowledge of the mechanisms underlying this tradeoff is limited. Our study suggests that DEL1 functions as a negative regulator of SA and defense in growing tissue and places DEL1, via the hormone SA, at the intersection of plant growth and immunity.

RESULTS

DEL1 impacts powdery mildew growth and reproduction on *A. thaliana*

Misexpression of *DEL1* resulted in visibly altered *G. orontii* growth on mature, fully expanded leaves of *A. thaliana* plants infected at 4 weeks (Figures 1A-B). *del1-1* knockout plants were more resistant to *G. orontii*, with powdery mildew in isolated spots and/or covering ≤ 20% of the leaf area compared to wild type (WT) plants in which assessed leaves exhibited coverage of 20-50% (Figure 1C). Conversely, a *DEL1* overexpression line (*DEL1^{OE}*) was more susceptible to *G. orontii*, with average leaf coverage of 50%. Consistent with the visual scoring, the number of asexual reproductive structures, known as conidiophores, per germinated conidium was significantly lower in *del1-1* compared with WT, while *DEL1^{OE}* supported more conidiophores per colony than WT (Figures 1D-E).

del1-1 knockout plants are slightly smaller than wild type

As shown in Figure 1A and B, *del1-1* rosette and leaf size appeared to be slightly smaller than WT. Measurements of average rosette diameter for *del1-1* vs. WT confirmed this to be statistically significant with *del1-1* rosette diameter on average 82% of WT (p ≤ 0.001), while *DEL1^{OE}* rosette diameter was not reproducibly different from WT (n≥18 per genotype, average of 3 experiments).

Impact of *DEL1* on *G. orontii* growth and reproduction is not due to altered cell ploidy or cell death

As leaves develop and expand, individual cells in a leaf exhibit a range of ploidy (e.g. Melaragno et al., 1993). At 4 ½ weeks, we observed WT basal mesophyll leaf ploidy to range from 8 to 64C, with a mean of 16C (Figure 3.2A). In response to *G. orontii*, ploidy in mesophyll cells underlying the infection site at 5 dpi shifted upward, to a mean of 64C similar to previous results (Chandran et al. 2010, 2013). Basal mesophyll ploidy distribution in leaves of uninfected *del1-1* plants was similar to WT, as was the *G. orontii* -induced shift in ploidy (Figure 3.2A). In all cases, cell DNA ploidy correlated with nuclear size (Figure 3.3). The ploidy index, a single value that integrates the ploidy distribution information, was similar for WT and *del1-1* uninfected and infected mesophyll cells, with a statistically significant *G. orontii*-induced shift in mesophyll cell ploidy underlying the fungal feeding structure (Figure 3.2B). By contrast, basal
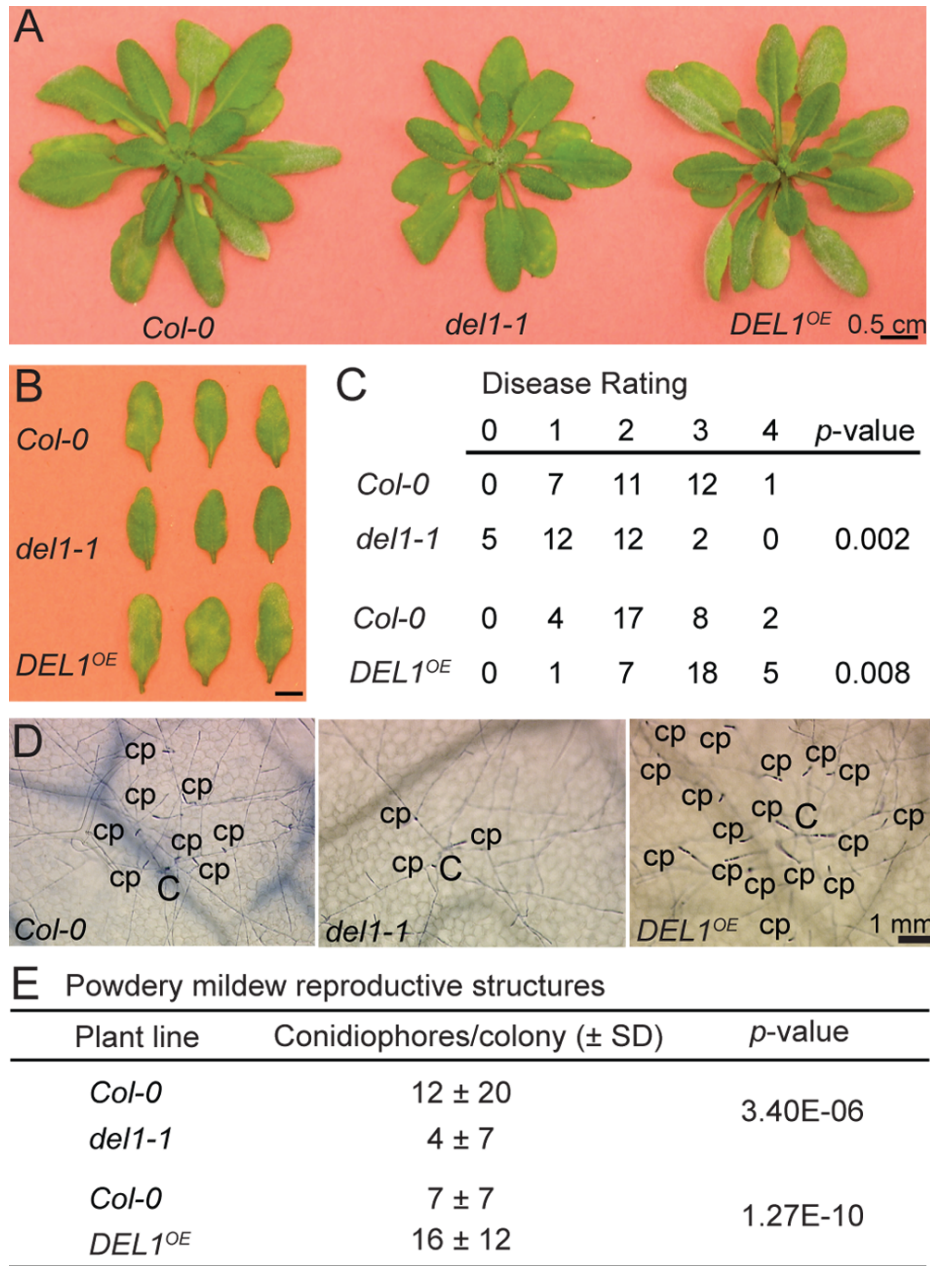
Figure 3.1 Misexpression of *DEL1* results in altered powdery mildew growth and reproduction on *A. thaliana*

(A-B) Visible *G. orontii* growth and reproduction is reduced on leaves of *del1-1* and enhanced on *DEL1^OE^* compared to WT *Col-0* at 11 dpi. Bar= 0.5 cm. **(C)** Number of plants with disease rating at 11 dpi uses scoring system: 0- no visible symptoms of infection, 1- isolated spots, 2- ~20% coverage of infected leaves, 3- ~50% coverage, 4- 100% coverage. n=31 per genotype; p-values from two-sided Fisher's exact test. **(D)** Conidiophores (cp) per initial germinated conidium (C) in WT, *del1-1* and *DEL1^OE^* visualized by trypan blue staining at 5 dpi. **(E)** No. of cp per colony on WT, *del1-1* and *DEL1^OE^* at 5 dpi. Data are mean ± SD of ≥90 colonies per genotype; p-values from Student's t-test. Each experiment was repeated at least three times with similar results.
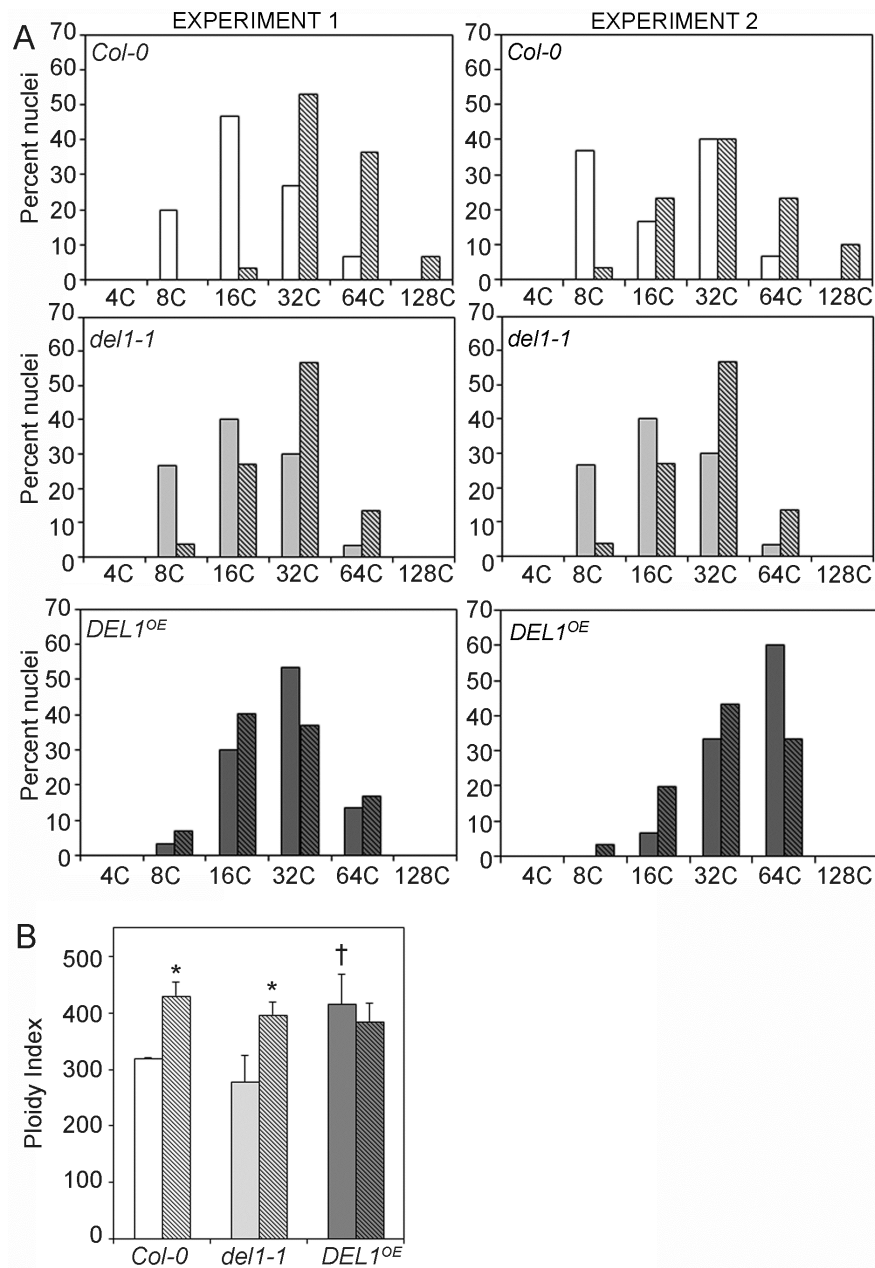
Figure 3.2. Impact of *DEL1* on *G. orontii* growth and reproduction is not due to effect on ploidy

(A) Ploidy distribution of mesophyll cells at the *G. orontii* infection site in WT, *del1-1* and *DEL1^OE* at 5 dpi from two independent experiments. Uninfected (plain bars); infected (hatched bars). n=30 nuclei per genotype per experiment. (B) Average ploidy index ±SD for WT, *del1-1* and *DEL1^OE* at 5 dpi from uninfected (plain bars) and infected (hatched bars) leaf samples of two independent assays. n=30 nuclei per genotype per experiment. Ploidy index= (%4C nuclei*1) + (%8C nuclei*2) + (%16C nuclei*3) + (%32C nuclei*4) + (%64C nuclei*5). p<0.005, from Fisher's exact test for infected vs. uninfected (*) and uninfected mutant vs. WT (†).
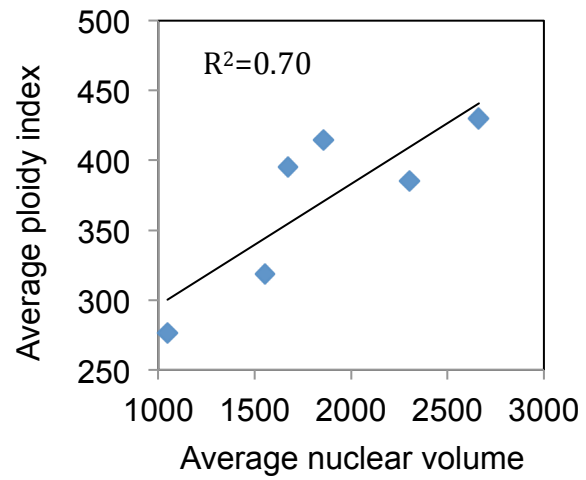
Figure 3.3. Nuclear DNA content is proportional to nuclear size
Ploidy index is proportional to nuclear volume (μm^3). Data is average of two independent experiments. R^2 was determined using linear regression analysis.
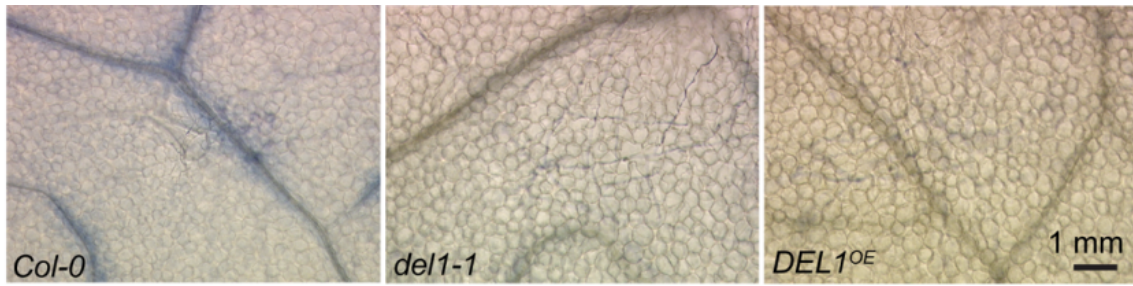
Figure 3.4. *G. orontii* **resistance of** *del1-1* **is not associated with cell death**
Absence of cell death indicated by lack of trypan blue staining in mesophyll cells underlying the haustorial complex-containing epidermal cell at 5 dpi. Each experiment was repeated at least twice with similar results.

mesophyll ploidy was elevated in $DEL1^{OE}$ compared to WT, but the *G. orontii*-induced shift to higher ploidy levels

did not occur. Because the basal mesophyll ploidy index of $DEL1^{OE}$ was significantly higher than that of WT, the induced mesophyll ploidy index in cells underlying the fungal feeding structure was not statistically different from WT, despite the lack of induced endoreduplication. Therefore, final induced mesophyll ploidy in cells underlying the fungal feeding structure was not appreciably different from WT for either *del1-1* or $DEL1^{OE}$ (Figure 3.2B). This indicated altered induced mesophyll ploidy was not responsible for the powdery mildew phenotypes.

Since enhanced resistance of *A. thaliana* mutants to powdery mildews can be due to activated cell death responses (Micali et al., 2008) and misexpression of mammalian atypical E2Fs impacts apoptosis (Lammens et al., 2009), we examined whether cell death is activated in *del1-1* or $DEL1^{OE}$ leaves compared to WT. Similar to WT, cell death was not observed in epidermal or mesophyll cells of *del1-1* or $DEL1^{OE}$ constitutively or 5 dpi with *G. orontii* (Figure 3.4).

Microarray analysis of *del1-1* suggests altered SA-associated defense responses are responsible for the *G. orontii* phenotypes of *del1-1* and $DEL1^{OE}$

To provide insight on process(es) contributing to the enhanced resistance of *del1-1* to *G. orontii*, we performed microarray analysis of leaves from *del1-1* and WT, *G. orontii* -infected and uninfected plants. Lack of *DEL1* impacted basal (uninfected) gene expression (436 genes), with a much reduced effect 5 dpi with *G. orontii* (113 genes). Thirty-four genes exhibited altered regulation in both datasets. More than 75% of these genes exhibited enhanced expression in *del1-1* compared to WT, consistent with DEL1's known function as a transcriptional repressor. Moreover, the extent of enhanced expression was more dramatic in the uninfected samples than in the infected samples indicating basal expression, not induction, to be most impacted.

Functional process analysis of genes with altered expression in uninfected *del1-1* vs. WT did not show 'Cell Cycle' or other related categories to be statistically enriched. Instead 'Cell Rescue, Defense, and Virulence' and 'Interaction with the Environment' categories were most enriched (Table 3.1A), with these genes being in the up-regulated gene set. No process categories were statistically enriched in the down-regulated gene set of uninfected *del1-1* vs. WT or in the total, up-, or down-regulated gene sets of *G. orontii* – infected *del1-1* vs. WT; this was likely due to the limited number of genes in these datasets.

As shown in Table 3.1A, the basal expression of genes involved in Defense/Stress response was elevated in *del1-1* including those associated with SA accumulation and SA-dependent defense responses (Table 3.1B). For example, the SA biosynthetic gene *ICS1* exhibited constitutively elevated expression in *del1-1*, as did the SA-dependent defense gene *Pathogenesis-related Protein 1* (*PR-1*).

Enhanced resistance and size phenotypes of *del1-1* are SA-dependent

RT-qPCR analysis showed basal expression of *ICS1* and *PR-1* was elevated in *del1-1* compared to WT in agreement with the microarray data (Figures 2A-B). Furthermore, total SA accumulation (free SA plus SAG) was elevated in *del1-1* compared to WT (Figure 3.5C, Figure 3.6). By contrast, free SA alone was not statistically different in *del1-1* versus WT.

Parallel analysis of $DEL1^{OE}$ found an opposite pattern of response with basal *ICS1* expression and total SA accumulation reduced in $DEL1^{OE}$ compared to WT (Figure 3.6). *PR-1* expression in $DEL1^{OE}$ was similar to WT, consistent with a lack of SA-induced defense in WT and $DEL1^{OE}$.

Table 3.1. Microarray analysis of *del1-1* indicates up-regulation of plant defense responses including genes required for SA synthesis and accumulation in the absence of pathogen challenge.

(A) *Arabidopsis* Munich Information Center for Protein Sequences functional process categories impacted in uninfected *del1-1* versus WT *Col-0* are shown with the number of genes in each category compared with the total number of genes in each category on the ATH1 array. BIOMAPS analysis was performed on genes up-regulated 1.5 fold or higher (p≤0.05) in *del1-1* compared to WT. Functional categories that met a p-value cut-off of < 5.00E-05, calculated using Fisher exact test, are shown.

MIPS functional process category	No. of genes in each category	No. of genes in each category on ATH1 array	*p*-value
CELL RESCUE, DEFENSE AND VIRULENCE	42	1176	9.53E-11
stress response	22	714	3.67E-05
disease, virulence and defense	17	348	1.03E-06
INTERACTION WITH THE ENVIRONMENT	34	1296	7.56E-06
cellular sensing and response to external stimulus	34	1161	7.22E-07
response to biotic stimulus	11	202	3.38E-05
calcium binding	10	158	2.31E-05

(B) Expression of genes required for SA synthesis and accumulation is constitutively up-regulated in *del1-1*. vs. WT (1.5-fold change threshold and p≤0.05).

Locus ID	Gene Name	Description	Function	*del1-1* versus WT ratio
At1g74710	*ICS1*	Isochorismate synthase	Total SA accumulation	4.4
At4g39030	*EDS5*	MATE transporter	Total SA accumulation	6.1
At5g13320	*PBS3*	GH3 acyl-adenylate/thioesterforming enzyme	Total SA accumulation	10.6
At2g14610	*PR1*	Pathogenesis-related protein	SA-dependent defense	32.0
At1g75040	*PR5*	Pathogenesis-related protein	SA-dependent defense	18.6
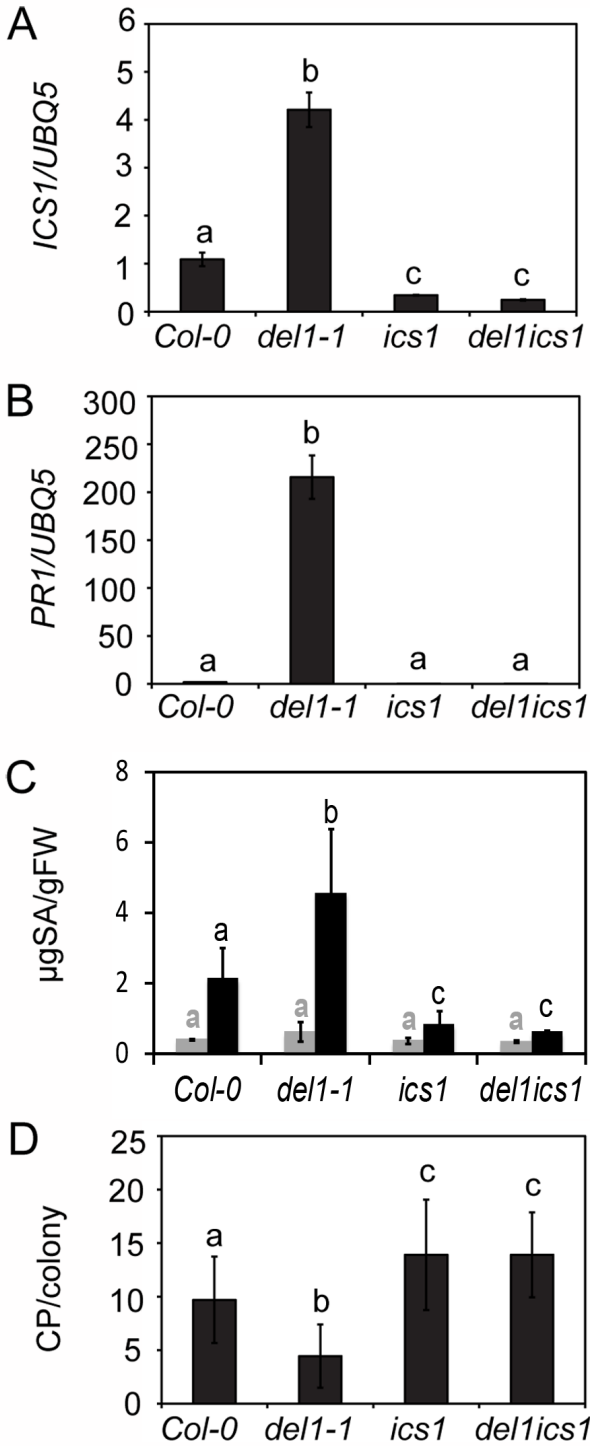
Figure 3.5. DEL1 controls basal levels of SA

(A-B) *ICS1* and *PR-1* transcripts measured in leaves of WT, *del1-1*, *ics1* and *del1-ics1* plants by RT-qPCR. All values were normalized to the *UBQ5* housekeeping gene. Data are mean ± SD, n=3.
(C) Free (grey) and total (black) SA accumulation in leaves of WT, *del1-1*, *ics1* and *del1-ics1* plants. Data are mean ± SD, n=3.
(D) Number of conidiophores (CP) per colony on WT, *del1-1*, *ics1* and *del1-ics1* leaves 5d after *G. orontii* infection. Data are mean ± SD of ≥90 colonies per genotype; p<0.005.

Letters indicate statistically significant differences between genotypes; p<0.05 unless specified. For all assays, independent experiments gave similar results.

Figure 3.6. Misexpression of *DEL1* alters basal SA-associated gene expression and total SA levels
(A&B) *ICS1* and *PR-1* transcripts assessed by RT-qPCR, normalized to housekeeping gene *UBQ5*. Shown are mean ±SD, n=3.
(C) Free and Total SA (free SA plus SA glucosides). Shown are mean ± SD, n=3. Letters indicate statistical differences, $p < 0.05$. An independent experiment gave similar results.

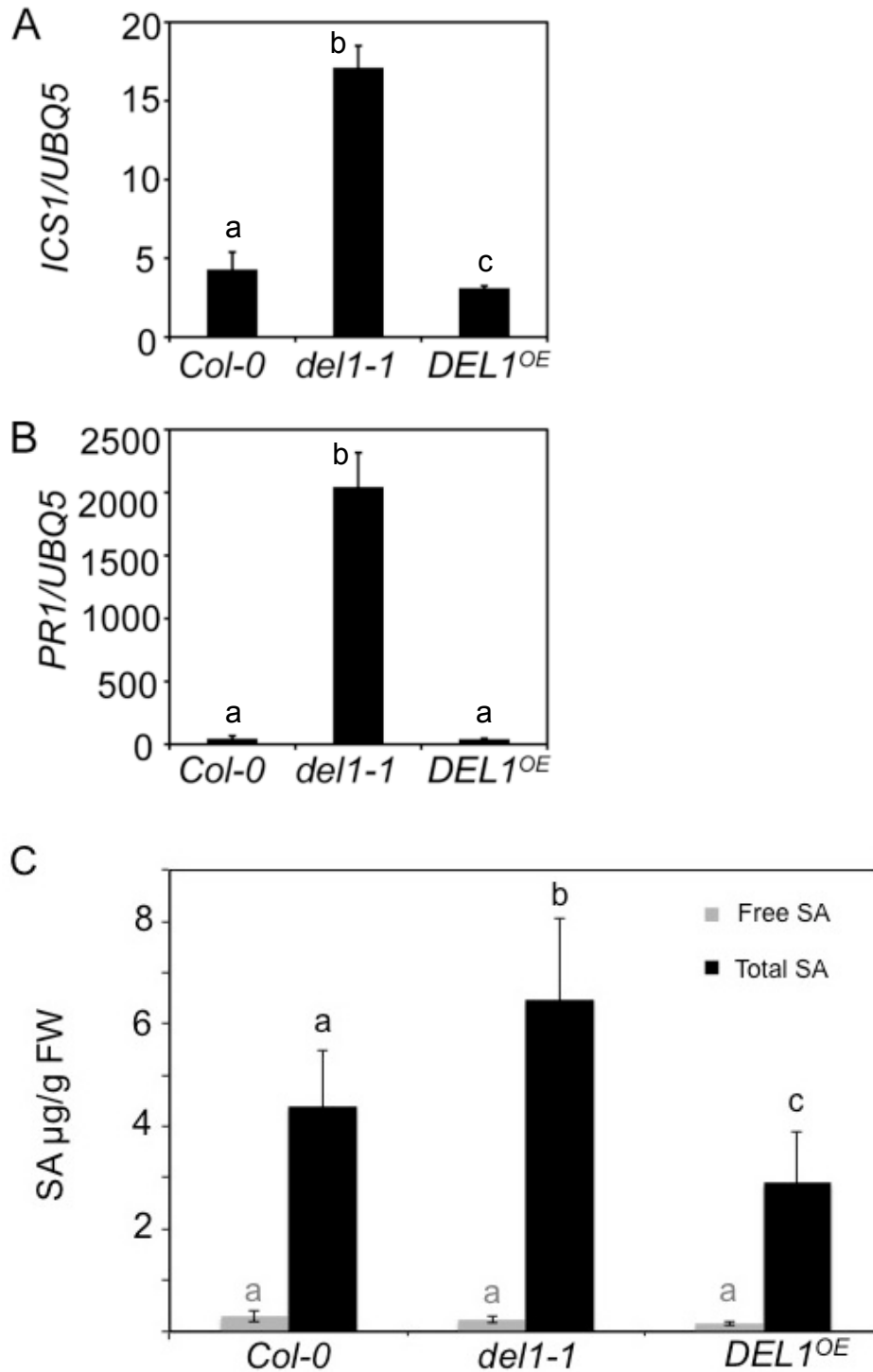To determine whether elevated basal SA synthesis and response is responsible for the enhanced resistance of *del1-1* to *G. orontii*, a *del1-ics1* double mutant was created. In the double mutant, basal *PR-1* expression was no longer elevated (Figure 3.5B), and total SA accumulation was significantly lower than WT and similar to that of *ics1* (Figure 3.5C). Moreover, *del1-ics1* was more susceptible to *G. orontii* than WT (Figure 3.5D), similar to the *ics1* mutant, indicating the enhanced resistance of *del1-1* to *G. orontii* is SA-dependent.

Because enhanced basal SA can result in enhanced resistance to a variety of (hemi)-biotrophic pathogens that includes *Pma*, we examined *Pma* ES4326 bacterial growth in WT, *del-1*, and *del1-ics1* plant leaves. *del1-1* plants were more resistant to *Pma*, with 10-fold fewer colony forming units/cm^2 leaf area than WT at 3 dpi (Figure 3.7). Similar to our results with *G. orontii*, the enhanced resistance of *del1-1* to *Pma* was no longer observed in the *del1-ics1* double mutant (Figure 3.7). Instead, *del1-ics1* double mutants exhibited enhanced bacterial growth comparable to that routinely reported for *ics1* (e.g. Dewdney et al. 2000).

In addition, the reduction in rosette size of *del1-1* can be attributed to elevated basal total SA, as this phenotype was not evident in the *del1-ics1* double mutant (Figure 3.2).

EDS5, a regulator of SA biosynthesis, is a DEL1 target

To ascertain the mechanism by which DEL1 controls basal SA levels, we searched for E2F binding sites (WTTSSCSS; W=A/T; S=C/G) using PLACE (Higo et al. 1999) in the 1 kbp sequence upstream of the translational start site of genes known to impact SA accumulation that also showed elevated expression in *del1-1* compared to WT (Table 3.1B). Of these genes, only the SA transporter *EDS5* contains an E2F-binding site (AAACCGCG) in its promoter. The E2F site is located 55 bp upstream of the translational start site, in reverse orientation (Figure 3.8B). Like the SA biosynthetic mutant *ics1*, *eds5* mutants accumulate dramatically reduced levels of SA after pathogen inoculation and exhibit enhanced susceptibility to virulent pathogens (Nawrath et al. 2002). Moreover, co-expression analysis of curated *Arabidopsis* microarray data using ATTED-II (Obayashi et al. 2009) showed expression of *ICS1* and *EDS5* to be highly correlated across pathogen treatment datasets (r^2=0.8). Therefore, we proposed *EDS5* to be a direct target of DEL1.

To test our hypothesis, we performed chromatin immunoprecipitation (ChIP) assays on WT and *del1-1* leaves using a DEL1-specific antibody (Lammens et al., 2008). Since DEL1 is expressed in actively dividing cells, expanding leaves of WT and *del1-1* were used for the assay. ChIP DNA was screened by qPCR with primers spanning the identified E2F-binding site for an enrichment of the *EDS5* promoter in WT versus *del1-1*. Primer pairs designed to amplify promoter regions of the *PHR1* (AT1G12370) gene previously shown to be bound by DEL1 (Radziejwoski et al., 2011) were used as a positive control. Similar to *PHR1* (Figure 3.9), ChIP-qPCR with primers spanning the predicted E2F-binding site of *EDS5* clearly resulted in an enriched precipitation of the *EDS5* promoter in WT versus *del1-1* samples (Figure 3.8C). Within the *EDS5* promoter, enrichment occurred at the E2F-binding site, but not in a distal (control) region (Figure 3.8D).

DEL1 is primarily expressed in dividing cells with its expression decreasing as leaves age (Lammens et al. 2008; Radziejwoski et al., 2011). If *EDS5* is repressed by DEL1, its expression should increase with leaf age. Analysis of published microarray data from an *Arabidopsis* leaf developmental series showed this to be the case (Figure 3.10). To confirm these results of others, we examined leaf age-dependent expression of *DEL1* and *EDS5* in 3-week-old WT plants. As expected, we found *DEL1* expression was highest in leaf 10 (youngest leaf) with reduced
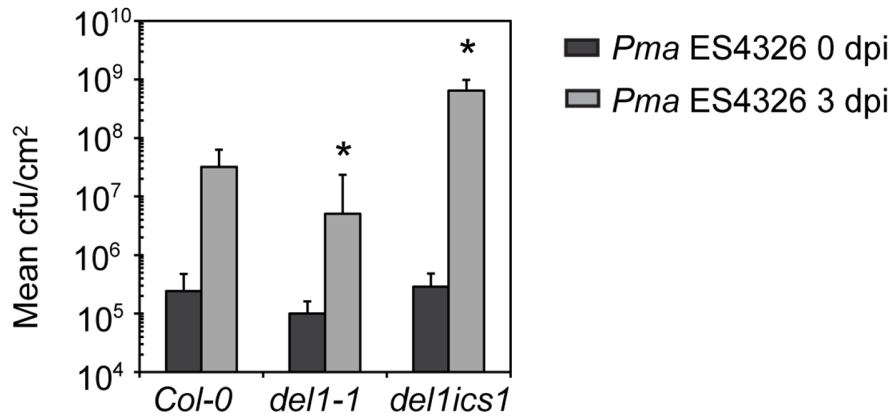
Figure 3.7. Enhanced resistance of *del1-1* to *Pma* ES4326 is SA-dependent.
Growth of *Pma* ES4326 assessed in WT, *del1-1* and *del1-ics1* leaves inoculated with bacterial suspension (OD_{600}=0.0002) in 10 mM $MgSO_4$ and harvested at 0 and 3 dpi. Mean cfu (colony forming units)/cm^2 ±SD, n=8-9 per genotype.
 *$p<0.05$, from Student's t-test for comparison to WT. An independent experiment gave similar results.

	Rosette diameter (cm)		
	Col-0	*del1-1*	*del1-ics1*
Mean (±SD)	4.9 ± 1.0	4.4 ± 0.8	4.9 ± 0.6
p-value		0.03	0.92

N=34 per genotype; p-value for difference from WT was derived using Student's t-test. An independent experiment gave similar results.

Table 3.2. Smaller plant size of *del1-1* is rescued in *del1-ics1* double mutant.
Rosette diameter of four-week-old wild type *Col-0*, *del1-1*, and *del1-ics1* double mutant plants.

expression in older leaves (Figure 3.8E). *EDS5* showed the opposite pattern with low expression in younger leaves and highest expression in leaf 5, the oldest leaf (Figure 3.8E). Taken together, our results indicate that DEL1 can bind to the *EDS5* promoter via the E2F-binding site and repress its transcription. Because EDS5, like ICS1, is required for SA accumulation, our data suggests DEL1 represses SA accumulation and associated defense in growing tissue through repression of basal *EDS5* gene expression (Figure 3.8F).

DISCUSSION

During plant development, cell proliferation is often followed by endoreduplication associated with cell expansion and/or differentiation. Reduced levels of the atypical E2F protein DEL1 is (in part) responsible for this transition as *DEL1* overexpression reduces leaf cell endoreduplication and expansion in dividing cells, while leaves of *del1-1* exhibit increased cell DNA ploidy and size (Vlieghe et al., 2005). To our initial surprise, leaf mesophyll cell ploidy was unaltered in *del1-1* and leaf/rosette size was smaller than WT. Furthermore, *DEL1^{OE}* leaf mesophyll cell ploidy was elevated, not reduced, with no statistically significant impact on leaf/rosette size. *DEL1* is normally expressed in dividing cells and initial studies focused on leaves or other organs with actively dividing cells, often of the epidermis. By contrast, our study was conducted on specific mesophyll cells of unstressed fully-expanded leaves of mature 4 ½ week old plants grown in environmentally controlled chambers. Therefore, any alteration associated with an accelerated/delayed transition from mitosis to the endocycle in dividing cells due to misexpression of *DEL1* was probably minimized by our controlled growth environment and/or compensated for during plant development to maturation. Furthermore, although endoploidy correlates with cell size in certain situations, altered cell/leaf size can also be attributed to ploidy-independent processes such as cell wall extensibility and/or turgor (in Cookson et al., 2006).

Since there was no difference in the *G. orontii*- induced mesophyll ploidy index of WT, *del1-1*, and *DEL1^{OE},* the impact of misexpression of *DEL1* on powdery mildew growth and reproduction could not be attributed to an effect on ploidy. Furthermore, we determined that the enhanced resistance of *del1-1* was not due to activated cell death responses. Instead, microarray analyses of *del1-1* and WT plants showed the primary transcriptional impact of *del1-1* to be on basal defense gene expression, which was up-regulated and highly enriched in *del1-1* compared to WT. This included genes required for the synthesis and accumulation of the plant defense hormone salicylic acid, such as the SA biosynthetic gene *ICS1* and the SA transporter *EDS5* as well as downstream defense genes regulated by SA (e.g. *PR-1*).

SA-dependent defense limits growth and reproduction of compatible powdery mildews (Micali et al., 2008), acting as a resistance determinant. When pathogen-induced SA accumulation is severely limited, as it is in *ics1*, SA-dependent gene expression is dramatically reduced and *G. orontii* growth and reproduction is enhanced (Chandran et al., 2009; Wildermuth et al., 2001). We found basal total SA accumulation and SA-dependent gene expression were elevated in *del1-1*, which was more resistant to *G. orontii*. Analysis of the *del1-ics1* double mutant showed the enhanced resistance of *del1-1* to *G. orontii* to be SA-dependent, as elevated basal total SA, SA-dependent gene expression, and enhanced resistance were no longer observed. Instead the *del1-ics1* double mutant phenocopied the *ics1* mutant, which was more susceptible to *G. orontii* than WT with minimal total SA accumulation and *PR-1* expression. *del1-1* also exhibited enhanced resistance to the virulent bacterial pathogen *Pma* ES4326, similar
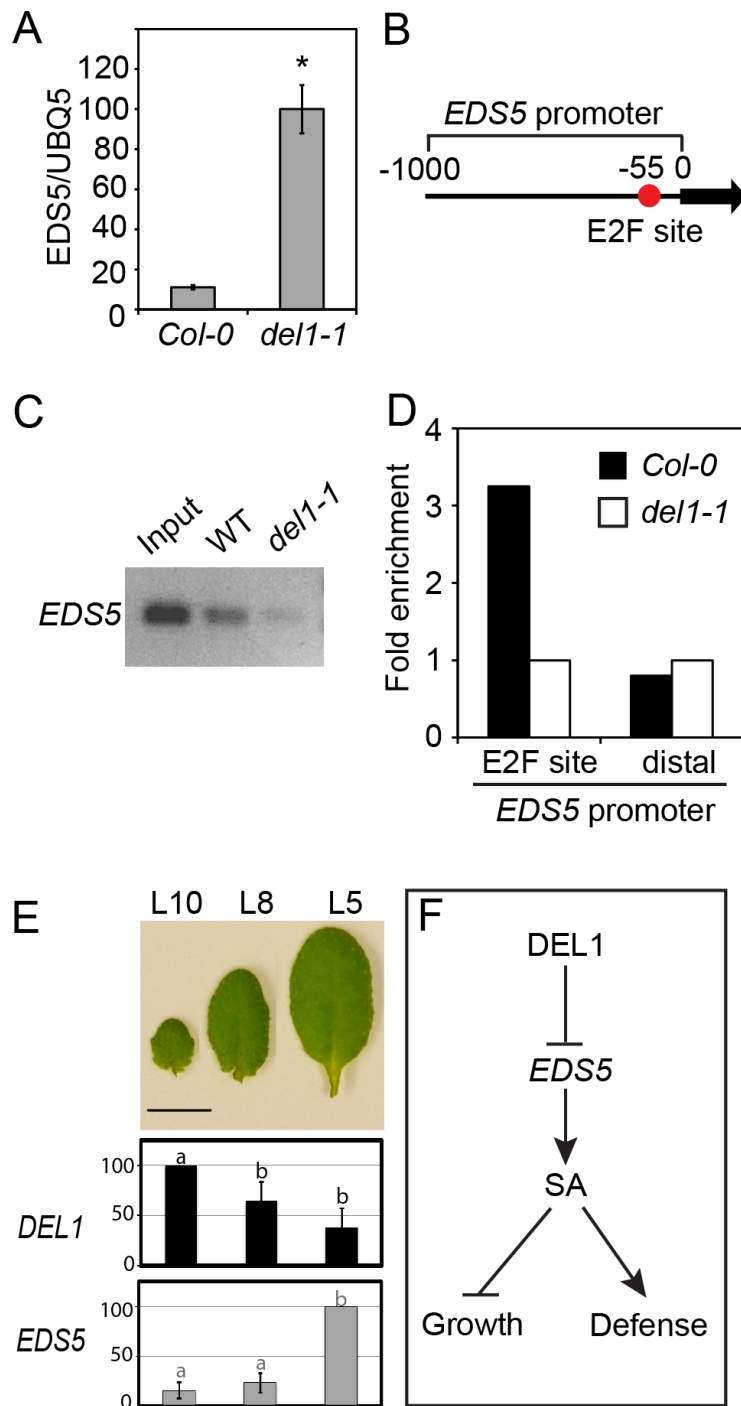
Figure 3.8 *EDS5* is a DEL1 target

(A) *EDS5* transcripts measured in leaves of WT and *del1-1* plants by RT-qPCR. All values were normalized to the housekeeping gene *UBQ5*. Data are mean ± SD, n=3; *p<0.05 using Student's t-test.

(B) *EDS5* promoter showing E2F-binding site 55 bp upstream of translational start site.

(C) ChIP analysis showing enriched binding of DEL1 to the *EDS5* promoter in WT compared to *del1-1*.

(D) qPCR of ChIP samples with primers spanning the predicted E2F-binding site of the *EDS5* promoter compared with a distal region lacking the E2F-binding site. All values were normalized to the *UBQ5* housekeeping gene.

(E) Relative change in *DEL1* and *EDS5* transcripts with leaf age. Transcripts for the tenth (L10), eighth (L8) and fifth (L5) leaf of WT plants were determined by RT-qPCR. Values were normalized to *UBQ5* and are shown as % of highest value (set to 100). Data are mean ± SD, n=3; letters indicate statistically different values, p<0.05. Bar=1cm.
For all panels, independent experiments gave similar results.

(F) Proposed role for DEL1 as a mediator of plant growth and defense via the hormone salicylic acid. DEL1 controls basal SA levels in proliferating tissue through the transcriptional repression of *EDS5,* an SA transporter required for robust total SA accumulation. Limited basal SA accumulation prevents activation of plant immunity and promotes growth.
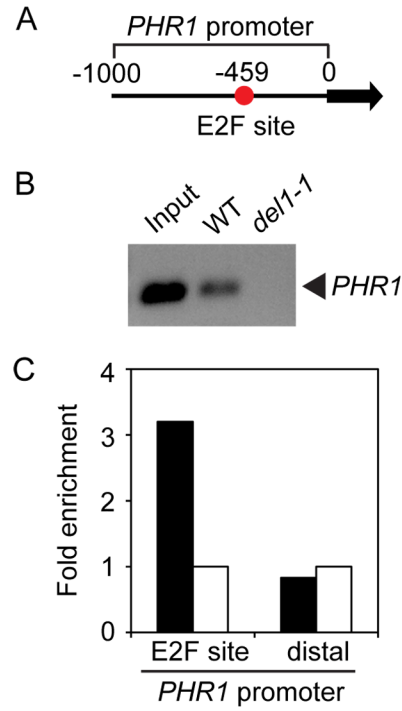
 Figure 3.9. ChIP analysis showing binding of DEL1 to the *PHR1* promoter.
(A) E2F site shown in red on the *PHR1* promoter.
(B-C) qPCR of ChIP samples shows an enrichment of the *PHR1* promoter fragment
containing the E2F-binding site and not a distal site in WT compared to *del1-1*. An
independent experiment gave similar results.
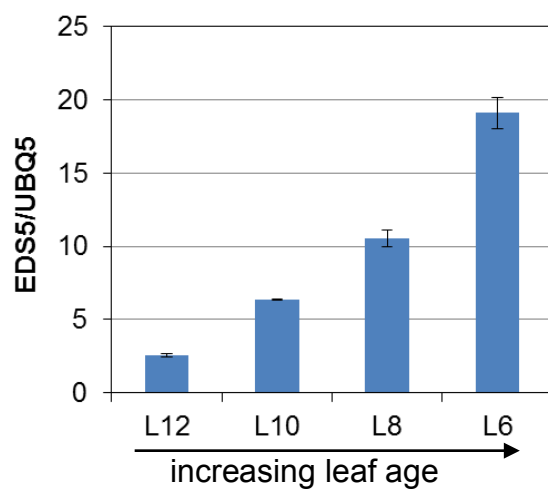
Figure 3.10. *EDS5* **expression during leaf development from the Gene Expression Map of Arabidopsis Development (Schmid et al., 2005,** *Nature Genetics* **37:501).**
Absolute expression of *EDS5* (±SD) was normalized to that of housekeeping gene *UBQ5* from *Arabidopsis* ATH1 microarray data for different age leaves (L) from 17-day-old WT Col-0 plants grown under continuous light; n=3. Leaves increase in age from youngest (L12) to oldest (L6). Note that *DEL1* is not on the *Arabidopsis* ATH1 microarray.

to that observed for other mutants with modestly elevated basal SA and no cell death (e.g. *cpr1* (Bowling et al., 1994)). Again, enhanced resistance was SA-dependent.

In our study, the slightly smaller size of *del1-1* was also a consequence of elevated basal SA as this phenotype was no longer evident in the *del1-ics1* double mutant. Mutants with elevated basal total SA are typically smaller in size than WT plants, with reduction in stature dependent on the level of SA. For example, the smaller stature of *cpr1-1* plants was attributed to moderately elevated basal total SA in the absence of cell death (Jirage et al., 2001; Bowling et al., 1994). Furthermore, transgenic *A. thaliana* plants that constitutively express bacterial SA synthesis genes exhibit a range in elevated basal total SA and growth reduction (Mauch et al., 2001). By contrast, when robust SA accumulation is prevented, plants are often larger, with the impact dependent on growth conditions and stress exposure (Rivas-San Vicente and Plasencia, 2011). Allocation of plant resources to SA-mediated defense redirects resources from growth and reproduction (e.g. Heidel et al. 2004). Therefore, fine control of these processes in a developmental context is critical. Our results suggest DEL1 acts via the hormone SA to restrain defense in growing tissue.

Furthermore, DEL1's impact on SA likely results from its direct transcriptional repression of the SA transporter *EDS5*. DEL1 is a conserved eukaryotic (atypical) E2F transcription factor that binds the E2F *cis*-acting regulatory element (e.g. Lammens et al. 2008; Radziejwoski et al. 2011). We found DEL1 binds at the E2F site of the *EDS5* promoter and *EDS5* expression is anti-correlated with that of *DEL1* during leaf development. Lack of *EDS5* function severely limits SA synthesis, presumably through feedback inhibition when SA is unable to be transported out of the plastid where it is synthesized (Nawrath et al. 2002; Serrano et al. 2013). Moreover, both *eds5* and *ics1* mutants exhibit dramatic reductions in SA-dependent defense gene expression and allow enhanced growth of (hemi)-biotrophic pathogens (Nawrath et al. 2002; Wildermuth et al., 2001).

In addition to *G. orontii* and *Pma*, *del1-1* mutants have also been shown to be more resistant to UV, osmotic stress, and root nematodes (Radziejwoski et al., 2011; Cookson et al., 2006; de Almeida Engler et al., 2012). Both DNA damage repair and plant defense/immune responses are known to be highly integrated and controlled by SA (Spoel and Dong, 2012). Moreover, *ICS1*, *EDS5*, and SA are induced in response to UV stress (Nawrath et al. 2002). Previous work demonstrated that DEL1 restrains UV-induced DNA damage repair responses in 2½ week old plants by repressing expression of the photolyase repair gene *PHR1* (Radziejowski et al., 2011). Similar to our findings with *ICS1* and *EDS5*, DEL1 appeared to control basal *PHR1* expression, not its induction (by UV), with *DEL1* expression greater in younger actively dividing leaves. We found DEL1 binds the promoters of both *EDS5* and *PHR1* in expanding leaves suggesting a potential role for SA in the enhanced UV-B resistance of *del1-1*. Furthermore, although reduced nematode development/reproduction on *del1-1* was attributed to its impact on cell division in syncytia/gall formation (de Almeida Engler et al., 2012), it may also result from the up-regulation of SA defense responses, which are known to enhance resistance to nematodes (Wubben et al., 2008).

Therefore, although the literature to date focuses on the function of the *Arabidopsis* atypical E2F DEL1 as a repressor of the endocycle in mitotically active cells, we propose that the primary function of DEL1 is more general – to restrain (a)biotic stress response in growing tissue, with its impact on the endocycle as one component of this response. Herein, we show DEL1 acts through its repression of the hormone SA to limit plant immunity. Moreover, we speculate that DEL1 may also act via SA to restrain other (a)biotic stresses including genotoxic stress. Like

DEL1, atypical mammalian E2Fs function as repressors at the intersection of growth and stress response. However, in contrast to DEL1, they have been shown to promote (genotoxic) stress tolerance while restraining proliferation (Hazar-Rethinam et al., 2008; Zalmas et al., 2008; Carvajal et al., 2012). Given our findings with DEL1, further investigation to ascertain whether atypical mammalian E2Fs also modulate biotic stress tolerance and innate immunity is warranted.

EXPERIMENTAL PROCEDURES

Plant lines, growth conditions, and *G. orontii* infection

del1-1 (E2Fe/DEL1 KO mutant) and *DEL1^{OE}* transgenic line 2 in the *A. thaliana* WT Columbia-0 (*Col-0*) background were described previously (Vlieghe et al., 2005). The *del1-ics1* double mutant was created by crossing *del1-1* with *eds16-1* aka *sid2-2* and *ics1-2* (Wildermuth et al., 2001) as described (Text 3.1). Plants were grown in growth chambers at 22ºC, 70% RH and a 12 h photoperiod with photosynthetically active radiation = 150 µmol m-2 s-1. Fully expanded mature leaves (3 per plant) of 4-week-old plants were used for all assays unless specified. As in Chandran et al. (2009), powdery mildew infections used a moderate inoculum of *G. orontii* MGH isolate with a settling tower. Mutants were compared to WT within the same box. Each experimental set included all genotypes vs. WT. *G. orontii* microscopic phenotypes were assessed for 9 leaves per genotype per experiment. For data in Figure 3.5, WT values did not differ appreciably from box to box allowing direct comparison of all genotypes.

Quantification of *G. orontii*-induced ploidy

For each line, three leaves were harvested at 5 dpi from infected and uninfected control plants in parallel, with nine leaves examined per genotype. Nuclear DNA quantitation of three mesophyll cells underlying the fungal feeding structure or similar mesophyll cells from leaves of uninfected plants was performed as described in Chandran et al. (2010) with DAPI stained DNA quantified by 3D reconstruction of serial confocal microscopic images for 30 nuclei per genotype per experiment.

RNA isolation, microarray hybridization and analysis

Three leaves were harvested at 5 dpi from infected and uninfected control plants per sample and total RNA extracted using the RNeasy Plant Mini kit (Qiagen, Valencia, CA). Target labeling, microarray hybridizations to Affymetrix ATH1 arrays and array scanning were performed by the Functional Genomics Laboratory (UC Berkeley). Microarray analysis was performed using Partek Genomics Suite (v6.6 beta, Partek Inc., St. Louis, MO). Expression values (log_2) for two independent biological replicates were extracted using robust multiarray analysis with perfect match correction and quantile normalization. Genes with ≥1.5 fold change in *del1-1* versus WT samples and p-value ≤0.05 were computed using a one-way Analysis of Variance. TAIR9 gene functional descriptions were employed. Biomaps in Virtual Plant (Katari et al., 2010) was used to identify statistically enriched functional processes. Gene expression data is deposited in the NCBI Gene Expression Omnibus (accession GSE40973).

Quantitative PCR (qPCR) and Chromatin Immunoprecipitation (ChIP)

For RT-qPCR, first strand cDNA synthesis used Superscript II or III Reverse Transcriptase (RT) from Invitrogen. qPCR used SYBR Premix Ex Taq (TaKaRa) or iTaq™ Universal SYBR Green

Supermix (Biorad) in an ABI 7300 instrument. The ChIP assay was performed using ~1.5 g of expanding leaves (leaves 6-9) from 3-week-old *A. thaliana* WT or *del1-1* plants as per Gendrel et al. (2005). DEL1-specific antibodies (Lammens et al. 2008) were used with BSA-blocked Protein A sepharose beads (Sigma, P-3391) to immunoprecipiate the DEL1-DNA complexes. Primer information is provided in Table S2.

Measurement of total SA levels
Leaf free and total SA (free SA plus SA glucosides) extraction and quantitation by HPLC with fluorescence detection was performed per (Nobuta et al., 2007).

***Pseudomonas syringae* pathogen assay**
Fully expanded mature leaves (3 per plant) of four-week-old plants were inoculated with *P. syringae* pv. *maculicola* ES4326 in 10 mM $MgSO_4$ at OD_{600}= 0.0002 or buffer alone using a needleless syringe per Glazebrook et al. (1996). Bacterial growth was assayed by grinding two 0.25 cm radius leaf discs per sample in 10mM $MgSO_4$ at 0 or 3 dpi and plating dilutions on King's B medium with streptomycin. Buffer-inoculated controls showed no bacterial growth at 0 or 3 dpi.

Table 3.2. Primers for qPCR and/or RT-PCR

Locus	Gene Name	Forward primer	Reverse primer
At1g74710	*ICS1*	GAATTTGCAGTCGGGATCAG	AATTAATCGCCTGTAGAGATGTTG
At2g14610	*PR1*	GAAAACTTAGCCTGGGGTAGC	TTCATTAGTATGGCTTCTCGTTCA
At4g39030	*EDS5*	ATCATATCCGAGATGCATAGACTG	CGAACATTAGTGTGAGACAACCA
At3g48160	*DEL1*	CCGTTACTTCTCCTTCTTCCATACC	CTCTAAACCAGCAGTTGGATATGTACC
At3g62250	*UBQ5*	GAAGACTTACACCAAGCCGAAG	TTCTGGTAAACGTAGGTGAGTCC
Primers for ChIP			
PHR1 (at E2F site)		GTGTAATGTGTATAGATGTTCGGG	GTTAGTTACGCTGTTAGGAGAGC
PHR1 (distal)		CATATCATGAGGAATGATAATCACTCTTTC	CATACGCTCACGCTAGTCGTTTG
EDS5 (at E2F site)		AAACACGTGGTGATTAGAGAGTAG	GGATCCGTCTTGTTTTGGAC
EDS5 (distal)		GAAATCGCGTGGAAGTCG	GAATCTCTTCTGATGTCAAAGACG

Primers are shown 5'-3'. *DEL1* primers are from Vlieghe et al. 2005. *PHR1* ChIP primers are from Radziejwoski et al. 2011.

Text 3.1. Genotyping *del1-ics1* double mutant

A. Nucleotide sequence flanking deletion site in *ics1-2* (*eds16-1*) mutant

The *ics1-2 (eds16-1)* mutation is a deletion of 6747 bp (3893 bp upstream and 2854 bp downstream of the ICS1 ATG). The deletion extends from exon 5 of At1g74700 into exon 9 of At1g74710. The sequence flanking the deletion is as follows:

CCCAAGATTTGGCTTTTTTGTTAAACCTTGGACACTTCTTCATGCAGGGGAGGAGTTT
ATTATAAGGAAAGATCTCAAAGTCAAAGCCTTTAAGACATTCCATGTCATCCAAAGC
CAGGTTTATTTTAGTAAACTCGCATGAGATTTTCGATATCTTAGCGTTATGTGTCTTC
GTTGAATTCATGCTTTCGTTTGATATTTTGCAGGGTTATGTAGTGTATTCAACTAAAT
ATAAACTCAAGAAGGAATATATTGGCCTATCTGGAAATGAAATTAAGAACTTGAAG
GTTTCAGGTGTTGAGGTTTGTCTTTGATTTGCTTAATATTGCTTGTCAATTTTTTCTTA
TGTTTGTCTATCACAAAGTCAATAGTTTTGCAATGGTCTTTCCAAAGTATATAAGCCT
GTTTAATAAGTTTGGATTGTGGATTGTAGATTCTGTCTATAGTATAAAATATTGGCTG
CTCTGCATCCAACTCCAGCTGTTTGTGGGCTTCCAGCAGAAGAAGCAAGGCTTTTGA
TTAAGGAGATAGGTAAAATATCTACCTTGGTTCAAC

B. Genotyping *del1-ics1* double mutants.
F$_2$ plants of *del1-1* crossed with *eds16-1* were genotyped using the following primers: For *del1-*DEL1 FP 5'-GATGATGAGGATGATGATGAA-3', DEL1 RP 5'-CATTGACGACAAGACATTTGC-3'; GABI-KAT T-DNA 5'-ATATTGACCATCATACTCATTG-3'. For *eds16-1-* EDS16 FP sm108 5'-TTCTTCATGCAGGGGAGGAG-3', EDS16 FP sm30 5'-CAACCACCTGGTGCACCAGC-3', EDS16 RP L1849 5'-AAGCAAAATGTTTGAGTCAGCA-3'. sm108 forward and L1849 reverse *EDS16* primers result in a 7,238 bp product for *Col-0* and 581 bp product for *eds16-1*. sm30 forward and L1849 reverse *EDS16* primers yield a 879 bp product for *Col-0* and no product for *eds16-1*. F$_3$ seeds from a confirmed homozygous double mutant line were used for all experiments.

REFERENCES

Berckmans, B., and De Veylder, L. (2009). Transcriptional control of the cell cycle. Curr Opin Plant Biol 12, 1: 7.

Bowling, S.A., Guo, A., Cao, H., Gordon, A.S., Klessig, D.F., and Dong, X. (1994). A mutation in Arabidopsis that leads to constitutive expression of systemic acquired resistance. Plant Cell 6, 1845-1857.

Carvajal, L.A., Hamard, P-J., Tonnessen, C., and Manfredi, J.J. (2012) E2F7, a novel target is up-regulated by p53 and mediates DNA damage-dependent transcriptional repression. Genes Dev 26, 1533-1545.

Chandran, D., Inada, N., Hather, G., Kleindt, C.K., and Wildermuth, M.C. (2010) Laser microdissection of Arabidopsis cells at the powdery mildew infection site reveals site-specific processes and regulators. Proc Natl Acad Sci USA 107, 460-465.

Chandran, D., Rickert, J., Cherk, C., Dotson, B.R., and Wildermuth, M.C. (2013). Host cell ploidy underlying the fungal feeding site is a determinant of powdery mildew growth and reproduction. Mol Plant-Microbe Interact 26, 537-545.

Chandran, D., Tai, Y.C., Hather, G., Dewdney, J., Denoux, C., Burgess, D.G., Ausubel, F.M., Speed, T.P., and Wildermuth, M.C. (2009). Temporal Global Expression Data Reveals Known and Novel Salicylate-Impacted Processes and Regulators Mediating Powdery Mildew Growth and Reproduction on Arabidopsis. Plant Physiol 149, 1435-1451.

Chen, H.Z., Ouseph, M.M., Li, J., Pecot, T., Chokshi, V., Kent, L., Bae, S., Byrne, M., Duran, C., Comstock, G., et al. (2012). Canonical and atypical E2Fs regulate the mammalian endocycle. Nat Cell Biol 14, 1192-1202.

Cookson, S.J., Radziejwoski, A., and Granier, C. (2006). Cell and leaf size plasticity in Arabidopsis: what is the role of endoreduplication? Plant Cell Environ 29, 1273-1283.

de Almeida Engler, J., Kyndt, T., Vieira, P., Van Cappelle, E., Bouldolf, V., Sanchez, V., Escobar, C., De Veylder, L., Engler, G., Abad, P., et al. (2012). CCS52 and DEL1 genes are key components of the endocycle in nematode-induced feeding sites. The Plant Journal 72, 185-198.

Dempsey, D.A., Vlot, A.C., Wildermuth, M.C., and Klessig, D.F. (2011) Salicylic acid biosynthesis and metabolism. The Arabidopsis Book 2011; 9e0156. doi: 10.1199/tab.0156.

Dewdney, J., Reuber, T.L., Wildermuth, M.C., Devoto, A., Cui, J., Stutius, L.M., Drummond, E.P., and Ausubel, F.M. (2000) Three unique mutants of Arabidopsis identify eds loci required for limiting growth of a biotrophic fungal pathogen. Plant J 24, 205-18.

Gendrel, A.V., Lippman, Z., Martienssen, R., and Colot, V. (2005) Profiling histone modification patterns in plants using genomic tiling microarrays. Nat Methods. 2, 213-8.

Glazebrook, J., Rogers, E.E., and Ausubel, F.M. (1996). Isolation of Arabidopsis mutants with enhanced disease susceptibility by direct screening. Genetics 143, 973-982.

Hazar-Rethinam, M., Endo-Munoz, L., Gannon, O., and Saunders, N. (2011) The role of the E2F transcription factor family in UV-induced apoptosis. Int. J. Mol. Sci. 12,8947-8960.

Heidel, A.J., Clarke, J.D., Antonovics, J., and Dong, X. (2004). Fitness costs of mutations affecting the systemic acquired resistance pathway in Arabidopsis thaliana. Genetics 168, 2197-2206.

Higo, K., Ugawa, Y., Iwamoto, M., and Korenaga, T. (1999) Plant cis-acting regulatory DNA elements (PLACE) database: Nucleic Acids Res. 27, 297-300.

Jirage, D., Zhou, N., Cooper, B., Clarke, J.D., Dong, X., and Glazebrook, J. (2001). Constitutive salicylic acid-dependent signaling in cpr1 and cpr6 mutants requires PAD4. Plant J 26, 395-407.

Katari, M.S., Nowicki, S.D., Aceituno, F.F., Nero, D., Kelfer, J., Thompson, L.P., Cabello, J.M., Davidson, R.S., Goldberg, A.P., Shasha, D.E., et al. (2010). VirtualPlant: a software platform to support systems biology research. Plant Physiol 152, 500-515.

Lammens, T., Boudolf, V., Kheibarshekan, L., Zalmas, L.P., Gaamouche, T., Maes, S., Vanstraelen, M., Kondorosi, E., La Thangue, N.B., Govaerts, W., et al. (2008). Atypical E2F activity restrains APC/CCCS52A2 function obligatory for endocycle onset. Proc Natl Acad Sci U S A 105, 14721-14726.

Lammens, T., Li, J., Leone, G., and De Veylder, L. (2009). Atypical E2Fs: new players in the E2F transcription factor family. Trends Cell Biol 19, 111-118.

Lee, H.O., Davidson, J.M., and Duronio, R.J. (2009) Endoreduplication: polyploidy with purpose. Genes Dev 23, 2461-2477.

Mauch, F., Mauch-Mani, B., Gaille, C., Kull, B., Haas, D., and Reimmann, C. (2001). Manipulation of salicylate content in Arabidopsis thaliana by the expression of an engineered bacterial salicylate synthase. Plant J 25, 67-77.

Melaragno, J.E., Mehrotra, B., and Coleman, A.W. (1993). Relationship between Endopolyploidy and Cell Size in Epidermal Tissue of Arabidopsis. Plant Cell 5, 1661-1668.

Micali, C., Gollner, K., Humphry, M., Consonni, C., and Panstruga, R. (2008). The powdery mildew disease of Arabidopsis: a paradigm for the interaction between plants and biotrophic fungi. The Arabidopsis Book; doi: 10.1199/tab.0115.

Nagl W. (1976) DNA endoreduplication and polyteny understood as evolutionary strategies. Nature 261,614-5.

Nawrath, C., Heck, S., Parinthawong, N., and Métraux, JP. (2002). EDS5, an essential component of salicylic acid-dependent signaling for disease resistance in Arabidopsis, is a member of the MATE transporter family. Plant Cell 14(1):275-86.

Nobuta, K., Okrent, R.A., Stoutemyer, M., Rodibaugh, N., Kempema, L., Wildermuth, M.C., and Innes, R.W. (2007). The GH3 Acyl Adenylase Family Member PBS3 Regulates Salicylic Acid-Dependent Defense Responses in Arabidopsis. Plant Physiol 144, 1144-1156.

Obayashi, T., Hayashi, S., Saeki, M., Ohta, H., and Kinoshita, K. (2009) ATTED-II provides coexpressed gene networks for Arabidopsis. Nucleic Acids Res 37, D987-91.

Radziejwoski, A., Vlieghe, K., Lammens, T., Berckmans, B., Maes, S., Jansen, M.A.,

Knappe, C., Albert, A., Seidlitz, H.K., Bahnweg, G., et al. (2011). Atypical E2F activity coordinates PHR1 photolyase gene transcription with endoreduplication onset. EMBO J 30, 355-363.

Rivas-San Vicente, M., and Plasencia, J. (2011). Salicylic acid beyond defense. Its role in plant growth and development. . J Exp Bot 62, 3321-3338.

Serrano, M., Wang, B., Aryal, B., Garcion, C., Abou-Mansour, E., Heck, S., Geisler, M., Mauch, F., Nawrath, C., and Metraux, J.P. (2013) Export of salicylic acid from the chloroplast requires the MATE-like transporter EDS5. Plant Physiol 162, 1815-1821.

Spoel, S.H., and Dong, X. (2012). How do plants achieve immunity? Defence without specialized immune cells. Nat Rev Immunol 12, 89-100.

Vlieghe, K., Boudolf, V., Beemster, G.T., Maes, S., Magyar, Z., Atanassova, A., de Almeida Engler, J., De Groodt, R., Inze, D., and De Veylder, L. (2005). The DP-E2F-like gene DEL1 controls the endocycle in Arabidopsis thaliana. Curr Biol 15, 59-63.

Wildermuth, M.C. (2010). Modulation of host nuclear ploidy: a common plant biotroph mechanism. Curr Opin Plant Biol 13, 449-458.

Wildermuth, M.C., Dewdney, J., Wu, G., and Ausubel, F.M. (2001). Isochorismate synthase is required to synthesize salicylic acid for plant defence. Nature 414, 562-565.

Wubben, M.J., Jin, J., and Baum, T.J. (2008). Cyst nematode parasitism of Arabidopsis thaliana is inhibited by salicylic acid (SA) and elicits uncoupled SA-independent pathogenesis-related gene expression in roots. Mol Plant Microbe Interact 21, 424-432.

Zalmas, L.P., Zhao, X., Graham, A.L., Fisher, R., Reilly, C., Coutts, A.S., and La Thangue, N.B. (2008) DNA-damage response control of E2F7 and E2F8. EMBO Rep. 9, 252-259.

CHAPTER 4 – CONCLUSIONS

In our current evolving climate, new challenges will emerge as pathogen distributions continue to geographically shift onto new host species, while altered CO_2, temperature and drought may influence molecular interactions between microbial components and plant response signaling and resistance mechanisms (Elad and Pertot, 2014). As such, an understanding of the mechanisms governing SA biosynthesis will be key for responding to these future challenges. Manipulation of endogenous SA synthesis and accumulation can have major impacts on plant fitness. These effects can be severe – constitutive defense gene expression, tissue necrosis and dwarfism – or largely absent until pathogen challenge. As detailed in Chapters 2 and 3, *CM1* and *DEL1* mutant plants represent a continuum of low-level defense priming by endogenous SA, and illustrate new approaches for modulating increased disease resistance in plants by influencing metabolic flux of chorismate products.

In Chapter 1, I detail data that show chorismate mutases CM1 and CM3 are structurally similar to bacterial IPL enzymes, and function through a similar reaction mechanism. However, *in planta* assays do not demonstrate that these enzymes augment SA synthesis via IPL activity, but rather can repress it when they are overexpressed and their activity is not bound by negative allosteric regulation. Accordingly, reducing naive expression of *CM1* results in elevated basal total SA, which confers resistance to a bacterial pathogen through mediating early responses to infection (Fig. 4.1). Further testing of complemented lines will provide confirmation that this phenotype is due to a reduction of *CM1* expression, and metabolite profiling can be employed to detail additional primary and secondary metabolism shifts due to chorismate misallocation, similar to that used in (Huang et al., 2010; Tzin et al., 2012).

While CM1 activity appears to modulate chorismate concentrations and indirectly affect flux to SA, *del1*'s increased SA is likely mediated through enhanced export and/or greater ICS1 activity (Fig. 4.1). We show that the SA exporter *EDS5* is a direct binding target for transcriptional repression by DEL1, and *DEL1* and *EDS5* expression are inversely correlated in leaves in an age-dependent manner. DEL1 has a known function in cell cycle regulation and control of entry into the endocycle (Vlieghe et al., 2005; Lammens et al., 2008), a process often manipulated by biotrophic pathogens, such as powdery mildew or root-knot nematodes (see our review at (Wildermuth et al., 2017)). The discovery that DEL1 also mediates expression of an SA hub suggests that it plays a broader role in coordinating developmental and stress response cues; evidence also shows that *DEL1* is responsive to light, and also coordinates expression of genes involved in UV-damage DNA repair (Radziejwoski et al., 2010; Berckmans et al., 2011). Additional DEL1 repression targets may be genetic regulators of SA synthesis and response, ie *PAD4*. The independent mechanisms by which *del1-1* and *cm1 #1* plants elevate SA synthesis suggest they could be additive, and genetic crosses might help further elucidate the mechanistic details of whether *cm1 #1* enhanced SA synthesis is limited by export, or coupled to plant age.

Modification of chorismate flux as virulence mechanism

The phenotypes displayed by plants in Chapter 2 highlight the importance of chorismate partitioning. Biotrophic pathogens from across the kingdoms of life have converged upon chorismate/isochorismate as a hub to manipulate SA and enhance virulence. These pathogens deploy secreted effector proteins that specifically alter chorismate and isochorismate directly to divert them from SA, or to convert them into other molecules that may aid the pathogen. In the smut fungus *Ustilago maydis*, the chorismate mutase effector Cmu1 has been detected
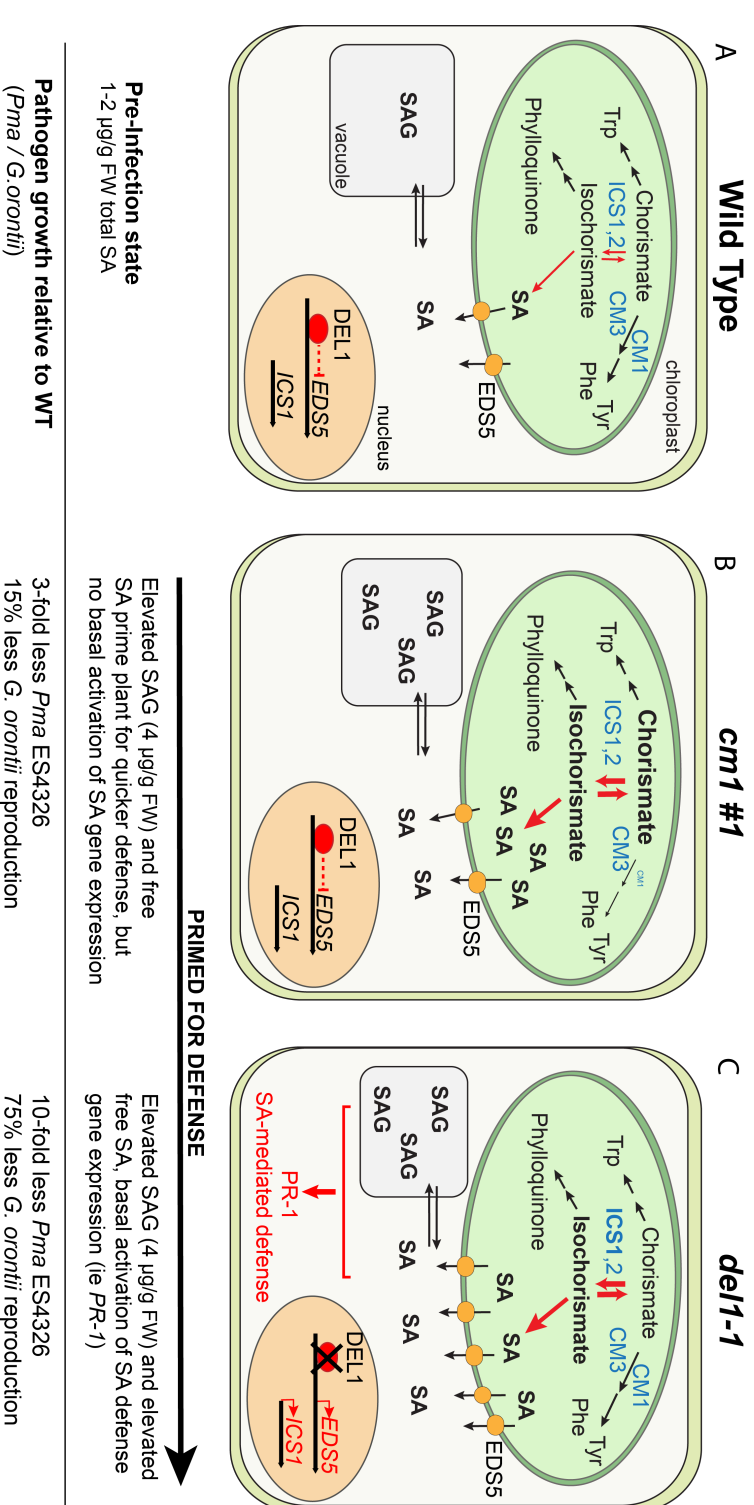
PRIMED FOR DEFENSE

	Wild Type	cm1 #1	del1-1
Pre-Infection state	1-2 µg/g FW total SA	Elevated SAG (4 µg/g FW) and free SA prime plant for quicker defense, but no basal activation of SA gene expression	Elevated SAG (4 µg/g FW) and elevated free SA, basal activation of SA defense gene expression (ie *PR-1*)
Pathogen growth relative to WT (*Pma / G.orontii*)		3-fold less *Pma* ES4326 15% less *G. orontii* reproduction	10-fold less *Pma* ES4326 75% less *G. orontii* reproduction

Figure 4.1 Model of basal SA accumulation and signaling in *cm1 #1* and *del1*
A) In the basal state of wild type leaves, SA synthesis and SAG accumulation occur at a slow rate, catalyzed by ICS1/ICS2, and export is mediated via EDS5. 4-week old plants accumulated between one to two µg/g FW of total SA. DEL1 represses *EDS5* expression in an age-dependent manner (dotted line), and *EDS5* expression increases with leaf age. **B)** In *cm1 #1*, *CM1* expression is reduced to 5% of wild type, chorismate concentration increases due to reduced flux to Phe and Tyr, and is reversibly converted to isochorismate by ICS1/2. SA synthesis is increased, but export to cytosol is limited by EDS5 and there is no activation of SA-mediated defense responses. SAG levels accumulate 3-fold more than wild type. **C)** In *del1-1*, lack of DEL1 results in 10-fold increase of *EDS5*, which enhances SA export from the plastid. Plastidic free SA is toxic at high levels and limits synthesis. Increased EDS5 and SA transport out of the plastid results in greater SA synthesis via ICS1. Elevated SAG and cytosolic SA reach threshold for SA-mediated defense activation (ie *PR-1*). Additional stress-responsive components normally restrained by DEL1 (not shown) are likely active and enhance this response. Upon pathogen challenge, *cm1 #1* exhibits moderate disease resistance, while *del1-1* exhibits greater resistance (Note: *del1-1* was assayed for *G. orontii* spore output as in Chapter 2, and had 75% less spores than wild type).

translocating from fungal to host plant cytosol, where it can dimerize with endogenous cytosolic *Zea mays* CM (Djamei et al., 2011). Chorismate flux to phenylpropanoids increases in plant cells upon infection of wild type *U.maydis* CL13 relative to strains with a *cmu1* deletion. Induced SA in the host plant is absent in smut infection carrying *Cmu1,* but increases at least 10-fold in plants infected with a smut fungus strain lacking the CM effector. Similarly, obligate root knot nematodes secrete CM effectors into root cells during early establishment of parasitism, presumably disrupting both auxin and SA accumulation (Doyle and Lambert, 2003; Vanholme et al., 2009). CM proteins are not commonly found among animals; these nematode effectors are thought to be the result of horizontal gene transfer with soil bacteria (Noon and Baum, 2016), and the CM from *Heterodera schachtii* shares sequence and predicted structural homology to bacterial CMs (Vanholme et al., 2009). Nematodes are sensitive to SA-mediated resistance responses in roots, and although SA increases in the shoots of infected plants, levels of SA in roots remained unchanged. This is possibly as a result of secreted CM activity (Wubben et al., 2008), though comparisons between root and shoot metabolism should be carefully made. These deployed CM proteins show similar impacts on SA to overexpression of *CM1* and *CM3* in *N. benthamiana*, which showed a reduction in induced SA accumulation (Chapter 2). Additional characterization of stable overexpression lines of wild type and allosteric insensitive CM1 I've developed using metabolite profiling and disease assays will provide further insight into this virulence strategy in native plants.

Effectors repertoires of filamentous pathogens *Verticillium dahliae* and *Phytopthora sojae* include secreted isochorismatase hydrolases (ISCH), which convert isochorismate into 2,3-dihydro-2,3-dihydroxybenzoate (DDHB). These effectors increase host susceptibility; SA levels are reduced in infected host plants relative to those without the effector, corresponding to a reduction in *PR-1* expression and increased pathogen growth (Liu et al., 2014). This effector confers a virulence advantage that extends beyond benefiting its native host. When the effector is transiently expressed in *N. benthamiana* and plants are induced by a related non-ISCH-carrying pathogen, plants with the effector protein had lower SA and exhibited a corresponding increase in DDHB(Liu et al., 2014). Given the dynamics between isochorismate and chorismate medited by ICS1, might these effectors also have a secondary role in reducing chorismate flux to phenylpropanoid metabolism by creating an isochorismate sink?

The supposed cytosolic localization of CM and ISCH effectors in the host plant raises interesting questions about the possible export of chorismate and isochorismate from the plastid. Plants typically have both plastidic and cytosolic chorismate mutases, suggesting that at least low levels of chorismate exist in the cytosol. *Arabidopsis* plants expressing a cytosolic-located bacterial SA synthase have elevated levels of basal total SA similar to that seen in *cm1 #1* and *del1-1* plants (Mauch et al., 2001), while plastidic localized protein generated 10-fold more SA. Further investigation into the spatial dynamics and mechanisms of chorismate concentration is warranted, as plants deficient in chorismate export to the cytosol may be less susceptible to the deleterious impact of this class of effector proteins. Conversely, it remains possible these effectors may localize to the plastid during infection.

Modulation of pre-infection SA through chorismate partitioning for agriculture

As seen in numerous mutants with high levels of basal SA, accompanying effects of defense gene signaling can also reduce plant size and reproduction (Canet et al., 2010). *CM1* and *DEL1* mutants suggest new approaches for modulating SA levels for plant priming. Previous approaches to genetically engineer elevated SA into tobacco and *Arabidopsis* introduced

bacterial SA synthesis enzymes (Verberne et al., 2000; Mauch et al., 2001) with varying impacts on overall plant fitness. Knockdown of *CM1* seems sufficient to increase basal SA in *Arabidopsis*, an effect that confers a degree of disease resistance, yet is not accompanied by the constitutive defense gene activation that typically reduces plant biomass yield (Chapter 2). This begs the question whether modulation of chorismate mutase activity or increasing flux of SA through increasing export from the chloroplast might serve as a strategy to increase pre-infection resistance in crop species such as tomato or soybean, which are both shown to utilize an ICS for SA synthesis (Uppalapati et al., 2007; Shine et al., 2016). Such a strategy could employ tissue-specific promoters to restrict the impact to vegetative structures. Based on their known kinetic parameters and differing infection phenotypes in genetic knockdown/out plants, there is likely a specialization of roles of CM1 and CM3 in *Arabidopsis*. Species with several plastidic CM isoforms might have functional redundancy, which may allow one to craft combinational knockouts and fine-tune flux to SA; one such example is soybean *Glycine max*, which possesses five putative plastidic isoforms that cluster with CM1, and is known to produce SA from isochorismate (Shine et al., 2016).

Outstanding questions remain, chiefly among them, how is isochorismate converted into SA in plants? A new large-scale mutant screen of 35,000 plants has identified 7 mutants that accumulate low levels of free SA upon infection with *Pma* ES4326 (Ding et al., 2015). This screen also identified seven new alleles of *EDS5*, two of *ICS1* and one for *PAD4*; these new mutants may be an IPL or reveal another mechanism by which SA is produced. Other potential candidates may be identified through association with *ICS1* or *EDS5*, as metabolite channeling might be employed to enhance SA synthesis. Lastly, examination of other chorismate-utilizing enzymes may reveal latent IPL function.

REFERENCES

Berckmans B, Lammens T, Van Den Daele H, Magyar Z, Bogre L, De Veylder L (2011) Light-Dependent Regulation of DEL1 Is Determined by the Antagonistic Action of E2Fb and E2Fc. PLANT Physiol **157**: 1440–1451

Canet J V., Dobón A, Ibáñez F, Perales L, Tornero P (2010) Resistance and biomass in Arabidopsis: A new model for Salicylic Acid perception. Plant Biotechnol J **8**: 126–141

Ding Y, Shaholli D, Mou Z (2015) A large-scale genetic screen for mutants with altered salicylic acid accumulation in Arabidopsis. Front Plant Sci. doi: 10.3389/fpls.2014.00763

Djamei A, Schipper K, Rabe F, Ghosh A, Vincon V, Kahnt J, Osorio S, Tohge T, Fernie AR, Feussner I, et al (2011) Metabolic priming by a secreted fungal effector. Nature **478**: 395–398

Doyle EA, Lambert KN (2003) *Meloidogyne javanica* Chorismate Mutase 1 Alters Plant Cell Development. Mol Plant-Microbe Interact **16**: 123–131

Elad Y, Pertot I (2014) Climate Change Impacts on Plant Pathogens and Plant Diseases. J Crop Improv **28**: 99–139

Huang T, Tohge T, Lytovchenko A, Fernie AR, Jander G (2010) Pleiotropic physiological consequences of feedback-insensitive phenylalanine biosynthesis in Arabidopsis thaliana.

Plant J **63**: 823–835

Lammens T, Ronique Boudolf V, Kheibarshekan L, Zalmas LP, Gaamouche T, Maes S, Vanstraelen M, Kondorosi E, Thangue NB La, Govaerts W, et al (2008) Atypical E2F activity restrains APC/C CCS52A2 function obligatory for endocycle onset.

Liu T, Song T, Zhang X, Yuan H, Su L, Li W, Xu J, Liu S, Chen L, Chen T, et al (2014) Unconventionally secreted effectors of two filamentous pathogens target plant salicylate biosynthesis. Nat Commun **5**: 4686

Mauch F, Mauch-Mani B, Gaille C, Kull B, Haas D, Reimmann C (2001) Manipulation of salicylate content in Arabidopsis thaliana by the expression of an engineered bacterial salicylate. Plant J **25**: 67–77

Noon JB, Baum TJ (2016) Horizontal gene transfer of acetyltransferases, invertases and chorismate mutases from different bacteria to diverse recipients. BMC Evol Biol **16**: 74

Radziejwoski A, Vlieghe K, Lammens T, Berckmans B, Maes S, Jansen MA, Knappe C, Albert A, Seidlitz HK, Nther Bahnweg G, et al (2010) Atypical E2F activity coordinates PHR1 photolyase gene transcription with endoreduplication onset. EMBO J **30313**: 355–363

Shine MB, Yang JW, El-Habbak M, Nagyabhyru P, Fu DQ, Navarre D, Ghabrial S, Kachroo P, Kachroo A (2016) Cooperative functioning between phenylalanine ammonia lyase and isochorismate synthase activities contributes to salicylic acid biosynthesis in soybean. New Phytol **212**: 627–636

Tzin V, Malitsky S, Zvi MM Ben, Bedair M, Sumner L, Aharoni A, Galili G (2012) Expression of a bacterial feedback-insensitive 3-deoxy-d-arabino-heptulosonate 7-phosphate synthase of the shikimate pathway in Arabidopsis elucidates potential metabolic bottlenecks between primary and secondary metabolism. New Phytol **194**: 430–439

Uppalapati SR, Ishiga Y, Wangdi T, Kunkel BN, Anand A, Mysore KS, Bender CL (2007) The phytotoxin coronatine contributes to pathogen fitness and is required for suppression of salicylic acid accumulation in tomato inoculated with Pseudomonas syringae pv. tomato DC3000. Mol Plant Microbe Interact **20**: 955–965

Vanholme B, Kast P, Haegeman A, Jacob J, Grunewald W, Gheysen G (2009) Structural and functional investigation of a secreted chorismate mutase from the plant-parasitic nematode Heterodera schachtii in the context of related enzymes from diverse origins. Mol Plant Pathol **10**: 189–200

Verberne MC, Verpoorte R, Bol JF, Mercado-Blanco J, Linthorst HJ (2000) Overproduction of salicylic acid in plants by bacterial transgenes enhances pathogen resistance. Nat Biotechnol **18**: 779–783

Vlieghe K, Boudolf V, Beemster GTS, Maes S, Magyar Z, Ana Atanassova, Janice de Almeida Engler, Ruth De Groodt, Dirk Inze´, Veylder L De (2005) The DP-E2F-like Gene DEL1 Controls the Endocycle in Arabidopsis thaliana. Curr Biol **15**: 59–63

Wildermuth MC, Steinwand MA, Mcrae AG, Jaenisch J, Chandran D (2017) Adapted Biotroph Manipulation of Plant Cell Ploidy. Annu Rev Phytopathol **55**: 537–64

Wubben MJE, Jin J, Baum TJ (2008) Cyst nematode parasitism of Arabidopsis thaliana is inhibited by salicylic acid (SA) and elicits uncoupled SA-independent pathogenesis-related gene expression in roots. Mol Plant Microbe Interact **21**: 424–432

APPENDIX I: Physiologically relevant concentrations of SA do not affect CM1 activity

INTRODUCTION AND RESULTS

Pathogen-induced SA biosynthesis generally is mediated by transcriptional upregulation and increased protein of *ICS1,* which has a K_m for chorismate that allows it to be highly competitive with other chorismate-utilizing enzymes. Chorismate serves as a branch point between synthesis of aromatic amino acids phenylalanine, tyrosine and tryptophan and partitioning is tightly controlled. AS and CM enzymes are sensitive to the accumulation of these chorismate derivatives via allosteric feedback on their enzyme activities (Tzin and Galili, 2010; Westfall et al., 2014), which can reroute metabolite flux between different pathway branches. Insensitive mutants that cannot respond to allosteric cues tend to accumulate excessive product and derivatives (Li and Last, 1996; Hughes et al., 2004). As such, relative pools of these allosteric effectors greatly influence overall flux of chorismate to specific pathways. Research focus has largely centered on production of aromatic amino acids and their impact on indole- and phenylpropanoid pathways. Could SA also serve as an allosteric effector for chorismate mutases?

Two possible forms of SA-mediated regulation on CM1 could exist. As SA concentration increases in the plastid, it may inhibit CM1 activity to reinforce chorismate flux to SA biosynthesis. This mechanism could be through binding at the allosteric site (Chapter 1) or by competing with chorismate at the active site. Alternatively, SA could act as a positive activator of CM1, altering chorismate/isochorismate equilibrium to reduce SA synthesis and increase flux to phenylalanine for phenylpropanoid metabolism. This result could explain why SA synthesis is impaired in the *eds5* mutant, which likely experiences a local buildup of SA in the plastid (Serrano et al., 2013). As a third possibility, SA synthesis could be largely governed through relative kinetics and concentrations of ICS1 or other enzymes, such as an increase in DAHPS activity and no allosteric effect on CM1 exists.

To investigate this question, I conducted *in vitro* assays on recombinant protein CM1 at 500 μM, near the K_m, with varied concentrations of SA ranging from 0.5 μM to 5 mM. Activity was consistent across multiple experiments for the two enzymes at lower concentrations of SA, yet more variable at 5 mM. I found that CM1 activity is unaffected by SA in all physiological concentrations (Appendix Fig. A1). PchB was unaffected by SA at low concentrations, similar to results in (Gaille et al., 2002), who found PchB to be insensitive to the reaction product pyruvate, along with phenylalanine, tyrosine and tryptophan. Interestingly, I found PchB activity increased in the presence of 5 mM SA, though the physiological significance of this result is unclear.

METHODS

SA competitive inhibition assay with recombinant CM1 and PchB

To determine whether SA can impact CM activity, varying concentrations of SA (0, 0.5 μM, 5 μM, 50 μM, 500 μM, 5 mM) were incubated with CM1 (100 ng recombinant protein) or PchB (1 μg protein) in 50 mM TRIS-HCl pH 7.7, 10 mM $MgCl_2$ and 500 μM chorismate in 100 μL reactions performed in triplicate in a microplate. Controls with no protein were included to account for non-enzymatic degradation of chorismate. Chorismate mutase activity of CM1 and PchB was monitored via loss of chorismate at A_{274} at 10-second intervals over 25 minutes and concentration calculated using its molar extinction coefficient.
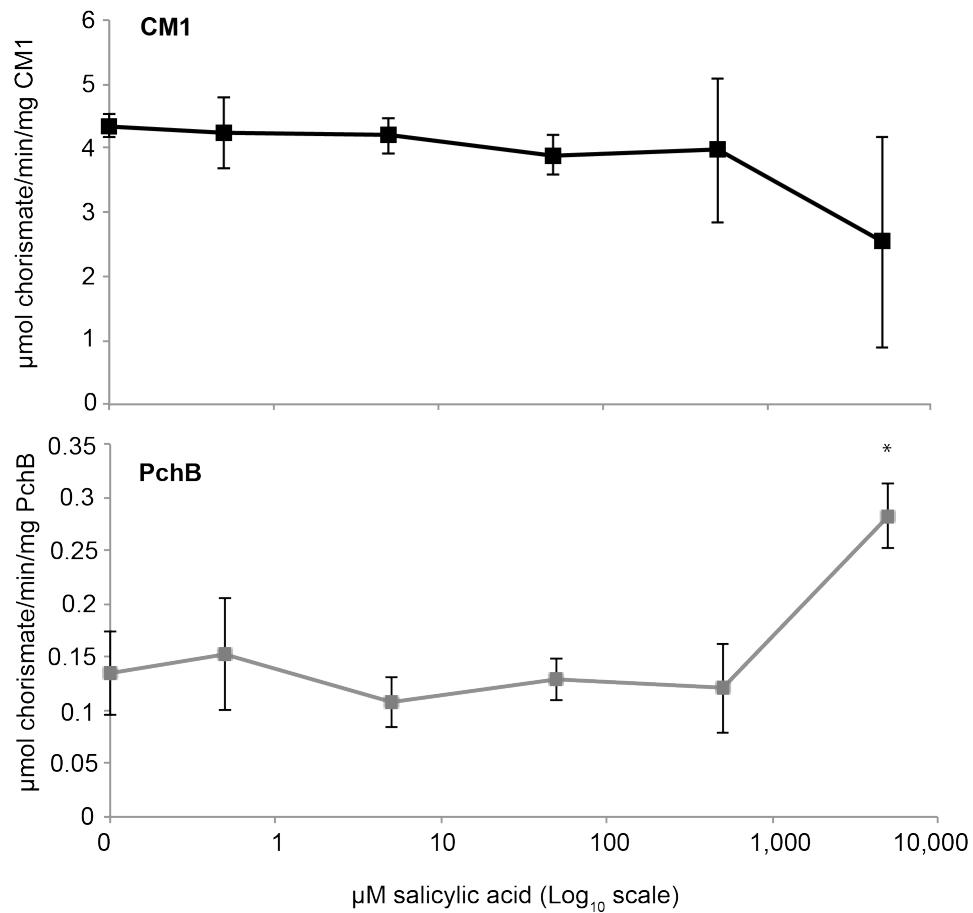
Figure A1: SA does not modulate CM1 activity *in vitro*
CM1 and PchB were incubated with 500 µM chorismate and varying concentrations of
SA and CM activity was monitored via spectrophotometry. Each data point represents the
average of 3 experiments, with standard error. Statistical significance was determined by
two-way ANOVA with Tukey post-hoc test (p <0.05).

REFERENCES

Gaille C, Kast P, Dieter H (2002) Salicylate biosynthesis in Pseudomonas aeruginosa. Purification and characterization of PchB, a novel bifunctional enzyme displaying isochorismate pyruvate-lyase and chorismate mutase activities. J Biol Chem **277**: 21768–21775

Hughes EH, Hong SB, Gibson SI, Shanks J V., San KY (2004) Expression of a feedback-resistant anthranilate synthase in Catharanthus roseus hairy roots provides evidence for tight regulation of terpenoid indole alkaloid levels. Biotechnol Bioeng **86**: 718–727

Li J, Last RL (1996) The Arabidopsis thaliana trp5 Mutant Has a Feedback-Resistant Anthranilate Synthase and Elevated Soluble Tryptophan. Plant Physiol **110**: 51–59

Serrano M, Wang B, Aryal B, Garcion C, Abou-Mansour E, Heck S, Geisler M, Mauch F, Nawrath C, Metraux J-P (2013) Export of Salicylic Acid from the Chloroplast Requires the Multidrug and Toxin Extrusion-Like Transporter EDS5. Plant Physiol **162**: 1815–1821

Tzin V, Galili G (2010) New Insights into the shikimate and aromatic amino acids biosynthesis pathways in plants. Mol Plant **3**: 956–972

Westfall CS, Xu A, Jez JM (2014) Structural evolution of differential amino acid effector regulation in plant chorismate mutases. J Biol Chem **289**: 28619–28628